Novel Transparent Composite Electrodes and Mixed Oxide Layers for Improved Flexible Electronics

by

Aritra Dhar

A Dissertation Presented in Partial Fulfillment
of the Requirements for the Degree
Doctor of Philosophy

Approved December 2014 by the
Graduate Supervisory Committee:

Terry Alford, Co-Chair
William Petuskey, Co-Chair
Andrew Chizmeshya
Stephen Krause

ARIZONA STATE UNIVERSITY

May 2015

ABSTRACT

Transparent conductive oxides (TCO) comprise a class of materials that exhibit unique combination of high transparency in the visible region along with high electrical conductivity. TCOs play an important role as transparent electrodes for optoelectronic devices such as solar cell panels, liquid crystal displays, transparent heat mirrors and organic light emitting devices (OLED). The most commonly used transparent electrodes in optoelectronic applications is indium tin oxide (ITO) due to its low resistivity (~ 10^{-4} Ω-cm) and high transmittance (~ 80 %). However, the limited supply of indium and the growing demand for ITO make the resulting fabrication costs prohibitive for future industry. Thus, cost factors have promoted the search for inexpensive materials with good electric-optical properties.

The object of this work is to study the structure-property-processing relationship and optimize a suitable transparent electrode with the intent to optimize them for flexible optoelectronics applications. The work focuses on improved processing of the mixed oxide (indium gallium zinc oxide, IGZO) thin films for superior optical and electrical properties. The study focuses on two different methods of post-deposition annealing-microwave and conventional. The microwave annealing was seen to have the dual advantage of reduced time and lower temperature, as compared to conventional annealing. Another work focuses on an indium free transparent composite electrode (TCE) where a very thin metal layer is inserted between the two TCO layers. A novel Nb_2O_5/Ag/Nb_2O_5 multilayered structure can exhibit better electrical and optical properties than a single layered TCO thin film. The focus for low cost alternative leads to a TiO_2/metal/TiO_2 based TCE. A systematic study was done to understand the effect of

metal thickness and substituting different metals (Ag, Cu or Au) on the opto-electrical properties of the TCEs. The $TiO_2/Ag/TiO_2$ with mid Ag thickness 9.5 nm has been optimized to have a sheet resistance of 5.7 Ohm/sq. average optical transmittance of 86 % at 550 nm and figure of merit with 61.4 $\times 10^{-3}$ Ω^{-1}. The TCEs showed improved optical and electrical properties when annealed in forming gas and vacuum. These dielectric/metal/dielectric multilayer TCEs have lower total thickness and are more efficient than a single-layer ITO film.

Dedicated to my family Shri Suhasis Kumar Dhar, Smt. Jaba Dhar,
and my wife Ms. Ankita Routh Dhar for their
eternal love and companionship

ACKNOWLEDGMENTS

I would like to take this opportunity to acknowledge the help, assistance and support of many individuals without whom this dissertation would not have been possible.

It is my honour to thank my research advisor Dr. T. L. Alford for his constant guidance, and invaluable suggestions during the past four years. It gives me immense pleasure to thank the members of my dissertation committee including Prof. T.L.Alford, Prof. William Petuskey, Prof. Stephen Krause and Prof. Andrew Chizmeshya for taking the time to review my work and provide constructive feedback amidst their busy schedule.

I am indebted to Dr. Shahriar Anwar for allowing me to use the hall measurement system and would like to convey my sincere gratitude to Tim Karcher for training me to do various experiments and modifications with the magnetron sputter system. I would also like to thank Barry Wilkens, David Wright, Diana Convey, and Kenneth Mossman of the CSSS staff for training and assistance with instrument usage.

I would also like to acknowledge the friendship and assistance of my lab mates Zhao Zhao, Sayantan Das and Arash Elhami. I would like to thank former labmates Dr. Rajitha Vemuri, Dr. Mandar Gadre and Dr.H.W.Choi for their valuable suggestions and providing me training on the operation of various lab instruments.

Last but not the least, I would like to thank my father Shri Suhasis Kumar Dhar and my mother Smt. Jaba Dhar without whose unconditional love and support this research journey would not have been possible. Their prayers have made me what I am today. At the same time, I would like to thank my wife, Ankita for being beside me through thick and thin and sharing my joys and sorrows during the last four years. I also thank my in-laws for having faith in me. My special thanks to Suratna, Sriloy, Subhadip, Sumit,

Sandipan, Anirban and Palash for making my PhD life fun-filled and adventurous and I am sure I will cherish this experience forever.

TABLE OF CONTENTS

Page

CHAPTER PAGE

CHAPTER PAGE

CHAPTER PAGE

LIST OF TABLES

LIST OF FIGURES

Figure Page

Figure Page

CHAPTER 1

INTRODUCTION

1.1 TRANSPARENT CONDUCTIVE OXIDES

Transparent conducting oxides (TCOs) are unique class of materials that are essential components for a large variety of optoelectronics applications. TCOs act as a transparent electrodes or electrical contacts in flat-panel displays, solar cells, electromagnetic shielding of CRTs used for video display terminals [1-4], electro chromic windows and low-emissivity windows in buildings. Transparent conducting oxides (TCOs) are wide band gap semiconductors which are optically transparent and show conductivities intermediate to metals and semiconductors. The key requirement for the TCO applications is that optical transmittance (%T) should be greater than 80%, while resistivity (ρ) is less than 10^{-4} Ω-cm [5,6]. In this regard, a substantial amount of research has been going to find an ideal material with optimum optical and electrical properties. A good understanding of the fundamental materials structure/property/processing relationships is required to elucidate the present challenge for achieving novel materials that retains optical transparency while becoming more electrically conductive.

As early as in 1907, the first TCO material was reported when Badeker oxidized a thin film of cadmium when annealed in air [7]. The heating resulted in incomplete oxidation of the cadmium and thus formed non-stoichiometric cadmium oxide with oxygen vacancies in its structure. The oxygen vacancies generated occupied defect

energy levels for facile electronic promotion and thus made the Cd-oxide optically transparent while remaining highly conducting. However, it was only after 1940 when the technological advances in transparent conducting oxides (TCOs) emerged due to commercialization needs for potential applications in industry.

In general, the conductivity of the TCOs is attributed to high carrier concentration (n) arising from defects (intrinsic and extrinsic), whose energy levels lie close to the conduction band. Now, a decrease of the resistivity can be possible with either an increase in the mobility or carrier concentration or both. However, higher carrier concentration also leads to an increase in the visible absorption. To an extent, many phenomenological approaches based upon well-understood physical principles have been reported to achieve materials having these properties. An overview of these approaches will be presented along with an idea to further the development of TCO technology. Thus to understand progress made in this field, it is essential to first introduce the physics involved in these semiconductors.

In order to evaluate the performance of a TCO thin film, a figure of merit (FOM), $\varphi_{TC,}$ (as defined by Haacke [8]) was estimated using the following relationship:

$$\varphi_{TC} = \frac{T_{av}^{10}}{R_{sh}} \qquad (1.1)$$

where, T_{av} is the average transmittance and R_{sh} is the sheet resistance, generally expressed as $R_{sh}=\rho/d$ for thin films of uniform thickness d.

Theoretical modeling and empirical analysis suggest that the unique combination of low electrical sheet resistance and high optical transparency can be realized by selecting a wide band-gap metal oxide which could be either generated or degenerated through suitable incorporation of native donors or substitutional dopants into the host lattice.

1.1.1 Electrical properties

According to Boltzmann's conductivity equation, a material's conductivity is given by

$$\sigma = \frac{1}{\rho} = n\mu e \tag{1.2}$$

where σ, ρ, n, μ and e are electrical conductivity, resistivity, carrier concentration, carrier mobility and electronic charge, respectively.

Thus the conductivity is determined by the product of the mobility (μ) and carrier concentration of free electrons (n). In case of wide band gap semiconductors, the n and μ cannot be individually increased and hence limits the conductivity. With increase in n, carrier transport is restricted due to ionized impurity scattering. As a result, mobility decreases and the conductivity drop down. As the dopant concentration increases, the resistivity reaches minima and remains constant whereas the optical transparency window becomes narrower. It is known that the mobility exerts all the forces acting on the electron in the conducting solid. Thus, mobility can be summarized as [9, 10]:

$$\frac{1}{\mu} = \frac{1}{\mu_i} + \frac{1}{\mu_l} + \frac{1}{\mu_g} \tag{1.3}$$

where, μ_i represents ionized impurity scattering, μ_l accounts for lattice scattering, and μ_g for scattering at the grain boundaries. The effect and extent of these various scattering mechanisms must be taken into account to determine the conductivity in a material. The conductivity is related with excess oxygen vacancies or doped impurities. However, apart from ionized impurity scattering, there are other factors which affect mobility like lattice scattering, neutral impurity scattering, electron–electron scattering and grain boundary scattering. Impurity scattering (μ_i) is the one of the dominant scattering mechanism in TCOs. For highly degenerate metal oxides, the ionized impurity scattering is given by (Eq. 1.4) [11].

$$\mu_i = \frac{4e}{h}\left(\frac{\pi}{3}\right)^{\frac{1}{3}} n^{\frac{2}{3}} \tag{1.4}$$

In the case of polycrystalline TCOs, grain boundary scattering is the predominant scattering mechanism. Here, a large number of interface states are present which result in a space charge region in the grain boundaries. This transport phenomenon in polycrystalline thin films can be expressed by Petritz model [12], where the mobility (μ_g) is written as:

$$\mu_g = \mu_0 \exp(-\frac{\Phi_B}{k_B T}) \tag{1.5}$$

Where $\mu_0 = (\frac{S^2 e^2}{2\pi m^* k_B T})^{\frac{1}{2}}$

S is the grain size, e is the elementary charge, Φ_B is the grain boundary potential and k_B is the Boltzmann constant.

It was found in theoretical simulation that the mobility decreases with decrease in grain size and increase in the grain boundary potential [13, 14]. Apart from this, there are other scattering mechanisms that also affect the mobility in TCO films, but most of them tend to be active only at low temperature.

1.1.2. Optical properties

In order to achieve high transparency, TCO thin films must have a very low absorption coefficient in the near UV-VIS-NIR region. Figure 1.1 shows the typical transmittance spectrum of a wide band gap semiconductor TCO film, which exhibits three distinct regions of transmission [15].

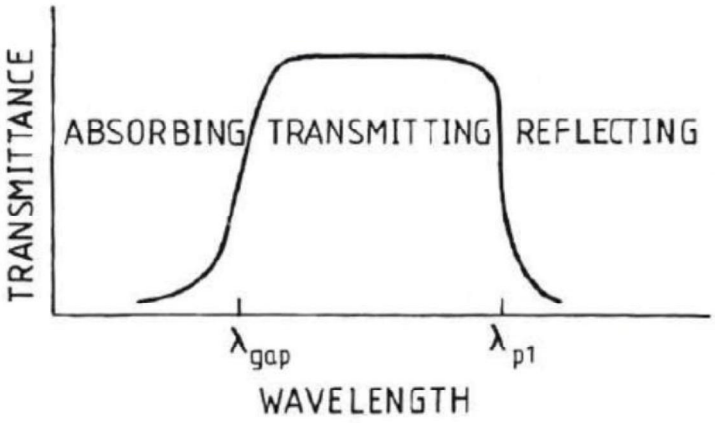

Fig1.1. Optical transmission spectrum of a typical TCO with λ_{gap} and λ_{pl} , respectively. Figure reproduced from Reference 15. Copyright 1979 Elsevier Ltd.

The optically transparent region is marked between the absorption edge (λ_{gap}) and the plasma edge (λ_{pl}), is also known as transparent window. The absorption edge (λ_{gap}) is related to bandgap absorption while the plasma edge (λ_{pl}) is due to free electron plasma absorption.

The important optical properties of TCOs are transmission (T), reflection (R), and absorption (A). They are determined by its refraction index (n), extinction coefficient (k), band gap (E_g), and film geometry. Other than the film geometry, all other factors depends on the structure and chemical composition of the material, whereas the geometry can be controlled by changing the film thickness and surface roughness.

Reflectivity is another important parameter which is affected by the degenerate nature of a semiconductor. At frequencies below the plasma frequency, it reflects and absorbs incident radiation. For most materials, the plasma frequency falls in the near-infrared part of the spectrum. From the Drude-Lorentz free electron model, the plasmon frequency (ω_p) can be expressed by the following equation [16]:

$$\omega_p = \sqrt{\frac{ne^2}{m\varepsilon_0}} \tag{1.6}$$

where n is the carrier density of electrons and ε_o is the permittivity of free space.

1.1.3 Work function

Work function (Φ) corresponds to the minimum amount of energy needed to remove an electron from the metal. It is the energy difference between Fermi energy and vacuum level. The factors affecting work function significantly are contamination, surface conditions and reactions *etc* [17-20]. In a nondegenerate semiconductor, the Fermi level is located within the band gap and thus is calculated as energy difference between valence bands maximum (VBM) and vacuum level. Thus, in case of semiconductors, the Φ is different from ionization energy whereas in metals, they are the

same thing. The Fermi level is defined as the point on the energy scale where the probability is just 50%.

The change in work function poses a similar challenge as balancing the electrical properties and the optical properties (%T and R) and. In organic optoelectronic devices, the work function of the electrode materials is very important to understand whether the electrode forms an Ohmic or a blocking contact for the respective charge carrier (holes or electrons).

1.2 TCO MATERIAL SELECTION

1.2.1 Doped and mixed oxides

Most of the research on TCO has focused on *n*-type semiconductors consisting of metal oxides. Indium-tin-oxide (ITO) have been the most popular TCO which had been widely used in various optoelectronics industry. However, since indium is rare and thus very costly, a lot of research has been going on to come up with new prospective transparent conducting oxides (TCOs) that are either indium free or contain a reduced amount of indium. [21-26]. Many types of metal oxides have recently attracted much attention have been newly developed in recent years to substitute the ITO [21-27]. A list of host materials and suitable dopants are shown in Table 1.1 for potential TCO thin-film materials reported up to now. The dopants are added to the host metal oxides for improved optical and electrical properties.

Binary	Dopant	Resistivity	Toxicity
ZnO	Al, Ga, B, In, Y, Sc,V, Si, Ge, Ti, Zr, Hf,//F	⊙	
CdO	In, Sn	⊙	××
In_2O_3	Sn, Ge, Mo, Ti, Zr, Hf, Nb, Ta, W, Te//F	⊙	×
Ga_2O_3	Sn	Δ	
SnO_2	Sb, As, Nb, Ta//F	○	
TiO_2	Nb, Ta	Δ	
Ternary			
$MgIn_2O_4$		Δ	
$GaInO_3$, $(Ga, In)_2O_3$	Sn, Ge	Δ	
$CdSb_2O_6$	Y	Δ	×
$SrTiO_3$	Nb, La	×	
Ternary	Multi-component	Resistivity	Toxicity
$Zn_2In_2O_5$, $Zn_3In_2O_6$	ZnO In_2O_3 system	○	
$In_4Sn_3O_{12}$	In_2O_3 SnO_2 system	○	
$CdIn_2O_4$	CdO In_2O_3 system	○	×
Cd_2SnO_4, $CdSnO_3$	CdO SnO_2 system	○	×
Zn_2SnO_4, $ZnSnO_3$	ZnO SnO_2 system	Δ	
	ZnO In_2O_3 SnO_2 system	○	
	CdO In_2O_3 SnO_2 system	○	×
	ZnO CdO In_2O_3 SnO_2 system	○	×

: ⊙Very good, ○: Good, Δ: Average, ×: Bad, ××: Very bad.

Table 1.1. Host and dopant materials in TCO thin films. Figure reproduced from Reference 26. Copyright 2007 Elsevier Limited.

Thus, doped ZnO, SnO_2, In_2O_3 and multicomponent oxides composed of various combinations of these binary compounds are potential TCOs. The indium-free candidate for an alternative TCO material is impurity- doped ZnO, such as Al:ZnO (AZO) and Ga:ZnO (GZO). There have been several reports of highly transparent AZO and GZO thin films for electrode to replace ITO [21-27]. Table 1.2 summarizes the minimum resistivities and the maximum carrier concentrations obtained for various doped ZnO films reported to date.

Dopant	Doping Content (at.%)	Resistivity (10^{-4} Ω cm)	Carrier Concentration (10^{20} cm^{-3})
Al	1.6–3.2	1.3	15.0
Ga	1.7–6.1	1.2	14.5
B	4.6	2.0	5.4
Y	2.2	7.9	5.8
In	1.2	8.1	3.9
Sc	2.5	3.1	6.7
Si	8.0	4.8	8.8
Ge	1.6	7.4	8.8
Ti	2.0	5.6	6.2
Zr	5.4	5.2	5.5
Hf	4.1	5.5	3.5
F	0.5	4.0	5.0

Table 1.2. Resistivities, Carrier Concentrations, and Dopant Content for ZnO Films Doped with Various Impurities. Figure reproduced from Reference 22. Copyright 2011, Cambridge University Press

Most of them exhibited good optical transmittance but lacked similar electrical properties when compared to ITO. Other examples of reduced indium content TCO materials are the multicomponent oxides such as In_2O_3-SnO_2, ZnO-In_2O_3, and ZnO-In_2O_3-SnO_2 (or Zn-In-Sn-O) [26, 27] Also reported in literature (table 1.3) are ternary compounds such as $Zn_2In_2O_5$ and $Zn_3In_2O_6$ (zinc indates) and $In_4Sn_3O_{12}$ (indium stannate) contained in the ZnO-In_2O_3 and In_2O_3-SnO_2 systems, respectively. However, these materials still lack good opto-electrical properties at room temperature and high temperature is required for dopant activity and hence not suitable for flexible plastic substrates.

TCO	In content [at.%]	Deposition temperature [°C]	Resistivity ρ [Ω cm]
ZnO–In_2O_3	50–80	RT	$2.9–3.5 \times 10^{-4}$
In_2O_3–SnO_2	50–90	RT	$4.5–5.5 \times 10^{-4}$
Zn–In–Sn–O	50–57	RT	$4.5–8.5 \times 10^{-4}$

Table 1.3. Obtainable properties of reduced-indium TCO thin films. Figure reproduced from Reference 38. Copyright 2007 Elsevier Limited

Table 1.3 summarizes a comparison of properties of reduced-indium-content TCO films and ITO. Even though the amount of indium used in these materials can be reduced approximately 50%, the underlying availability problem remains.

1.2.2 Transparent composite electrodes (TCEs)

Recently, insertion of a very thin metal layer sandwiched between the two TCO layers has been studied to develop a transparent composite electrode (TCE) with the desired electrical conductivity [28-33]. These TCEs have several advantages over convention *n*-doped oxide electrodes. The electrical conductivity is significantly improved. Also, high conductivity is attained in the as-deposited condition, thus obviating the need for high temperature processing in order to improve conductivity. This makes the films suitable for deposition on low temperature polymer substrates. The addition of a ductile metal layer also provides improved robustness under mechanical strain [28-33]. The transparent oxide layer deposited on top of the metal layer provides a protective cover from the environment while simultaneously serving as an anti-reflection layer. While traditional transparent conductors provide reasonably high transmittance values but are limited in their conductivity, these transparent oxide-metal-oxide multilayers can simultaneously provide very high transparency and conductivity. Although metals have high reflectivity, very thin films (< 15 nm) shows moderate transmittance in the visible region and the top dielectric layer helps to obtain a higher transparent effect by diminishing the reflection from the metal layer. This

oxide/metal/oxide (OMO) multilayer framework have lower total thickness and more efficient than a single-layer TCO film.

Considering the fact that the metal layer is the main contributing factor in determining the electrical conductivity of the TCO/metal/TCO structures, a glossary of electrical resistivity values are listed in Table 1.4 for bulk materials. Ag has the lowest resistivity of all metals, followed by Cu that has an only slightly higher value, below 2 μΩ-cm for both cases. However, for metal thin films, the transmittance and the sheet resistance highly depends on layer thickness [28-33]. There is a critical thickness below which the optical transmittance is lowered and resistivity increases. At the critical thickness, the metal islands become contiguous and finally form an uniform film with properties that differ considerably from the bulk metal [28].

Metal	Resistivity (μΩ cm) at 20 °C
Ag	1.6
Cu	1.7
Au	2.4
Al	2.8
Mg	4.6
W	5.6
Mo	5.7
Zn	5.8
Ni	7.8
In	8.0
Pt	10.0
Pd	11.0
Sn	11.5
Cr	12.6
Ta	15.5
Ti	39.0

Table 1.4 Electrical resistivity values of several bulk metals. Figure reproduced from Reference 28. Copyright 2011 Elsevier Limited.

In Table 1.5, a brief overview of various transparent composites electrodes had been compiled. It is seen that Ag, Cu and Au had been the most preferred choice of the metal inter layer. Pure silver is commonly used, but some Ag-based alloys including Cu, Au, and Pd in small proportions have also been utilized. The data suggests that sputtering had been the most suitable for this multilayered structure deposition. The advantage with sputtering apart from being a cheap method, is its reproducibility and high order of uniformity. This deposition process can be used easily on glass and flexible plastic substrates.

TCO/metal/TCO description	Substrate	T (%)	Rs (Ω/sq)
ITO 50 nm/Ag 8 nm/ITO 50 nm	Glass	89	15
GIO 40 nm/Ag 8 nm/GIO 40 nm	Glass	92.9	11.3
ITO 37 nm/Ag(PdCu) 8 nm/ITO 37 nm	Glass	89	10
AZO 40 nm/Ag(PdCu) 8 nm/AZO 40 nm	Glass	88	10
ITO 30 nm/Ag 8 nm/ITO 30 nm	PEN	85	6.8
ZnO 57 nm/Ag 9 nm/ZnO 40 nm	Glass	95	7
ITO 35 nm/Ag 10 nm/ITO 35 nm	PET	77	10
ITO 35 nm/Ag 10 nm/ITO 35 nm	Glass	80	9
SnO2 45 nm/Ag 10 nm/ITO 45 nm	Arton	85	7
GZO 30 nm/Ag 10 nm/GZO 40 nm	Glass	90.7	7
ITO 30 nm/Ag 10 nm/ITO 30 nm	Glass	90	6
ITO 40 nm/Ag 10 nm/ITO 40 nm	Glass	87	6
ITO 45 nm/Ag 10 nm/ITO 45 nm	Arton	86	6
AZO 40 nm/Ag 10 nm/AZO 40 nm	PET	85	6
ITO 50 nm/AgCu-alloy 10 nm/ITO 50 nm	Glass	83	5.7
ITO 50 nm/Ag 10 nm/ITO 50 nm	Glass	88	5
ZnO 35 nm/Ag 12 nm/ZnO 35 nm	PET	75	10
GZO 30 nm/Ag 12 nm/GZO 30 nm	PES	87.2	7
IZO 30 nm/Ag 12 nm/IZO 30 nm	PET	84.8	6.9
AZO 40 nm/Ag 12 nm/AZO 40 nm	Glass	82	7
GZO 40 nm/Ag 12 nm/GZO 40 nm	Glass	87	6
ITO 40 nm/Ag 12 nm/ITO 40 nm	PES	89.3	4.3
ITO 50 nm/Ag 14 nm/ITO 50 nm	PET	81	11
ITO 70 nm/Ag 14 nm/ITO 70 nm	PPC	68	6.5
IZTO 30 nm/Ag 14 nm/IZTO 30 nm	PET	86	5
IZO 40 nm/Ag 14 nm/IZO 40 nm	Glass	87.7	4.2
ITO 40 nm/Ag 15 nm/ITO 40 nm	Glass	85	4.2
ITO 42 nm/Ag 15 nm/ITO 42 nm	Glass	85	3.3
ITO 43 nm/Ag 16 nm/ITO 43 nm	Glass	79.4	8.9
ITO 40 nm/Ag 16 nm/ITO 40 nm	Glass	86.5	4.4
ITO 50 nm/Ag 17 nm/ITO 50 nm	PET	83.2	6.7
ITO 54 nm/Ag 20 nm/ITO 54 nm	Glass	75	3.5
ZnO 50 nm/Cu 5 nm/ZnO 50 nm	Glass	83	10
ZnO 30 nm/Cu 6 nm/ZnO 30 nm	PEN	88	10
AZO 40 nm/Cu 8 nm/AZO 40 nm	Glass	84	9
ITO 40 nm/Cu 14 nm/ITO 40 nm	Glass	69	6
ITO 30 nm/Cu 16 nm/ITO 30 nm	Glass	88	6
AZO 50 nm/Au 9 nm/AZO 50 nm	Glass	83	12
ITO 50 nm/Au 10 nm/ITO 40 nm	PC	72	5.6
IZO 40 nm/Au 12 nm/IZO 40 nm	Glass	81.0	5.5

Table 1.5 Optical transmittance (T) and sheet resistance (Rs) values reported for several TCEs. Figure reproduced from Reference 28. Copyright 2011 Elsevier Limited.

1.3 FLEXIBLE SUBSTRATE

The use of flexible substrate has attracted increasing research interest in various flexible electronic devices like foldable electronic displays, sensors, solar cells, medical device, deployable spacecraft structures, and even smart clothing for defense applications. The advantage with plastic substrate is that unlike glass, it has lighter weight, usually more robust and compact, and more cost effective. The most popular plastic substrates used for flexible displays include polycarbonate (PC), polyethylene terepthalate (PET), polyethylene napthalate (PEN), polyethersulfone (PES), and polyimide (PI) [1-5, 28-30]. The use of plastic substrates also enables cheap, highly efficient and high volume manufacture capabilities by using roll-to-roll processing. Although it is a very promising new technology, these polymer substrates are limited by either low processing temperature, average transparency, high gas permeability, low chemical resistance and average solvent durability. Furthermore, plastic substrates have drawbacks such as low thermal resistance and high thermal expansion that are critical during device fabrication. The ideal substrate for flexible display should have the dual combination of thermal and scratch resistant properties of glass along with the flexibility, robustness and low-cost processability of plastic. Table 1.6 shows a summary of the properties and maximum processing temperatures of the most common plastic substrates.

Plastic materials	**Maximum process temperature (^{o} C)**	**Properties**
Polyethylene terepthalate (PET)	120	Clear, moderate CTE, good chemical resistance, lowest cost
Polyethylene napthalate (PEN)	150	Clear, moderate CTE, good chemical resistance, inexpensive
Polycarbonate (PC)	155	Clear, good dimensional stability, poor solvent resistance, expensive
Polyethersulfone (PES)	230	Clear, good dimensional stability, poor solvent resistance, expensive
Polyimide (PI)	275	Orange color, high CTE, good chemical resistance, expensive

Table 1.6. Processing temperatures and properties of flexible substrates.

1.4 APPLICATIONS

1.4.1 Organic solar cells

Organic solar cells (OSCs) have recently attracted considerable interest for use in the next generation of renewable energy sources due to their simple cell structure, simple process, low cost, and possibility of continuous roll-to-roll process in the atmosphere [1-5, 28]. Interest in organic solar cells arises primarily from the potential of ease of processing, thus providing low cost and large area production based on continuous roll-to-roll coating. The power conversion efficiency has improved steadily through the use of new materials and novel structures. Therefore, it is imperative to develop cheap transparent electrode materials, which can be processed at the lowest possible temperature. However, most OSCs reported so far are usually fabricated on polycrystalline indium tin oxide (ITO) electrodes. Apart from ITO being scarce and costly, also it showed poor electrical conductivity below 300 ^{o} C. Thus indium free transparent electrodes have been explored as potential alternatives.

1.4.2 OLEDs and flat panel displays

Organic light-emitting diode (OLED) is an optoelectronic device which emits light due to the electroluminescence of thin films of organic semiconductors. OLEDs can be potentially used to make digital displays in devices such as computer monitors, television screens and also in portable systems such as mobile phones and personal digital assistants (PDAs) [1-5, 25-30]. A lot of present research is the development of white OLED devices for use in solid-state lighting applications. Flexible OLEDs are developed on flexible substrates and are light weight and bendable. Organic light-

emitting devices are ideal for flat panel display applications due to their full color gamut and thin form factor. Fabrication of OLED devices with dielectric-metal-dielectric based transparent composite electrodes showed significant improvements in the performance of these devices [28]. TCEs provide lower ohmic losses in the anode which are especially advantageous for high-brightness and passive-matrix displays. Dielectric-metal-dielectric structures show promise for use as a transparent composite electrode in flexible displays. They provide significantly better electrical conductivity compared to most commonly used ITO, and improved bending properties.

1.4.3 Transparent heat mirrors

Transparent heat mirrors are thin films with high transmittance in the visible range and high reflectance in the near infrared to IR range. They have potentially several important applications in solar/thermal/electric conversion, solar heating, solar photovoltaic conversion, and window insulation [1-5]. Thus the conjugate combination of visible transmission and IR reflectivity suggested the potential use of transparent heat mirrors as wavelength selective coatings to increase the efficiency of solar-energy collection. Transparent heat-reflective films can be of two types: (1) single-layer films of wide band gap highly degenerated semiconductors, *e.g.,* ITO, SnO_2, and ZnO; (2) multilayer films consisting of oxide layers with a thin metal layers, *e.g.,* Metal oxide/M/Metal Oxide. It was studied that the multilayer transparent heat-reflective thin films showed higher reflectance in the far-infrared region than single layered films.

1.5 THESIS ORGANIZATION

This chapter has given an introduction to and some motivation for the research on transparent conductive oxides (TCO) and finally the impetus to move to a multilayered transparent composite electrode (TCEs). Here, we discussed on the background of various ongoing research on TCOs and TCEs and also on the importance of flexible substrates for next generation flexible electronics.

Chapter 2 focuses on the optimization of a mixed oxide – Indium gallium zinc oxide (IGZO) on both glass and flexible PEN substrates. The effect of thickness and annealing on the structural, optical and electrical properties of IGZO had been studied in details. The wettability of the IGZO thin film was also analyzed.

Chapter 3 discusses the improved processing of the above mixed oxide IGZO thin films for superior optical and electrical properties. The study focuses on two different methods of post-deposition annealing- microwave and conventional. The microwave annealing was seen to have the dual advantage of reduced time and lower temperature, as compared to conventional annealing.

Chapter 4 presents an indium free transparent composite electrode. This dielectric/metal/dielectric multilayered structure can exhibit better electrical and optical properties than a single layered TCO thin film. The research started with using Nb_2O_5 as the metal oxide and inserting a very thin film of Ag between the two layers. The research focuses on the detailed structure-property relationship with increase in Ag thickness. The optimized TCE showed sheet resistance of 7.2 Ω/sq and an average optical transmittance of 86 % at 550 nm.

Chapter 5 discusses on the post-deposition annealing of the above mentioned $Nb_2O_5/Ag/Nb_2O_5$ TCE for improved opto-electrical properties. The samples were annealed upto 150 ^oC in various environments like air, O_2, vacuum and forming gas.

Chapter 6 focuses on the same TCE structure with a very cheap material like TiO_2 as a low cost alternative to ITO. The multilayer stack has been optimized to have sheet resistance of 5.7ohm/sq and an average optical transmittance of 86 % at 550 nm. The multilayer with mid Ag thickness 9.5 nm has the best figure of merit with 61.4 x 10^{-3} Ω^{-1}.

Chapters 7 and 8 are on the effect of different inter metal layers (Cu and Au) on the structural, optical and electrical properties of TiO_2/metal/TiO_2. Although the resistivity of bulk Cu is lower than Au, the optical transmittance of the Cu-based TCEs is lower compared to Au. As a result, The FOM of Au based TCE was higher than that of Cu.

Finally, Chapter 9 presents the conclusion and proposed future work

CHAPTER 2

INFLUENCE OF FILM THICKNESS AND ANNEALING ON THE ELECTRO-OPTICAL PROPERTIES AND WETTABILITY OF INDIUM GALLIUM ZINC OXIDE (IGZO) THIN FILMS

2.1. INTRODUCTION

In recent years, high quality transparent conductive oxide (TCOs) thin films substrates are highly demanded for large scale optoelectronic applications such as flat panel displays, image sensors, electro chromic devices, organic light-emitting diodes (OLEDs) and photovoltaic devices applications [1-4]. TCOs have been the topic of many studies due to their high visible transparency and electrical conduction, which make them useful in various applications. Till date, Indium tin oxide (ITO) is the most popular electrode in optoelectronics industry. Recently, a lot of scientific research and commercial attention has been focused on new materials replacing ITO due to its high cost of fabrication and lack of low temperature dopant activation [5-6]. Potentials TCOs can be zinc-oxide (ZnO), gallium zinc oxide (GZO), aluminum zinc oxide (AZO), indium zinc oxide (IZO), indium gallium zinc oxide (IGZO) or metal oxide/metal/metal oxide multilayer structures using TiO_2, SnO_2, Nb_2O_5 *etc* [7-14]. Among them, IGZO is a new prospective material for its application as transparent electrode. The deposition processes of IGZO films include a variety of methods such as evaporation, sputtering, e-

beam and the sol-gel process. However, sputtering is the most desirable method due to high uniformity, good reproducibility and thus cheap process.

In the present work, we report the effect of thickness on the electrical and optical properties of IGZO thin films deposited on glass by RF sputtering. We also examined the effects of annealing to understand the thermal stability and wettability because it is significant in the device fabrication processes

2.2. EXPERIMENTAL DETAILS

The IGZO thin films of different thickness were deposited onto glass substrates at room temperature by RF sputtering of IGZO target (99.999% purity, 5.08 cm diameter and 0.64 cm thickness). Prior to the deposition, the glass substrates were ultrasonically cleaned in isopropyl alcohol and acetone, respectively and subsequently dried in N_2 gas. The base pressure of the sputter system prior to each deposition was approximately 1×10^{-7} Torr. The deposition was performed at a pressure of 10 mTorr and RF power of 100 W for IGZO in pure Ar gas (99.999%) without any vacuum break. The distance between the substrate and the target was maintained same at 6 cm for all the depositions. The sputtering target used in this study was pre-sputtered for 10 min prior to growth. The deposition time was varied between 3 to 15 minutes to achieve different thicknesses of IGZO thin film. Post-deposition, the thin films were subsequently annealed in air, forming gas (H_2/N_2), oxygen and vacuum at different temperatures upto 400 ^{o}C for 24 hours.

The IGZO film thicknesses were measured using variable angle spectroscopic ellipsometry (VASE) analysis. Sheet resistance was measured using four-point-probe technique equipped with a 100 mA Keithley 2700 digital multimeter. Hall measurements were done using an Ecopia HMS3000 tool by means of the Van der Pauw method at a constant magnetic field of 0.98 T applied perpendicular to the sample surface. The optical transmittance of the IGZO films was measured using an Ocean Optics double channel spectrometer (model DS200) in the wavelength range of 300–800 nm. Air was used as the reference for transmittance. The sources for visible and UV light were tungsten halogen and deuterium lamps, respectively. Surface topography was evaluated using atomic force microscopy (AFM) in acoustic mode (tapping mode), using a Molecular Imaging Pico scanning probe microscope system. The measurement of water contact angle was performed by a Kruss Easy Drop contact angle measurement system at ambient temperature. Double distilled de-ionized water (Millipore, MilliQ, USA) droplets with volume of ~2 µl were dropped onto the surface of all the IGZO films and the contact angle was recorded by the video window of DSA software.

2.3. RESULTS AND DISCUSSIONS

A systematic investigation was done in order to determine the effect of thickness and post-deposition anneal on the electrical and optical properties of IGZO thin films.

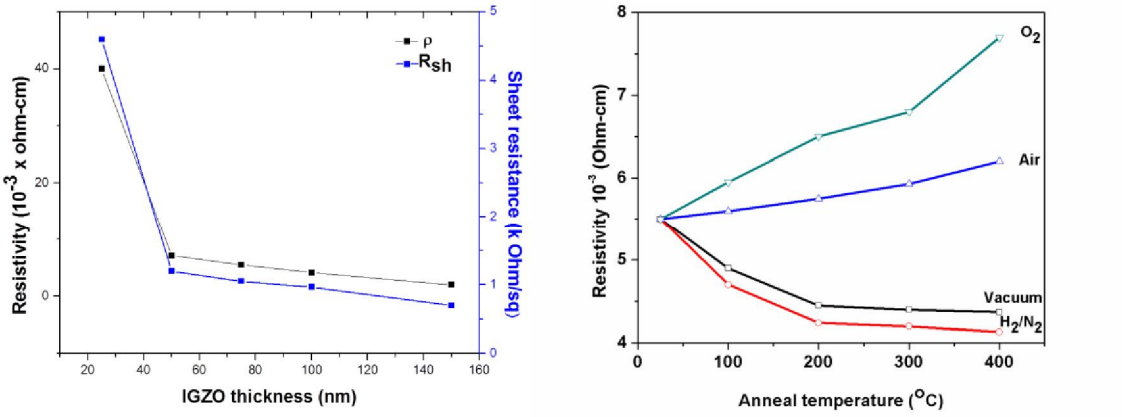

Fig.2.1. (a) Effect of IGZO thickness on resistivity and sheet resistance. (b) Resistivity of annealed IGZO thin films in different ambients.

Fig. 2.1(a) shows the effect of different thickness of as-deposited IGZO thin film on the electrical resistivity and sheet resistance. It was seen that both the resistivity and sheet resistance follows a similar tend with an initial sharp decrease in value followed by a gradual one. The resistivity dropped significantly from 5.5 x 10^{-3} Ω-cm to 5.5 x 10^{-3} Ω-cm with the increase in thickness from 25 nm to 50 nm. Thereafter, the resistivity of the IGZO thin film showed a gradual decrease to 5.5 x 10^{-3} Ω-cm till the thickness reaches to 150 nm. The sheet resistance also had a stiff drop from 4.6 K Ω of 25 nm IGZO film to 1.2 K Ω of a 50 nm thick film. Then it slowly decreases to 70 Ω at 150 nm. Figure 2.1(b) shows a graphical representation of the effect of thermal annealing of IGZO thin films in different ambients. The plot clearly indicates that with the increase in annealing temperature, the resistivity gradually decrease in vacuum and forming gas. However, it is seen to increase in O_2 and air atmosphere. Also, the increase is far more pronounced in only O_2 than air (~ 21% O_2 content). A possible explanation is that annealing in vacuum and forming gas creates more vacancies and thus improves the

conductivity of the thin films; whereas in case of air and O_2, the same vacancies are annihilated [26]. Also, vacuum and forming gas removes the adsorbed O_2 on the surface of the IGZO thin film and thus improves the electrical properties of the film [27].

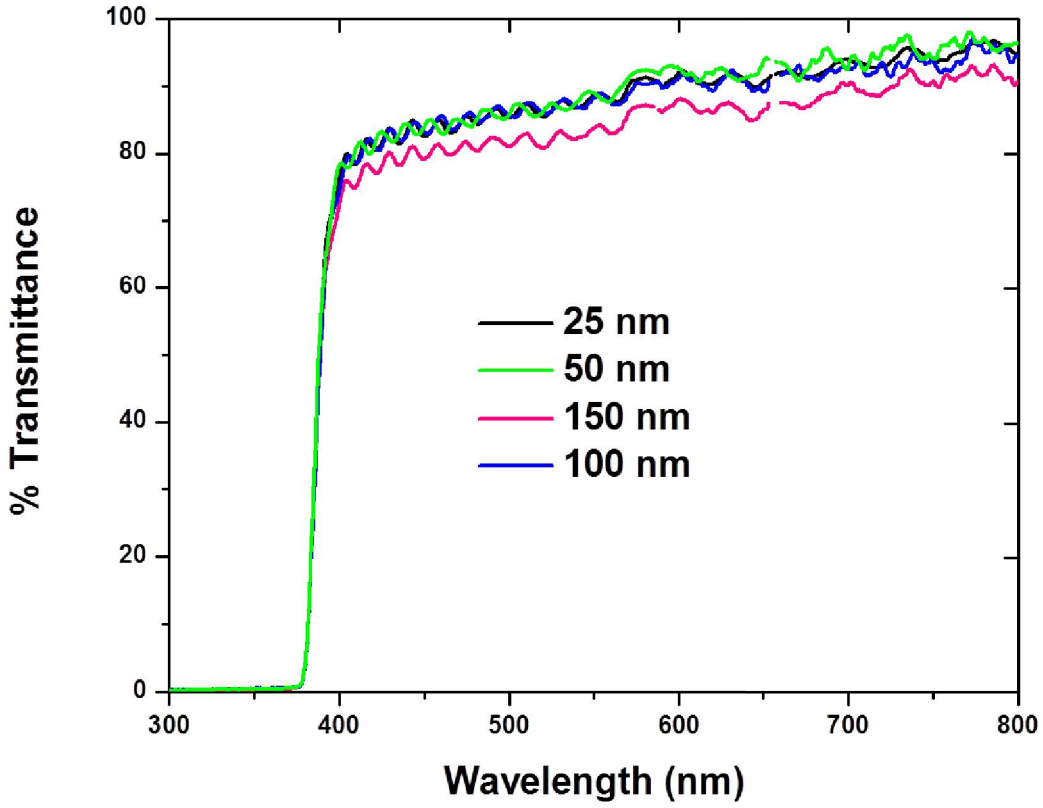

Fig.2.2 Optical transmittance spectra of various thickness of IGZO thin films

Figure 2.2 shows optical transmittance spectra of IGZO thin films for various thicknesses ranging from 25 nm to 150 nm on glass substrate. The average optical transmittances of IGZO films grown on glass substrates are around 80% in the visible region. The plot clearly suggests that with increasing film thickness, the transmittance gradually decreases and the transmittance edge shifts in the near infrared region. This can

be explained due to Plasmon excitation where the plasmon frequency (ω_p) can be expressed from Drude-Lorentz theory by the following equation [24-25]:

$$\omega_p = \sqrt{\frac{ne^2}{m\varepsilon_0}} \tag{2.1}$$

As thickness increases from 25 nm to 150 nm, the average transmittance of IGZO film in the visible region (wavelength from 300 nm to 800 nm) decreased from 91.3% to 85.2%. It is clear that the transparency in this range is determined by the surface morphology and structure of the IGZO film. As the film thickness, the surface scattering is slightly enhanced due to increase in surface roughness increases which resulted in a slight drop of the optical transparency in the visible range.

An AFM study on the surface roughness of the various IGZO thin films showed that the as-deposited sample has fairly high roughness and the roughness decreases gradually from *rms* value of 12 nm to 2.7 nm with the increase in anneal temperature upto 400 ^{o}C.

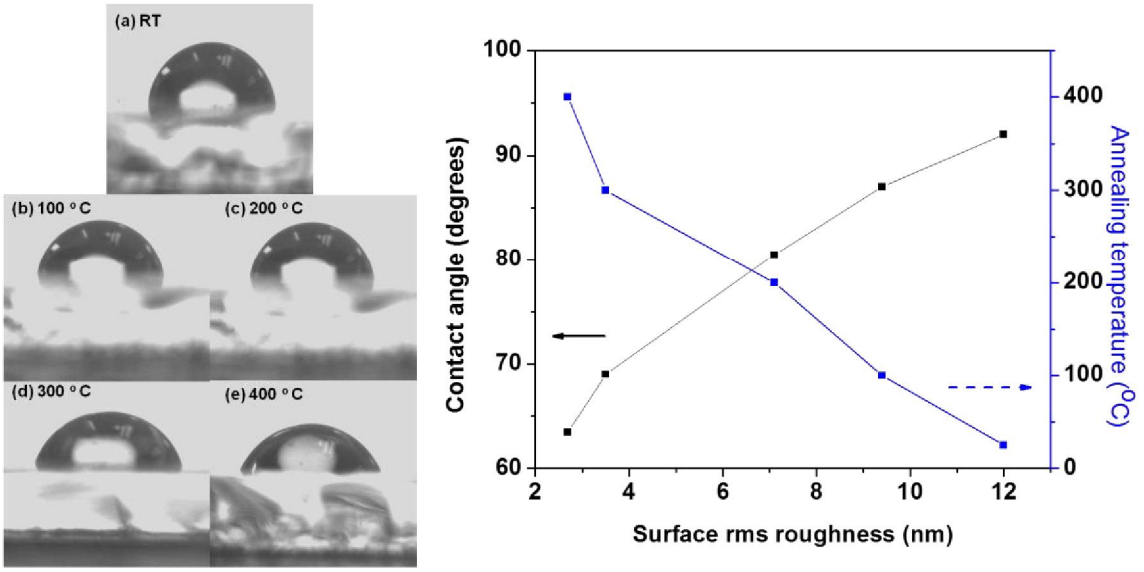

Fig.2.3. (a) Contact angle measurement of IGZO thin films annealed at different temperatures. (b) Comparative plot of contact angle and annealing with surface roughness

Figure 2.3. (a) shows the typical drop shape of a 2 µl droplet on the surface of as-deposited and annealed IGZO thin films. The wettability of the IGZO thin film surfaces was determined by the water contact angle measurement. Wetting deals with the three phases of materials: solid, liquid and gas. The degree of wetting (wettability) is determined by an intermolecular force when liquid comes in contact with a solid surface. The contact angle of as deposited film was around 92° against water and thus showed hydrophobic behavior. As the annealing temperature increased from room temperature to 400 ^{o} C, the contact angle decrease from 92^{o} to 63.5^{o} and thereby exhibit hydrophilic behavior. Thus, a gradual decrease in the contact angle was observed with increase in annealing temperature. The hydrophobic behavior of the un-annealed film actually mimics the “lotus effect” where the liquid drop on lotus leaf has high air pockets and solid asperities and thereby exhibits super hydrophobicity. In this case, due to high

surface roughness over the as deposited film, fraction of solid area in contact with the water drop is very low. As a result, the drop is in minimal contact on the solid surface which can be explained on the basis of Cassie–Baxter model. However, it was seen that annealing at high temperature tend to smoothen the surface and thus the contact angle gradually decreased exhibiting hydrophilic behavior as predicted by Wenzel model of homogenous wetting.

A figure of merit (FOM), $^{\varphi}_{TC,}$ (as defined by Haacke [27]) was estimated for each of the IGZO thin films using the following relationship:

$$\varphi_{TC} = \frac{T_{av}^{10}}{R_{sh}} \tag{2.2}$$

Where, T_{av} is the average transmittance and R_{sh} is the sheet resistance.

The 10 nm IGZO film showed the best FOM value of 20.3 x 10^{-4} Ω^{-1}. The annealed films show an improved FOM from 20.3 x 10^{-4} Ω^{-1} to 36.4 x 10^{-4} Ω^{-1} when compared to the as deposited sample. Also, the FOM is seen to improve in case of in vacuum and forming gas anneals in accordance to the improvement in both optical and electrical properties (as seen in Figures 2.2 and 2.3). The enhancement is however more in case of forming gas owing to better electrical properties and similar average transmittance compared to vacuum. However in O_2 and air ambients, the FOM actually decreases due to increase in sheet resistance with non-significant improvement in the optical properties.

2.4. CONCLUSION

A superior quality transparent conductive thin film of indium gallium zinc ozide (IGZO) was deposited and optimized onto glass substrates by RF sputtering at room temperature. The influence of film thickness and post-deposition annealing on the structural, optical and electrical properties was studied. The film thickness was optimized at 100 ^{o}C and the TCO showed improved optical and electrical properties at 400 ^{o}C in vacuum and forming gas. The 100 nm thick film had the best Haacke figure of merit (FOM) value of 20.3 x 10^{-4} Ω^{-1} and the FOM decreases to 36.4 x 10^{-4} Ω^{-1} in case of forming gas due to improved electrical properties. The wettability of both as-deposited and annealed thin films had been studied by contact angle measurements. The un-annealed IGZO film exhibited hydrophobic behavior while the annealed films were distinctly hydrophilic with contact angle of around 63.5° against water. Surface morphology appears to be the dominant controlling factor in wetting the thin film and efficiently controlled by post-deposition annealing. Thus IGZO can be used as a promising TCO in future opto-electronics applications.

CHAPTER 3

CONTROLLED MICROWAVE PROCESSING OF IGZO THIN FILMS FOR IMPROVED OPTICAL AND ELECTRICAL PROPERTIES

3.1. INTRODUCTION

In recent years, transparent conductive oxides (TCOs) have attracted sufficient amount of attention due to the high demand for optoelectronic devices such as solar cells, light emitting diodes (LEDs) and organic light-emitting diodes (OLEDs) [1-2]. Currently, indium tin oxide (ITO) is the most commonly used TCO material due to high electrical conductivity and high optical transparency in the visible region (~80%) [3]. However, ITO has several limitations. Notably, its lack of good electrical properties at room temperature and low supply of Indium makes it very expensive. Hence, the cost of ITO fabrication is very high.

In contrast to the disadvantages of ITO, several investigations had been done on various metal oxides like zinc-oxide (ZnO), gallium zinc oxide (GZO), aluminum zinc oxide (AZO), indium zinc oxide (IZO), indium gallium zinc oxide (IGZO), TiO_2, SnO_2, Nb_2O_5 *etc* [3-14]. These compounds are better alternatives due to their low toxicity, high carrier mobility, excellent environmental stability and superior chemical selectivity. Among them, IGZO is a new prospective material used as TCO on optoelectronic devices due to its high transmittance, low processing temperature and excellent surface smoothness [15-17]. However, the electrical resistivity of IGZO is still high for its

application as transparent electrode. To decrease the electrical resistivity of IGZO, several studies have been conducted to investigate the relationship between stoichiometry and electrical properties or controlling deposition parameters [15-19]. However, little attention has been paid on the influence of post-deposition processing parameters on optical, and electrical properties of IGZO [19-22]. Among the various deposition methods developed to prepare the IGZO films, sputtering is the most preferable process, because it allows uniform large area deposition, reproducible and easy process control [18]. In this paper, a detailed study on the optical and electrical properties of annealed IGZO thin films in different environments had been discussed. The results had been subsequently compared with microwave and conventional annealing to demonstrate lower temperature and less annealing time required in case of the former. Microwave annealing had emerged as an improved and controlled processing tool in recent years due to its rapid, volumetric heating and environment friendly [23-26]

3.2. EXPERIMENTAL DETAILS

The IGZO thin film were sputter deposited at room temperature onto glass substrate in a RF magnetron sputter deposition system. A sputter ceramic target of pure IGZO (99.999% purity, 5.08 cm diameter and 0.64 cm thickness) was used to deposit the oxide layer. The glass substrate was ultrasonically cleaned in isopropanol and acetone and subsequently dried before deposition.

The sputtering was performed in pure argon atmosphere (99.999%) at a pressure of 10 mTorr RF power of 100 W for IGZO without any vacuum break. The thickness of

the IGZO thin films were approximately 100 nm as measured by optical ellipsometry. Hall measurements were done using a Ecopia HMS3000 tool by means of the Van der Pauw method. A magnetic field of 0.98 T was applied perpendicular to the sample surface. Four-point-probe technique was used for sheet resistance measurements. Optical transmittance of the multilayers were measured using an Ocean Optics double channel UV-Vis spectrometer (model DS200) in the wavelength range of 300–800 nm with air reference for transmittance.

The films were subsequently annealed by conventional methods in air, forming gas (H_2/N_2), oxygen and vacuum at different temperatures for 24 hours. A microwave oven was used for the microwave annealing. The system used single frequency 2.45 GHz microwaves generated by a 1200 W magnetron source. The IGZO samples were encapsulated in a quartz tube filled with different gas environments during the microwave anneals.

3.3. RESULTS AND DISCUSSION

A systematic investigation was done in order to determine the effect of anneal parameters on the electrical and optical properties of IGZO thin films in different environments. Hall measurements and four point probe data shows that the electrical resistivity and sheet resistance of the 100 nm thick un-annealed IGZO thin film is 5.5 x 10^{-3} Ω-cm and 1047 Ω/sq, respectively. The films were subsequently annealed in air,

forming gas (H_2/N_2), oxygen and vacuum at different temperatures upto 500 ^{o} C for 24 hours and the results are summarized in the following Table 3.1.

Temperature	**Resistivity 10^{-3} (ohm-cm)**				**Sheet Resistance (ohm/sq)**			
(^{o}C)	**Vacuum**	**Forming**	**Air**	**O_2**	**Vacuum**	**Forming**	**Air**	**O_2**
25	5.5	5.5	5.5	5.5	1047	1047	1047	1047
100	5.3	5.1	5.4	6.3	976	914	1007	1174
200	4.9	4.7	5.5	6.8	922	837	1092	1252
300	4.65	4.4	5.6	6.95	794	616	1173	1315
400	4.5	4.2	6.1	7.9	657	532	1296	1376
500	5.8	5.6	6.4	8.4	1023	1015	1472	1739

Table 3.1. Resistivity and sheet resistance data of thermal annealed IGZO thin films.

From the above Table 3.1, it can be concluded that the IGZO films showed superior electrical properties on annealing in vacuum and forming gas. However, it exhibit inferior electrical behavior in air and O_2. The other important observation was that in case of forming gas and vacuum, both the resistivity and sheet resistance data decreased gradually with the increase in annealing temperature from room temperature to 400 ^{o} C but showed a sharp increase at 500 ^{o} C. The possible reason can be the damage of the IGZO thin films at such a high temperature. A similar comparative table (Table 3.2) for microwave annealing of the same IGZO samples in different annealing environments.

Figure3.1. shows a graphical representation of the effect of microwave annealing of IGZO thin films in different ambients as mentioned in Table 3.2. The plot clearly suggests that with the increase in annealing temperature, the resistivity gradually decrease

in vacuum and forming gas. However, the opposite trend is seen in case of air and O_2 atmosphere. The result can explained by the fact that annealing in vacuum and forming gas creates more vacancies and thus improves the conductivity of the thin films; whereas in case of air and O_2, vacancies are annihilated [26]. Also, vacuum and forming gas removes the adsorbed O_2 on the surface of the IGZO thin film. [27]

Temperature (^{o} C)	**Resistivity 10^{-3} (ohm-cm)**				**Sheet Resistance (ohm/sq)**			
	Vacuum	**Forming**	**Air**	**O_2**	**Vacuum**	**Forming**	**Air**	**O_2**
25	5.5	5.5	5.5	5.5	1047	1047	1047	1047
100	4.9	4.7	5.6	5.95	877	843	1025	1290
200	4.45	4.24	5.75	6.5	661	537	1134	1376
300	4.4	4.2	5.93	6.8	658	522	1216	1454
400	4.37	4.13	6.2	7.7	653	526	1315	1517
500	5.55	5.4	6.5	8.7	944	916	1532	1790

Table 3.2. Resistivity and sheet resistance data of microwave annealed IGZO thin films.

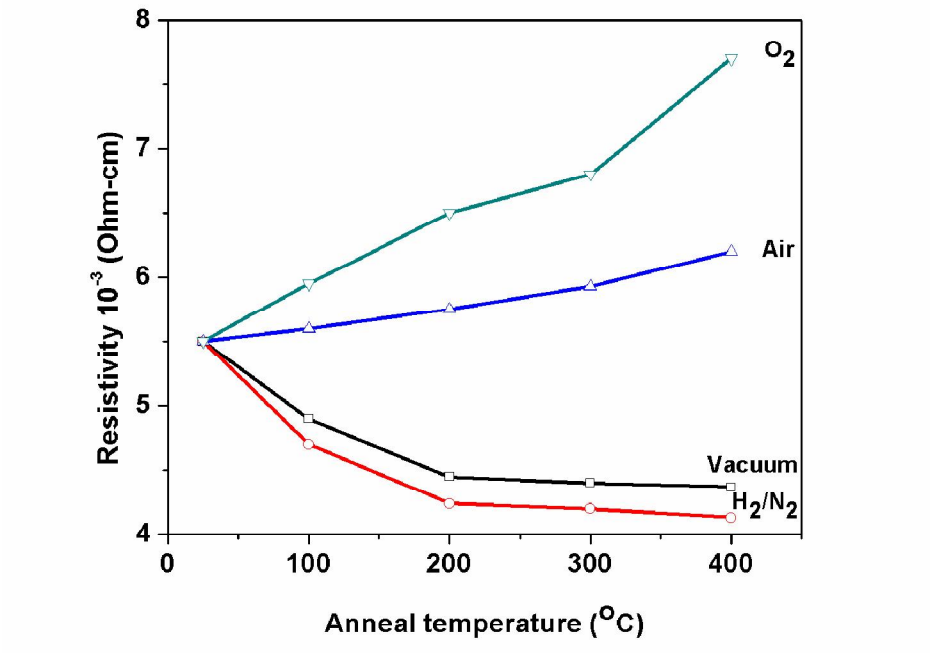

Fig.3.1. Resistivity of microwave annealed IGZO thin films in different ambient.

Figure 3.2 shows the comparative plots of resistivity with annealing time by conventional and microwave annealing, respectively. The IGZO films are annealed only in vacuum and forming gas (H_2/N_2) as these two environment showed superior electrical properties (Table. 3.1). While both anneals show a steady decrease in resistivity, the advantage with the microwave anneal is the lower temperature and a much reduced time. Due to the volumetric heating of the microwave, it is possible to attain 200 ^{o}C and 400 ^{o}C in just 4 and 7 minutes, respectively. Also, in 4 minutes at 200 ^{o}C, the resistivity of IGZO thin films after microwave annealing was lowered to 4.45 and 4.24 x 10^{-3} ohm-cm in vacuum and forming gas, respectively. However in conventional annealing at 400 ^{o}C, it took 24 hours to reach 4.5 and 4.2 x 10^{-3} ohm-cm in vacuum and forming gas, respectively. Also, in microwave annealing at 400 ^{o}C, the resistivity was further lowered to 4.4 and 4.1 x 10^{-3} ohm-cm in vacuum and forming gas, respectively.

Thus there is a dual advantage with microwave annealing in terms of both low temperature and reduced time.

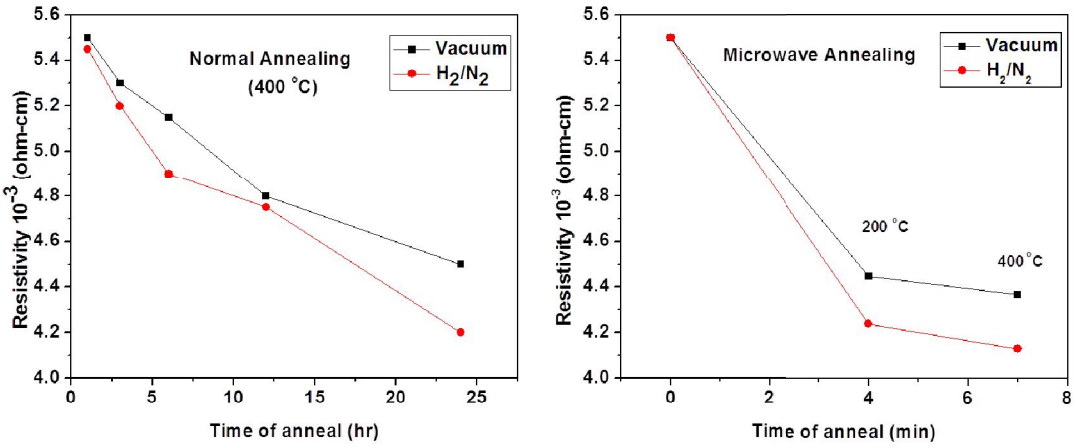

Fig.3.2. Comparative plot of resistivity for different methods of annealing- Normal and microwave.

Figures 3.3 show optical transmittance spectra for the as-deposited and annealed IGZO thin films on glass substrate. Figure 3.3(a) shows an improvement in optical transmittance when annealed in vacuum and forming gas but no significant change was observed on annealing in air and O_2. This can be explained on the basis of improved refractive indices with increase in annealing temperature. The refractive indexed also increased due to better packing density of grains and higher oxygen vacancies in the samples for vacuum and forming gas anneals [28]. The optical spectra clearly suggest a significant improvement in optical transmittance for the microwave anneal when compared to a conventional anneal. The optical transmittance of IGZO improves from 80% to almost 86% for the microwave anneal demonstrating the better volumetric heating of microwave annealing as shown in Fig. 3.3 (b).

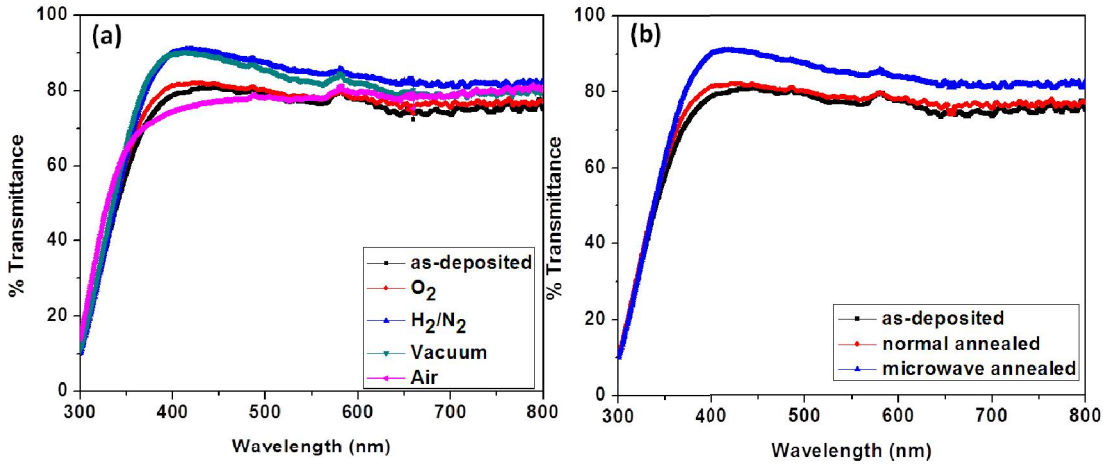

Fig.3.3. Optical transmittance spectra of IGZO thin films (400 ^{o} C): (a) microwave annealed in different atmospheres; (b) comparison between as-deposited and annealed samples.

A figure of merit (FOM), $\varphi_{TC,}$ (as defined by Haacke [29]) can be estimated to determine the performance of the IGZO thin films using the following relationship:

$$\varphi_{TC} = \frac{T_{av}^{10}}{R_{sh}} \tag{3.1}$$

where, T_{av} is the average transmittance and R_{sh} is the sheet resistance.

The IGZO thin films on microwave annealing show an improved FOM from 7.6 x 10^{-4} Ω^{-1} to 16.4 x 10^{-4} Ω^{-1} when compared to the normal anneal. Figures 3.2 and 3.3 suggest an improvement in both optical and electrical properties of the IGZO thin films when annealed in vacuum and forming gas, respectively; and thus improving the FOM. However in air and O_2 ambients, the FOM decreases due to decrease in sheet resistance with no significant improvement in the optical transmittance.

3.4. CONCLUSION

The IGZO thin films of 100 nm thickness were annealed in air, vacuum, forming gas and O_2 environments at different temperatures by both conventional and microwave methods. The microwave annealing showed improved optical and electrical properties in reduced time and lower temperature. Annealing in vacuum and forming gas resulted in better optical and electrical properties than in air and O_2. Thus microwave annealing can be used as an important tool for future materials and device processing.

CHAPTER 4

OPTIMIZATION OF Nb_2O_5/Ag/Nb_2O_5 MULTILAYERS AS TRANSPARENT COMPOSITE ELECTRODE ON FLEXIBLE SUBSTRATE WITH HIGH FIGURE OF MERIT

Flexible and transparent composite electrodes (TCE) have recently attracted a sufficient amount of attention due to rapid advances in flexible optoelectronics such as organic photovoltaics (OPV), flat panels and flexible organic light emitting diodes (OLEDs) for use as new generation displays[1-3]. TCEs that are fabricated on flexible substrates are important due to their ability to flex, robustness, light weight, curve, roll and fold for portability. Because the performances of flexible optoelectronic are critically affected by the electrode quality, it is important to develop high-quality flexible TCEs with low resistivity and high transparency as well as superior flexibility. Transparent conductive oxides (TCO) are widely used as electrode on OPVs or OLED devices. The TCO most commonly used for transparent electrodes in optoelectronic applications [4-5] is indium tin oxide [6-7] (ITO) due to its low resistivity (~ 10^{-4} Ω-cm), high transmittance (~ 80 %), and fabrication maturity. However, a-ITO film deposited on flexible substrates generally shows a fairly high resistivity due to limitations of process temperature and difficulty of dopant activation at temperatures below 300 ^{o}C. Also, the limited supply of indium and the growing demand for ITO make the resulting fabrication costs prohibitive for future applications. Thus, cost factors have promoted the search for inexpensive materials with good electric-optical properties. For these reasons, some

potential alternative materials such as pure zinc oxide (ZnO) or ZnO doped with metals [8-10] (*i.e* aluminum (Al), gallium (Ga), indium(In) *etc*) have been suggested as promising alternatives to flexible a-ITO electrodes. Another promising candidate is oxide/metal/oxide (OMO) multilayer [11-13] due to their low sheet resistances, high transparencies and flexibility because the dielectric/metal/dielectric multilayer system can suppress the reflection from the metal layer and obtain a higher transparent effect. These structures have lower overall thickness than a single-layer TCO film. Amongst metals, Ag is a good candidate for such multilayer films because of its low resistivity. Several advantages of transparent conductive multilayer films, with relatively lower thicknesses, have been reported over single layered TCO films [14]. The optical and electrical properties of the multilayer stack depend considerably on the thickness and deposition conditions of the Ag mid-layer. The Ag layer should be thin, uniform and continuous for high transmittance and low resistivity. ZnO is currently being investigated as a potential replacement for ITO. Other wide band gap metal oxides that had been studied as TCOs are TiO_2, MoO_3, SnO_2, Nb_2O_5 *etc*. The addition of a thin metal layer in the middle will decrease the effective resistivity of the multilayer without much loss in optical transmittance. Niobium oxides find a variety of applications in modern technology in different components ranging from optoelectronics, capacitors, oxygen sensors and as corrosion resistant material [15-17]. Apart from this, niobium oxide films are used as high refractive index layers in optical interference filters which consist of a multilayer stack of high and low refractive index materials. Among the different stoichiometries of niobium oxide, niobium pentoxide (Nb_2O_5) [15-17] is thermodynamically most stable. Nb_2O_5 dielectric film has a high transparency in the wavelength range from 380 nm to

900 nm. The Nb_2O_5 coatings show excellent chemical stability and corrosion resistance in both acidic and alkaline medium. It is chemically and thermally stable under hydrogen plasma processes that are commonly used for the production of solar cells.

In this work, the high transparency of Nb_2O_5 in visible region and low resistivity of thin Ag layer lead us to the detailed study of optical and electrical properties of Nb_2O_5/Ag/Nb_2O_5 (NAN) multilayers. The multilayers transparent conductive electrode have been deposited onto flexible substrates by sputtering at room temperature. The performance of this system has been evaluated using a figure of merit (FOM). The critical thickness of Ag to form a continuous conducting layer is found to be 9.5 nm based on electrical and optical analysis. A new conduction mechanism had been proposed before and after the critical thickness to explain the island growth mechanism of the Ag middle layer. Below the critical thickness, the NAN multilayer shows semiconductor behavior while metallic conduction was seen after the critical thickness.

4.2. EXPERIMENTAL DETAILS

The Nb_2O_5/Ag/Nb_2O_5 (NAN) multilayer thin films were deposited onto flexible Polyethylene naphthalate (PEN), glass and Si substrates by rf sputtering of Nb_2O_5 target (99.999 % purity) and dc sputtering of pure Ag target (99.99 % purity) at room temperature. PEN polymer substrates of 125 μm thickness (Dupont Teijin Films, Teonex® Q65) were used. The base pressure of the sputter system prior to each deposition was approximately $1x10^{-7}$ Torr. The deposition was performed at a pressure of 20 mTorr for Nb_2O_5 and 10 mTorr for Ag in pure Ar gas (99.999%). The Nb_2O_5 and

Ag were deposited using an rf power of 150 W and dc power of 40 W, respectively. The target-to-substrate distance was 6 cm and was maintained same for all the depositions. The deposition time for the top and bottom Nb_2O_5 layers was kept constant while Ag deposition time was varied between 24s and 64s. Bare Nb_2O_5 layers were also deposited under identical conditions on PEN to compare the physical properties.

Thickness and composition of the NAN multilayer films were determined using Rutherford backscattering spectrometry (RBS) The analysis was performed in a vacuum of 10^{-6} Torr using a 2 MeV He^{++} ion beam and total accumulated charge of 20 μC in a General Ionex Tandetron accelerator. Sample and detector were positioned in the Cornell geometry such that the backscatter detector is directly below the incident beam. The samples were tilted to 65° off normal incidence to increase the depth resolution. Energy spectra were obtained using a surface-barrier detector and the RBS data were analyzed using the RUMP[18] simulation program. The thicknesses of top and bottom Nb2O5 layers were approximately 30 nm while Ag thickness varied between 5 to 13 nm.

The phase of the bare Nb_2O_5 and multilayers were investigated by X-ray diffraction (XRD) analysis using a Philips X'pert MPD diffractometer with a Cu *Kα* radiation source. The operating voltage and filament current were 45 kV and 40 mA, respectively. A glancing angle of 1° was used for the incident beam during the analysis. International Center for Diffraction data cards were used for phase identification.

The surface morphology of different thicknesses of Ag layers grown on the bottom Nb_2O_5 layer was analyzed by a scanning electron microscope (XL30 ESEM, Philips) at an operating voltage of 10 kV.

Optical transmittance of the multilayers were measured using an Ocean Optics double channel spectrometer (model DS200) in the wavelength range of 300–800 nm with an air reference for transmittance. Tungsten halogen and deuterium lamps were used as sources for visible and UV light, respectively.

Hall measurements were done using a HMS3000 instrument. Electrical resistivity, Hall mobility, and carrier concentration of the films were measured by means of the Van der Pauw method. A magnetic field of 0.98 T was applied perpendicular to the sample surface.

4.3. RESULTS

A systematic investigation is done in order to determine the effect of each layer on the optical and electrical properties of multilayer films. The most crucial factor that affects the performance of the electrode is the homogeneity of the metal layer. The thickness of Ag layer is not allowed beyond a certain threshold for high transmittance in the visible region. Hence, the deposition method of all three layers is optimized for achieving high conductivity as well as transparency of the NAN multilayers.

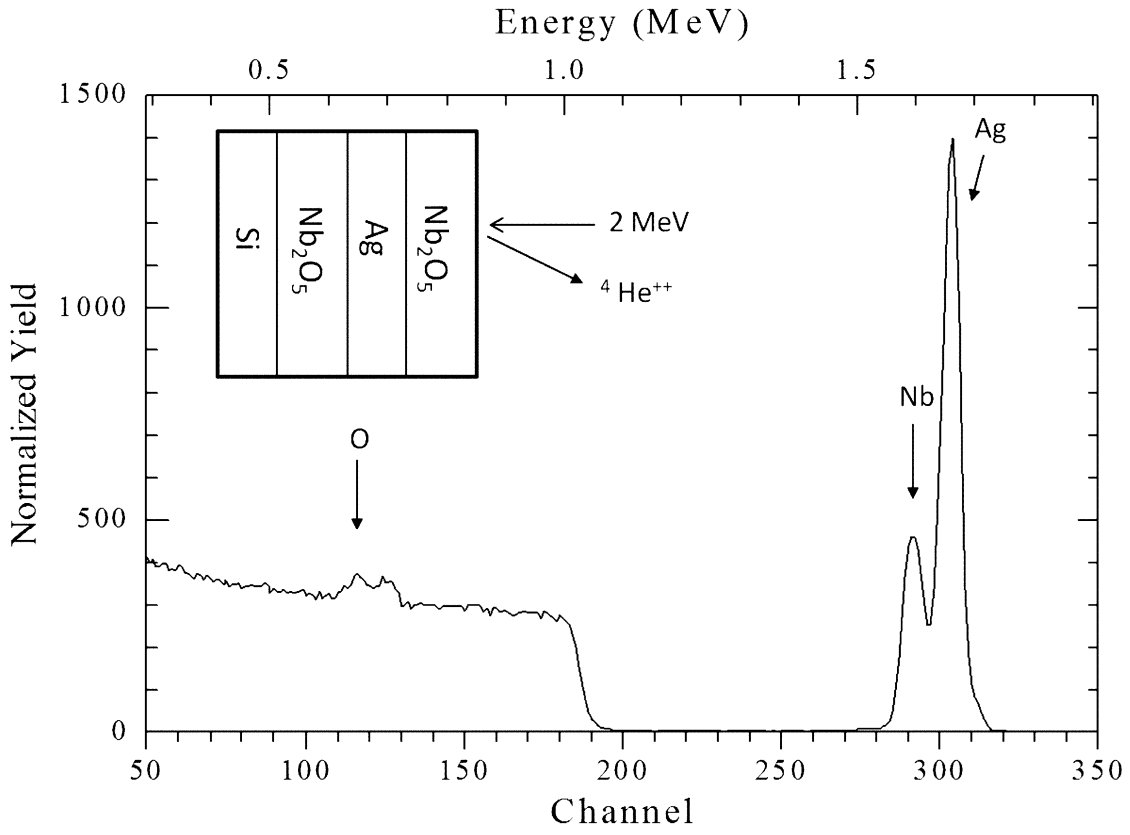

Fig. 4.1 RBS spectrum of Nb_2O_5/Ag/Nb_2O_5 thin film.

Figure 4.1 depicts the 2.0 MeV RBS spectrum of a Nb_2O_5/Ag/Nb_2O_5 thin film. It is used to determine the stochiometry and thickness of the NAN multilayer. The channel region at 280–300 corresponds to the Nb peak from Nb_2O_5 and that between 300-320 corresponds to the Ag peak. Oxygen peaks (in the 100–150 channel region) indicate the presence of oxygen in the top and bottom Nb_2O_5layers. The peak height and width (*i.e*, peak area) of the Ag signal increases with increasing Ag thickness. As the thickness of the top and bottom Nb_2O_5 layer remains constant in all the NAN multilayers, only the Ag

peak varies. A typical RUMP [18] calculation was done to determine the stochiometry of Nb-oxide is found to be $Nb_2O_{4.9}$

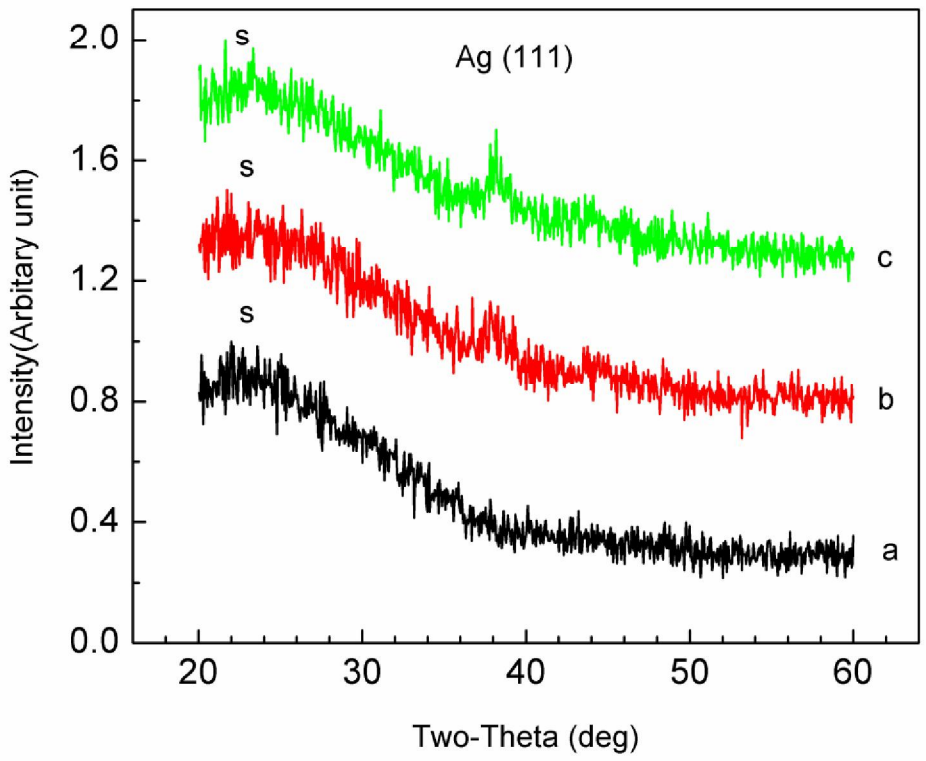

Fig.4.2 XRD patterns from Nb_2O_5/Ag/Nb_2O_5 thin film: (a) bare Nb_2O_5, (b) 5 nm Ag, (c) 13 nm Ag.

The crystalline structure of different multilayers was determined by XRD measurements. Figure 4.2 presents the XRD patterns of as deposited bare Nb_2O_5, NAN multilayers with 5 nm and 13 nm thickness of Ag layer. Although Nb_2O_5 is amorphous, there was the presence of the characteristic (111) peak of Ag in the multilayered structure. The broad peaks around 25^o labelled "s" corresponds to the substrate.

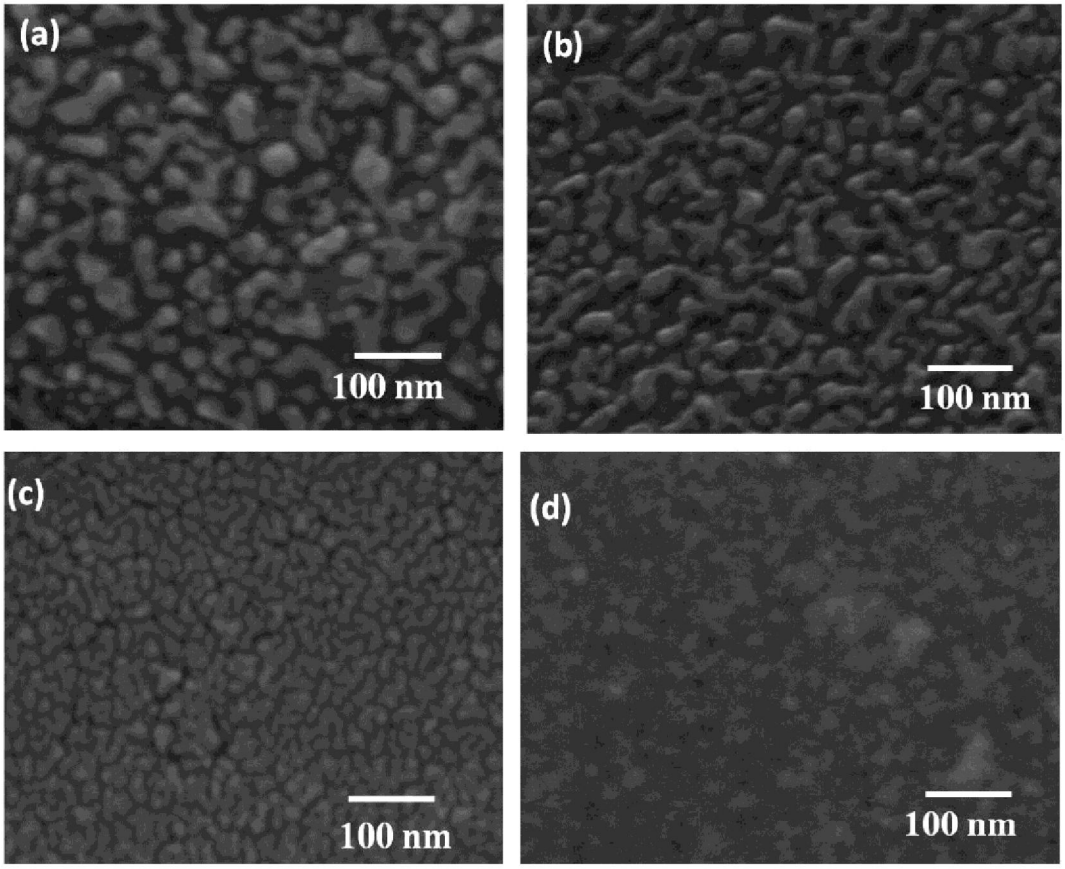

Fig.4.3 SEM images of Ag thin film deposited on bottom Nb_2O_5 surface with different Ag thickness (a) 5 nm, (b) 7 nm, (c) 9.5 nm, (d) 13 nm (Image blurring is due to charging).

Figure 4.3 shows the SEM images of different effective Ag thickness deposited on Nb_2O_5 bottom layer. When the effective Ag thickness was 5 nm, there are large amount of islands which are separated from each other. As the effective Ag thickness increases to 7 nm, the density of Ag islands increases and space between the islands decreases. But as the Ag approaches the critical thickness around 9.5 nm, all the

Ag islands are coalesced and a semi-continuous layer is formed with holes. Finally at 13 nm a continuous layer forms.

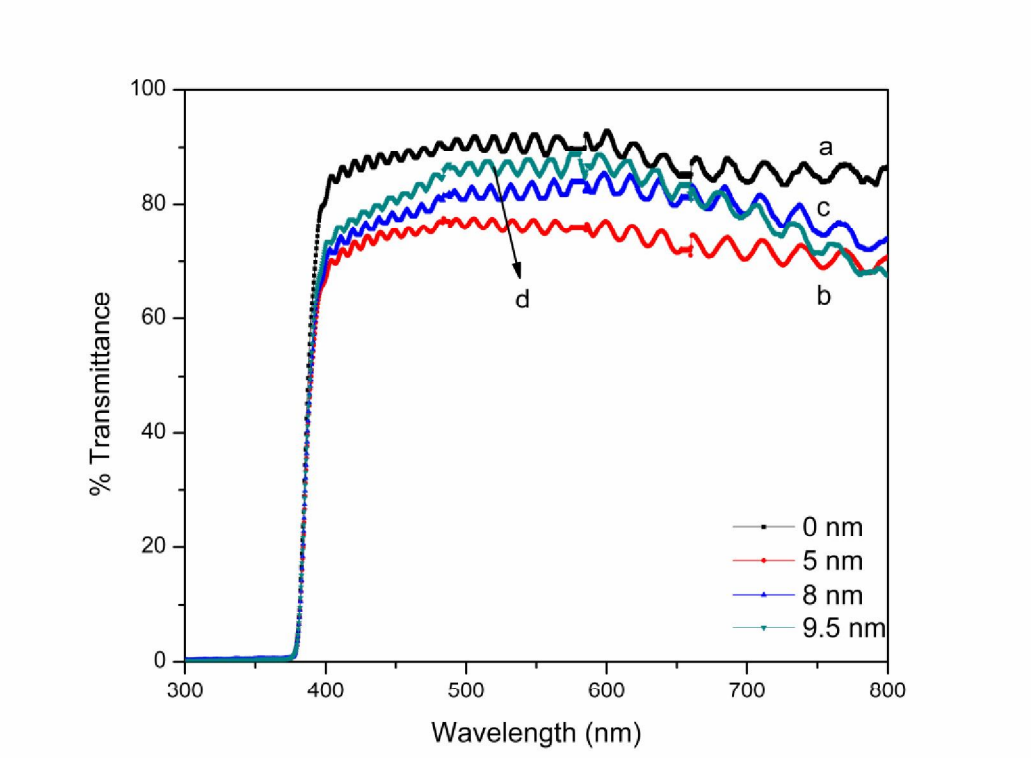

Fig. 4.4.1 Optical transmittance spectra from NAN multilayer films as a function of Ag thickness on the PEN substrate before critical thickness: (a) bare Nb_2O_5, (b) 5 nm Ag, (c) 8 nm Ag, and (d) 9.5 nm Ag.

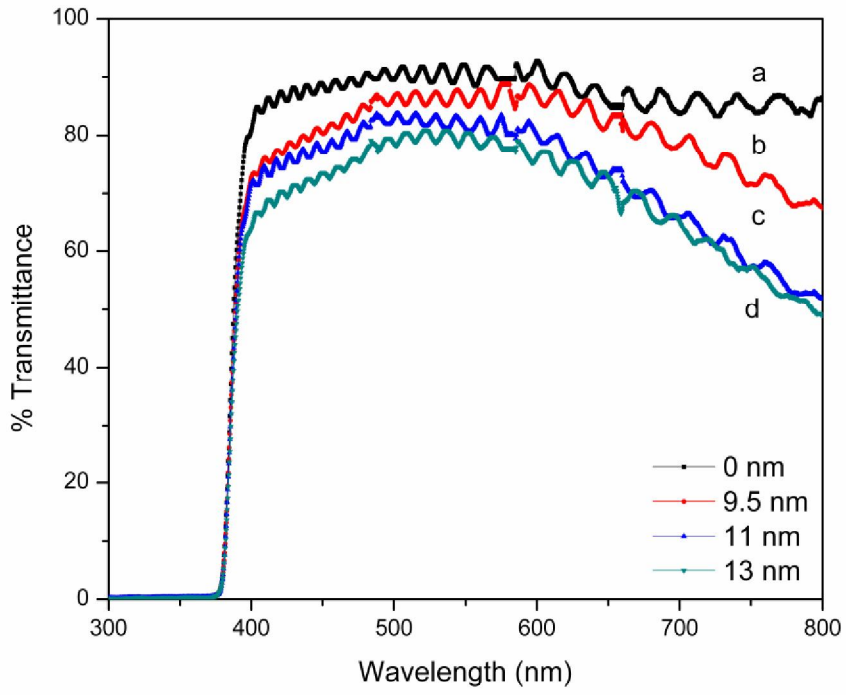

Fig. 4.4.2 Optical transmittance spectra from NAN multilayer films as a function of Ag thickness on the PEN substrate after critical thickness: (a) bare Nb_2O_5, (b) 9.5 nm Ag, (c) 11 nm Ag, and (d) 13 nm Ag.

Figures 4.4.1 and 4.4.2 show optical transmittance spectra for NAN multilayers on PEN substrate as a function of silver thicknesses. The maximum optical transmittance of the pure single-layer Nb_2O_5 film is about 90 % in the visible region. NAN multilayers show a maximum transmittance at ~550 nm wavelength. For the NAN multilayer electrodes in Figs. 4.4, increasing the Ag thickness above 8 nm resulted in a remarkable increase in its optical transmittance with average optical transmittance around 86 % for 9.5 nm Ag thickness. At a lower effective Ag thickness of 5 nm, a fairly low

transmittance of 76 % was observed at a wavelength of 550 nm due to the absorption of the aggregated Ag islands. Also, the decrease in transmittance is due to scattering of light from the isolated Ag islands. However, increasing Ag thickness lead to the improvement of the transmittance because the continuous Ag layer has less scattering loss[19,20]. But further increasing the Ag thickness above 9.5 nm resulted in a gradual decrease in the transmittance from ~ 86 % to 78 % for 13 nm Ag thickness even though this multilayer had the lowest sheet resistance. This was attributed to the increase in plasmon absorption and reflectivity of the mid Ag layer.

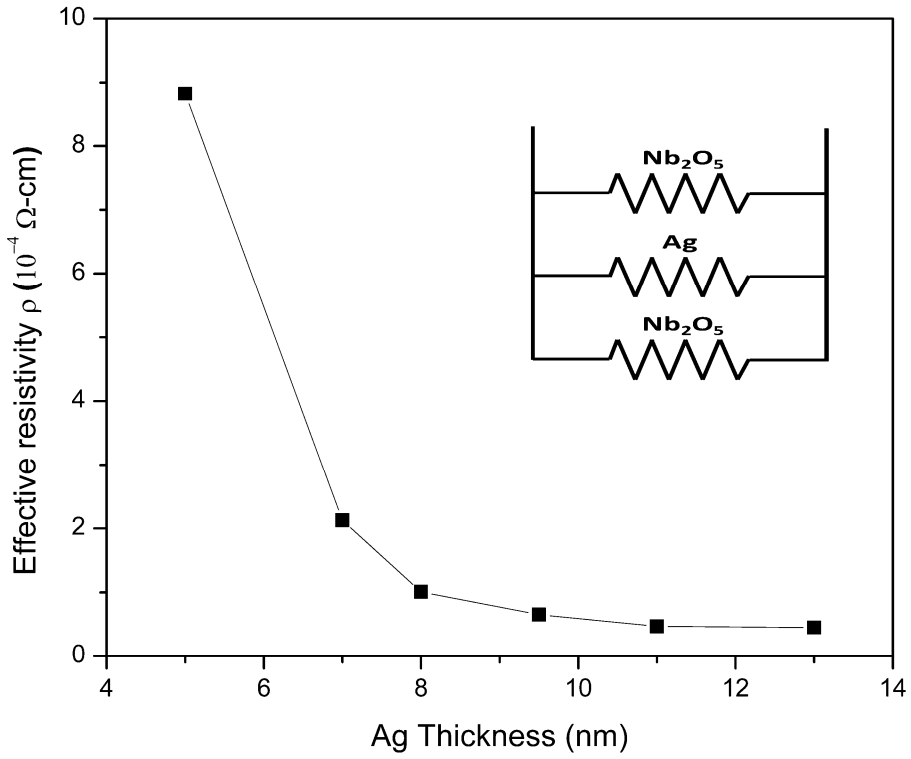

Fig.4.5 Effective resistivity of Nb_2O_5/Ag/Nb_2O_5 multilayer films as a function of Ag thickness.

Figure 4.5 shows the effect of Ag mid-layer on the effective resistivity of NAN multilayers where resistivity decreases with increasing thickness of the Ag mid-layer in the multilayer. Nb_2O_5 is an insulator with resistivity of the order 10^7 Ω-cm. On depositing a 5 nm Ag film between the Nb_2O_5 layers, the resistivity decreases to 8.8 $x10^{-4}$ Ω-cm which suggests that there is a 11 fold decrease in resistivity in NAN multilayers when compared to bare Nb_2O_5. As the effective Ag thickness is increased from 5 nm to 13 nm, the effective resistivity gradually decreases down to 4.45 x 10^{-5} Ω-cm. A more detailed investigation of Fig.4.5 shows that the resistivity of the NAN multilayers drops significantly for structures with effective Ag thicknesses greater than 5 nm indicating the presence of small Ag island structures in case of 5 nm deposition. However, there is a slow decrease in the resistivity of the multilayers from 7 to 13 nm with NAN multilayers approaching the resistivity of bulk silver. The change in resistivity of the NAN multilayer films with increasing Ag thickness can be explained using the following basic relation:

$$\rho = \frac{1}{n\mathrm{e}\mu} \tag{4.1}$$

where, ρ is the resistivity, n is the number of charge carriers, e is the charge of the carrier and μ is the mobility[19]. From this equation we see that changes in mobility and carrier concentration, both can affect the resistivity.

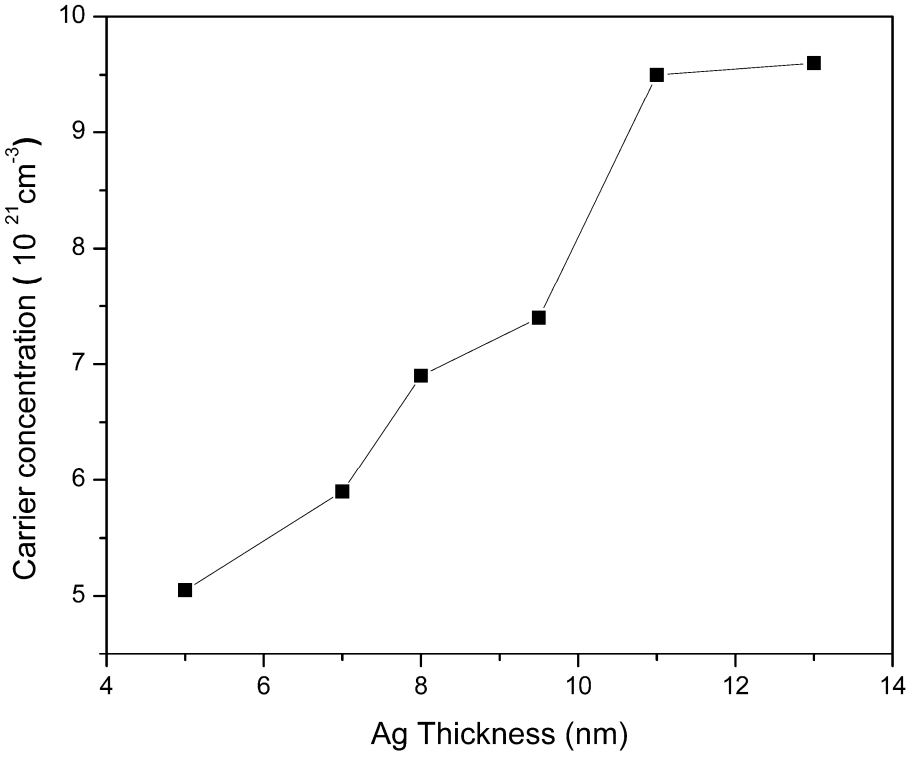

Fig. 4.6 Carrier concentrations of NAN multilayer films as a function of Ag thickness.

Figure 4.6 shows the change in carrier concentration as a function of Ag thickness for NAN multilayers. The plot indicates that carrier concentration depends strongly on the Ag thickness. The carrier concentration of the NAN multilayer has increased from 5 x 10^{21} to 9.6 x 10^{21} cm^{-3} upon increase of effective Ag thickness from 5 to 13 nm. Hence, metallic conduction is dominant in this NAN system.

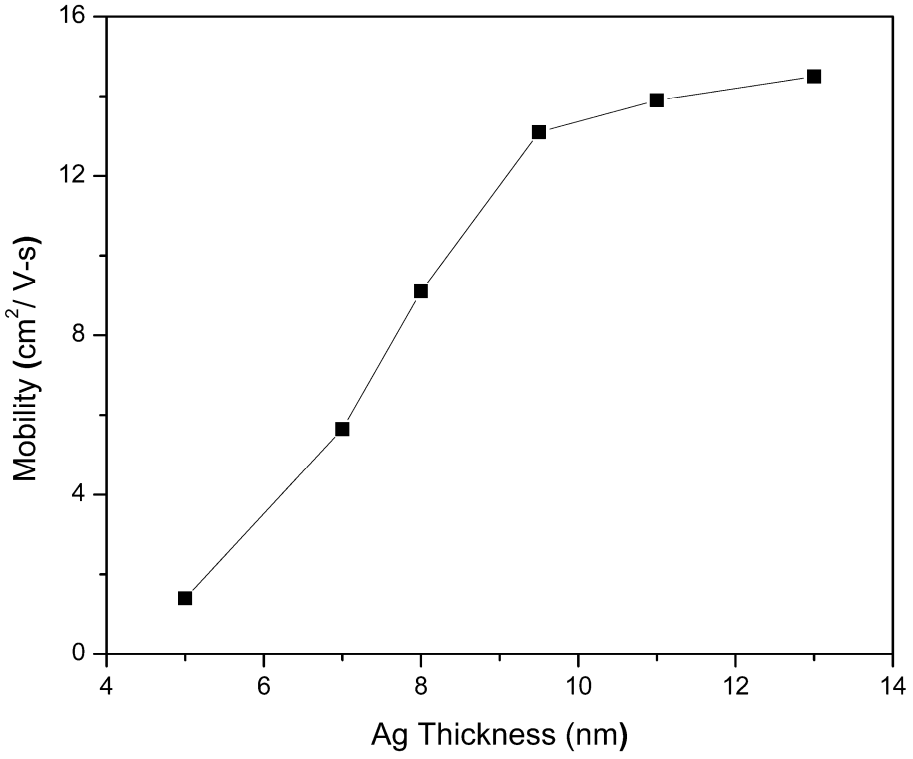

Fig.4.7 Hall mobility of NAN multilayer films as a function of Ag thickness.

Figure 4.7 shows the Hall mobility of NAN multilayer thin films as a function of Ag thickness. There is a rapid increase in Hall mobility that occurs with increasing effective Ag layer thickness from 1.4 cm^2 /V s at 5 nm to 13.1 cm^2 /V s at 9.5 nm, respectively. After 9.5 nm there is a gradual increase of mobility with increase in Ag thickness. There are many scattering mechanisms such as phonon scattering, grain-boundary scattering, surface scattering, interface scattering, and ionized-impurity scattering [20]. Since Nb_2O_5 is an intrinsic semiconductor and amorphous, we can rule out the possibility of ionized-impurity scattering. Interface scattering is predominant at

Nb_2O_5/Ag interface below the critical thickness which is 9.5 nm when there is presence of Ag island structures.

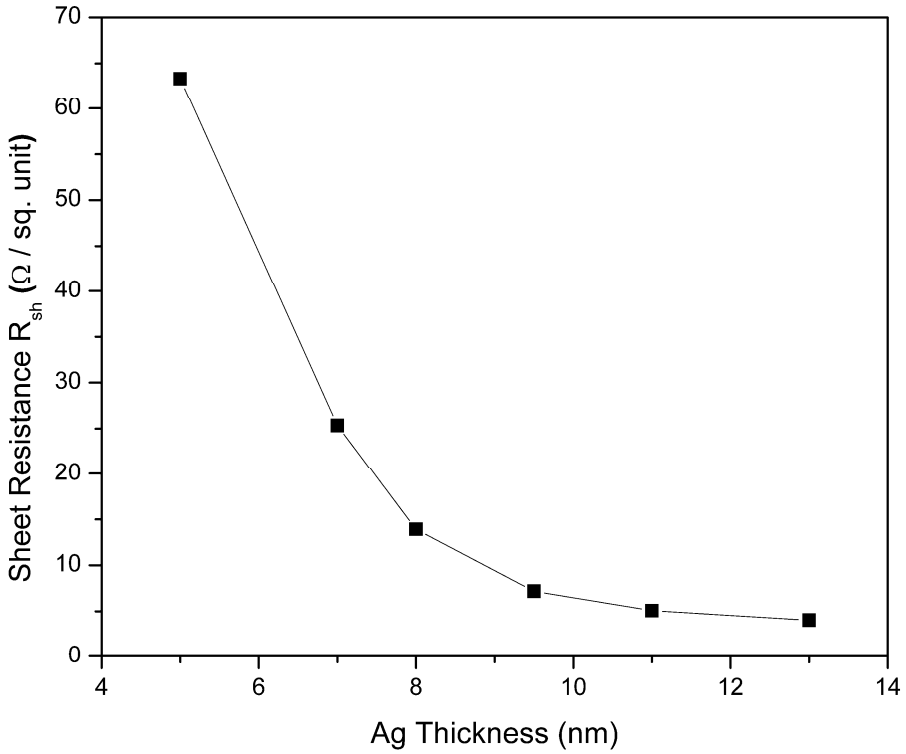

Fig.4.8 Sheet resistance of Nb_2O_5/Ag/Nb_2O_5 multilayer films as a function of Ag thickness.

Figure 4.8 shows the change in sheet resistance as a function of Ag thickness. Here also, we see a rapid decrease in sheet resistance from 63.3 Ω/sq to 13.9 Ω/sq as the effective mid-Ag layer increases from 5 to 7 nm. The sheet resistance curve follows similar trend to that of resistivity as a function of Ag thickness achieving data close to

bulk Ag on 13 nm thickness. The multilayer has a sheet resistance of 7.2 Ω/sq for the critical thickness of Ag layer.

A figure of merit, $\varphi_{TC,}$ (as defined by Haacke [21]) was estimated for each of the NAN multilayers using the following relationship:

$$\varphi_{TC} = \frac{T_{av}^{10}}{R_{sh}} \tag{4.2}$$

Where, T_{av} is the average transmittance and R_{sh} is the sheet resistance.

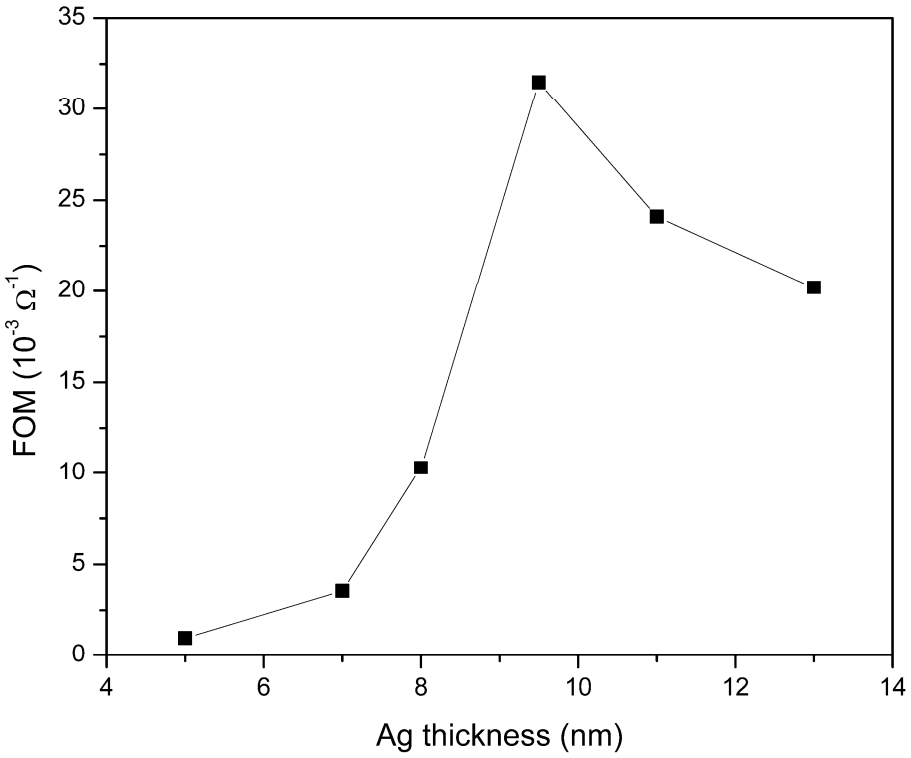

Fig.4.9 Figure of merit of NAN multilayer films as a function of Ag thickness.

Figure 4.9 shows a plot of φ_{TC} as a function of Ag thickness for all NAN multilayers. The multilayer with mid Ag thickness 9.5 nm has the best figure of merit with 31.5 x 10^{-3} Ω/sq. From the plot, we see that the best φ_{TC} is obtained when the Ag layer is just continuous for 9.5 nm Ag thickness sample. Below 8 nm, the poor FOM value corresponds to low average transmittance and high sheet resistance due to discontinuous Ag island growth as discussed earlier. The initial increase of FOM value till it reaches the best value and subsequent decrease corresponds to the similar trend in their average optical transmittance. This occurs while the sheet resistance decreases with increasing Ag thickness.

4.4. DISCUSSION

We know that a thin Ag film growing on crystalline bottom layer follow the Stranski–Krastanov[22,23] growth mechanism of a layer plus-islands growth model while Ag film growing on an amorphous Nb_2O_5 surface should follow the islands growth mechanism of Volmer-Weber model [23]. On the basis of island growth, we expect different conduction mechanism [24] before and after crtical thickness of Ag middle layer in our multilayer stack. It had been proposed that in case of continuous Ag film, when the islands are connected, there will be only metal conduction (*m*) as shown below:

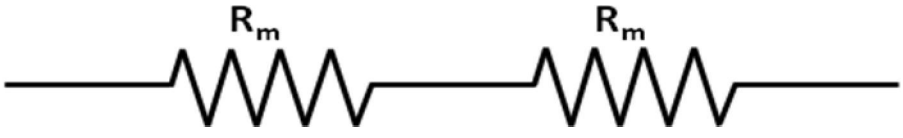

Fig.4.10 Schematic diagram of resistors in discontinuous Ag thin film with islands.

whose resistance (R^m) is defined by[24]:

$$R^m = \rho \frac{L_1}{s_1 d}(1 + \alpha T) \tag{4.3}$$

where L_1 is the distance from the centre to the edge of the island , ρ is the resistivity, T is temperature, α is the temperature coefficient of resistance, s_1 and d denotes the width and thickness of Ag thin film, respectively.

But in case of discontinuous metal films with islands, there will be a different resistance model which includes: metal conduction (m), dielectric conduction (d) and quantum tunneling (q_t) as shown below:

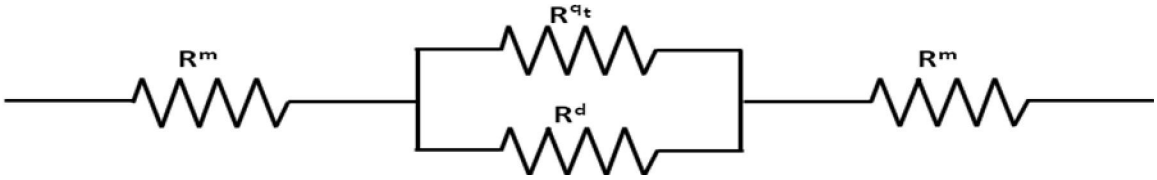

Fig.4.11 Schematic diagram of resistors in continuous Ag thin film.

Here, the surface coverage of the discontinuous Ag thin film will determine among dielectric (metal oxide) or quantum tunneling to take a predominant role in the conduction. The resistance of the dielectric (R^d) can be expressed by the formula [24]:

$$R^d = R^d_{sq} \frac{L_2}{s_2} \exp\left(\frac{E_a}{k_B T}\right) \tag{4.4}$$

where L_2 is the distance between two adjacent islands, s_2 is the width of the dielectric thin film, E_a is the activation energy of the dielectric resistance and k_B is Boltzmann's constant. Also, the quantum tunneling resistance (R^{qt}) can be defined by the following relation [24]:

$$R^{q_t} = \frac{h^2 L_2}{e^2 \left(2m\varphi\right)^{1/2} ds_2} \exp[\frac{4\pi L_2}{h}(2m\varphi)^{1/2}] \tag{4.5}$$

Where h is Plank's constant, φ is the potential barrier height for the dielectric–metal system, e and m are the charge and mass of electron, respectively.

Conduction through the dielectric dominates when the metal islands are very small and space between islands is large. As the islands grow, the separation between the islands decreases and some of the islands coalesce to form a continuous layer. This leads to a radical drop in resistance as observed in higher thickness region of Fig. 4.8. Quantum tunneling occurs between the larger islands with small gaps between them while bulk conduction occurs through the continuous layer.

It was observed that there is a parabolic increase in average optical transmittance with increasing Ag thickness and also the trend is different for middle (500-600 nm) and longer (near IR) wavelengths which can be explained based on scattering and absorption by the Ag mid-layer [19-20,25]. The difference at 500-600 nm wavelength region is due to light scattering at the Nb_2O_5/Ag interface in Ag isolated islands for effective Ag thickness below 8 nm and absorption of light due to interband electronic transitions from the 4d to unoccupied levels in the 5s band above Fermi level. As the effective Ag thickness increases, the Ag becomes a continuous layer from discontinuous islands which causes decrease in light scattering. In addition, as the islands in the film come closer together and are more densely packed, this plasmon absorption band shifts to longer wave length. In the longer wavelength (700-800 nm) region the transmittance decreased abruptly for larger Ag thickness (11-13 nm), a trend similar to that of a metal which

signifies that the multilayer is assuming the metallic behavior. The low transmission in the near IR region is due to plasmon-absorption-dependent reflection due to increase of electron carriers with increase in Ag thickness.

4.5. CONCLUSION

$Nb_2O_5/Ag/Nb_2O_5$ multilayer structures were deposited onto PEN to develop indium free transparent conductive films with low resistance. Hall measurements and sheet resistance data show that the conductivity of the NAN multilayer is solely due to the Ag mid-layer as the Nb_2O_5 is highly resistive. The multilayer stack has been optimized to achieve a sheet resistance of 7.2 Ω/sq and an average optical transmittance of 86 % at 550 nm. The multilayer with the middle layer Ag thickness of 9.5 nm has the best figure of merit of 31.5 x 10^{-3} Ω/sq. This is a very low resistivity flexible transparent electrode at room temperature obtained without using high substrate temperature or post-process anneals. Thus the NAN multilayers on PEN substrates can be used as transparent composite electrodes for solar cell and other display applications.

CHAPTER 5

EFFECT OF SILVER THICKNESS AND ANNEALING ON STRUCTURAL, OPTICAL AND ELECTRICAL PROPERTIES OF $Nb_2O_5/Ag/Nb_2O_5$ MULTILAYERS AS TRANSPARENT COMPOSITE ELECTRODE ON FLEXIBLE SUBSTRATE

5.1. INTRODUCTION

Transparent conductive oxides (TCO) are useful materials that exhibit unique combination of high transparency in the visible region along with high electrical conductivity. TCOs play an important role as transparent electrodes for flexible optoelectronic devices such as solar cell panels, liquid crystal displays and organic light emitting devices (OLED) [1-3] Other common applications for TCOs include heat mirrors, optical filters, low emittance films for advanced glazing, and protective or decorative coatings.

The material most commonly used for transparent electrodes in optoelectronic applications is indium tin oxide [4-5] (ITO) due to its low resistivity (~ 10^{-4} Ω-cm), high transmittance (~ 80 %), and fabrication maturity. However, the limited supply of indium and the growing demand for ITO make the resulting fabrication costs prohibitive for future industry. Thus, cost factors have promoted the search for inexpensive materials with good electric-optical properties. Pure zinc oxide (ZnO) or ZnO doped with metals [6-8] like aluminum (Al), gallium (Ga), indium (In) *etc* have been widely researched as a

promising candidate to replace ITO. Recently, electrical resistivity has been improved by inserting a thin metal or metal alloy film between two TCO layers [9-11]. These composites have significant lower resistivity than a single-layer TCO film. Amongst metals, Ag is a good candidate for such multilayer films because of its low resistivity [11].

Niobium oxide films has high refractive index and wide band gap (3.4-3.8 eV) and thus the dielectric film has a high transparency in the visible region. The Nb_2O_5 coatings show excellent thermal and chemical stability Thus the high transparency of Nb_2O_5 in visible region and low resistivity of thin Ag layer lead us to the detailed study of optical and electrical properties of Nb_2O_5/Ag/Nb_2O_5 (NAN) multilayers.

5.2. EXPERIMENTAL DETAILS

Multilayers of Nb_2O_5 and Ag were deposited at 20 mTorr pressure by rf magnetron sputter at 150 W and dc sputter at 40 W and 10m Torr pressure, respectively, onto flexible polyethylene substrate (PEN) substrates. The top and bottom Nb_2O_5 layers were approximately 30 nm thick while the silver thickness was varied between 5 to 13 nm. Thickness of the NAN multilayer films were determined using variable angle spectroscopic ellipsometry (VASE). Hall measurements by the van der Pauw technique were done using the Ecopia HMS 3000 instrument. Four-point-probe equipped with a 100 mA Keithley 2700 digital multimeter was used for sheet resistance measurements. Optical transmittance of the multilayers were measured using an Ocean Optics double channel spectrometer (model DS200) in the wavelength range of 300–800 nm with an air

reference for transmittance. Tungsten halogen and deuterium lamps were used as sources for visible and UV light, respectively. The thin film samples were annealed in vacuum, forming gas and O_2 environments upto 150 ºC for 3 hrs. Electrical and optical characterization was done for the as-deposited samples and also after each of the anneal steps.

5.3. RESULTS AND DISCUSSION

Figure 5.1 shows the effect of Ag mid-layer on the resistivity and sheet resistance of the NAN multilayers where both parameters decrease with increasing thickness of the Ag mid-layer. From the microstructure of the Ag thin film, it is clear that the Ag film deposited was discontinuous below the critical thickness (t_c) and gradually became continuous after t_c. Hence we expect different conduction mechanism before and after critical thickness.

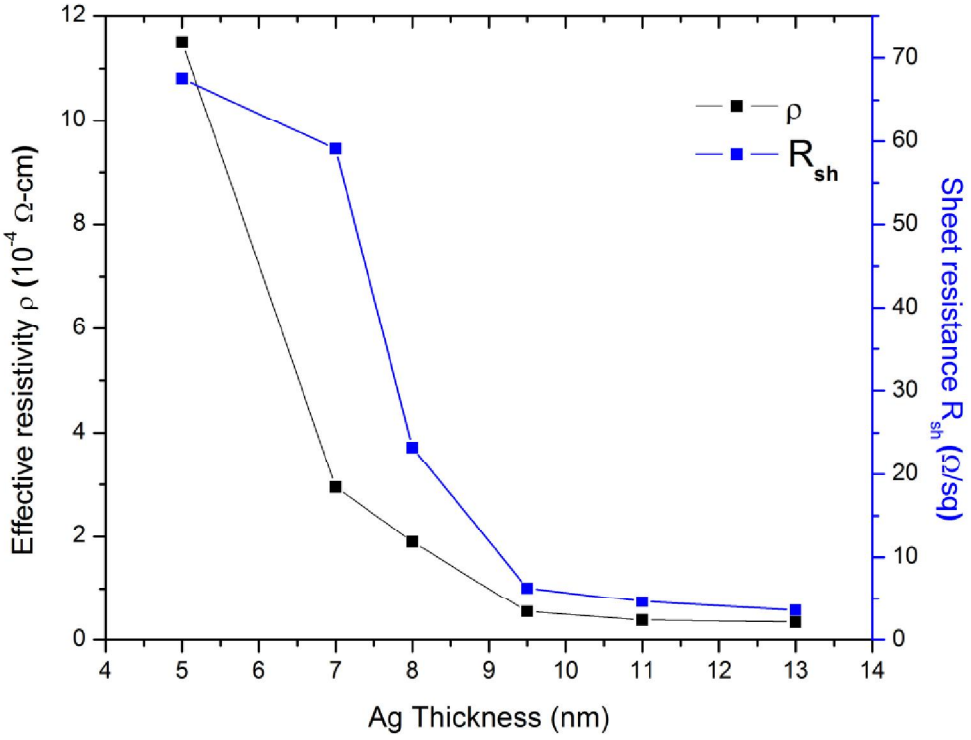

Fig.5.1. Effective resistivity and sheet resistance of Nb_2O_5/Ag/Nb_2O_5 multilayer films as a function of Ag thickness.

Nb_2O_5 has very high resistivity of the order 10^7 Ω-cm. On depositing a 5 nm Ag film between the Nb_2O_5 layers, the resistivity decreases to 8.8 x10^{-4} Ω-cm which suggests that there is a 11 fold decrease in resistivity in NAN multilayers when compared to bare Nb_2O_5. As the Ag thickness is increased from 5 nm to 13 nm, the effective resistivity gradually decreases down to 4.45 x 10^{-5} Ω-cm.

Conduction through the dielectric dominates when the metal islands are very small and space between islands is large. As the islands grow, the separation between the islands decreases and some of the islands undergo coalesce in large scale. This leads to a

radical drop in resistance as observed in lower thickness region of Fig. 5.1. Quantum tunneling occurs between the larger islands with small gaps between them while bulk conduction occurs through the contiguous layer. The conductivity (σ) in this region is governed by the following equation [18]:

$$\sigma \propto \exp(-2\beta L - \frac{W}{k_B T}) \tag{5.1}$$

where W is the island charging energy and β is the tunneling exponent of electron wave functions in the insulator.

In our study, Ag thin films were deposited on amorphous Nb_2O_5 surface and thus minimizations of surface and interfacial energies will be the driving force for the Ag grains to prefer (111) than (200) orientation as described by Zoo *et al* [20]. As a result, Ag thin film deposited on bottom Nb_2O_5 layer will have better grain texture orientation which will lead to decrease in grain boundary scattering and thus lower resistivity. When the Ag islands form a contagious layer, the decrease in resistivity is governed by the combined effect of the increase in carrier concentration of conducting electrons and mobility. At this stage, the dominant factor affecting resistivity was surface boundary scattering. The conductivity (σ) in this region behave according to the following equation [18] :

$$\frac{\sigma}{\sigma_0} \propto \frac{3}{4}(1-p)k\log\frac{1}{k} \tag{5.2}$$

where p is the fraction of the distribution function of the electrons arriving at the surface, σ_o represents the conductivity of the bulk metal, and $\kappa = t/\lambda_o$

However, the total resistance of the NAN multilayer is a result of parallel combination of the three individual layers of Nb_2O_5/Ag/Nb_2O_5 and can be shown as :

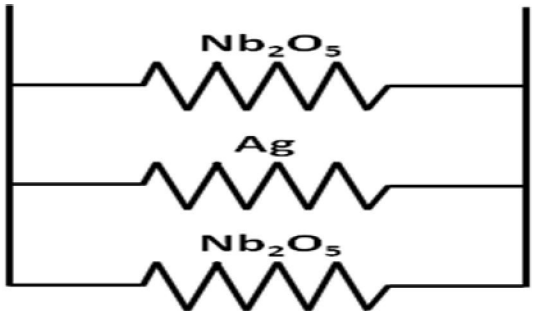

The change in effective resistivity of the NAN multilayer films with increasing Ag thickness can be explained using the following basic relation:

$$\rho = \frac{1}{ne\mu} \tag{5.3}$$

Where, ρ is the resistivity, n is the number of charge carriers, e is the charge of the carrier and μ is the mobility [19]. This equation suggest that both mobility and carrier concentration can affect the resistivity of the multilayers.

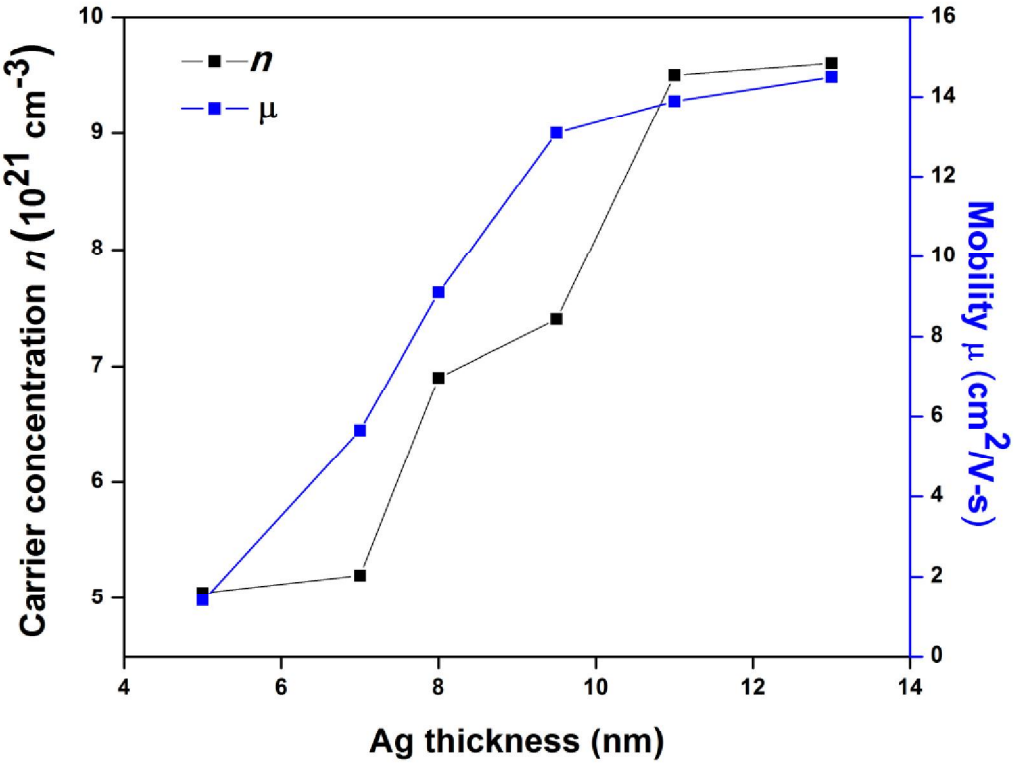

Fig.5.2. Carrier concentrations and mobility of NAN multilayer films as a function of Ag thickness.

Figure 5.2 shows the change in carrier concentration and mobility as a function of Ag thickness for NAN multilayers. The plot indicates that carrier concentration increases with increase in Ag thickness. The carrier concentration of the NAN multilayer has increased from 5 x 10^{21} to 9.6 x 10^{21} cm^{-3} upon increase of Ag thickness from 5 to 13 nm. There is a similar rapid increase in Hall mobility with increasing Ag layer thickness from 1.4 cm^2 /V s at 5 nm to 13.1 cm^2 /V s at 9.5 nm, respectively. Interface scattering is predominant at Nb_2O_5/Ag interface above the critical thickness while island boundary scattering takes place below the critical thickness.

Figure 5.3. shows optical transmittance spectra for $Nb_2O_5/Ag/Nb_2O_5$ (NAN) multilayers on PEN substrate as a function of silver thicknesses. The maximum optical transmittance of the pure single-layer Nb_2O_5 film is about 90 % in the visible region. NAN multilayers show a maximum transmittance of 86 % for 9.5 nm Ag thickness at ~550 nm wavelength.

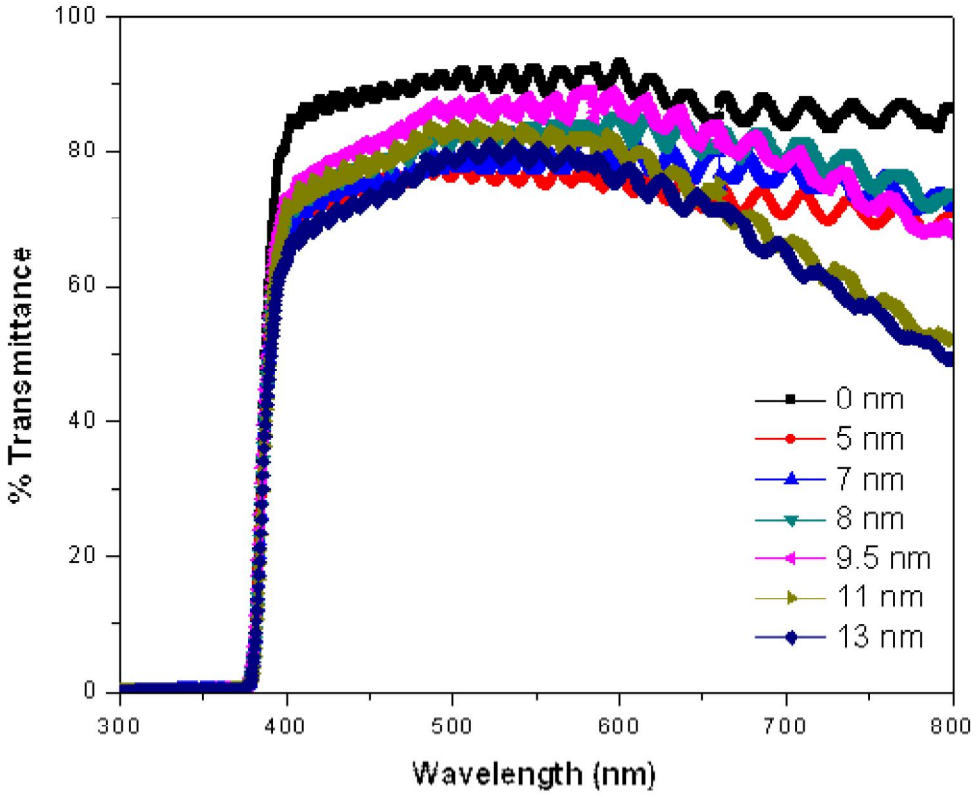

Fig.5.3. Transmittance spectra for $Nb_2O_5/Ag/Nb_2O_5$ (NAN) multilayers on PEN substrate as a function of silver thicknesses.

It was observed that there is a parabolic increase in average optical transmittance with increasing Ag thickness and also the trend is different for middle (500-600 nm) and longer wavelengths which can be explained based on scattering and absorption by the Ag mid-layer. The difference at 500-600 nm wavelength region is due to light scattering at the Nb_2O_5/Ag interface in Ag isolated islands for Ag thickness below 8 nm and absorption of light due to interband electronic transitions from the 4d to unoccupied levels in the 5s band above Fermi level. As the Ag thickness increases, the Ag becomes a continuous layer from discontinuous islands which causes decrease in light scattering. The decrease in optical transmittance for Ag thin film can be expressed as [21]

$$I = I_0[\frac{-4\pi\alpha x}{\lambda} + \delta] \tag{5.4}$$

Where α is called absorption constant, x is the depth from the surface and δ denotes the inter-band electronic transition term.

In the visible region, higher transmittance was observed which can also be explained on the coupling between the incident light and surface plasmon of the island like structures of Ag thin films[22]. However in the near IR (700-800 nm) region the transmittance decreased abruptly for larger Ag thickness (11-13 nm), which signifies that the multilayer is assuming the metallic behavior. In the near IR region, the low transmission is due to plasma-absorption-dependent reflection due to increase of electron carriers.

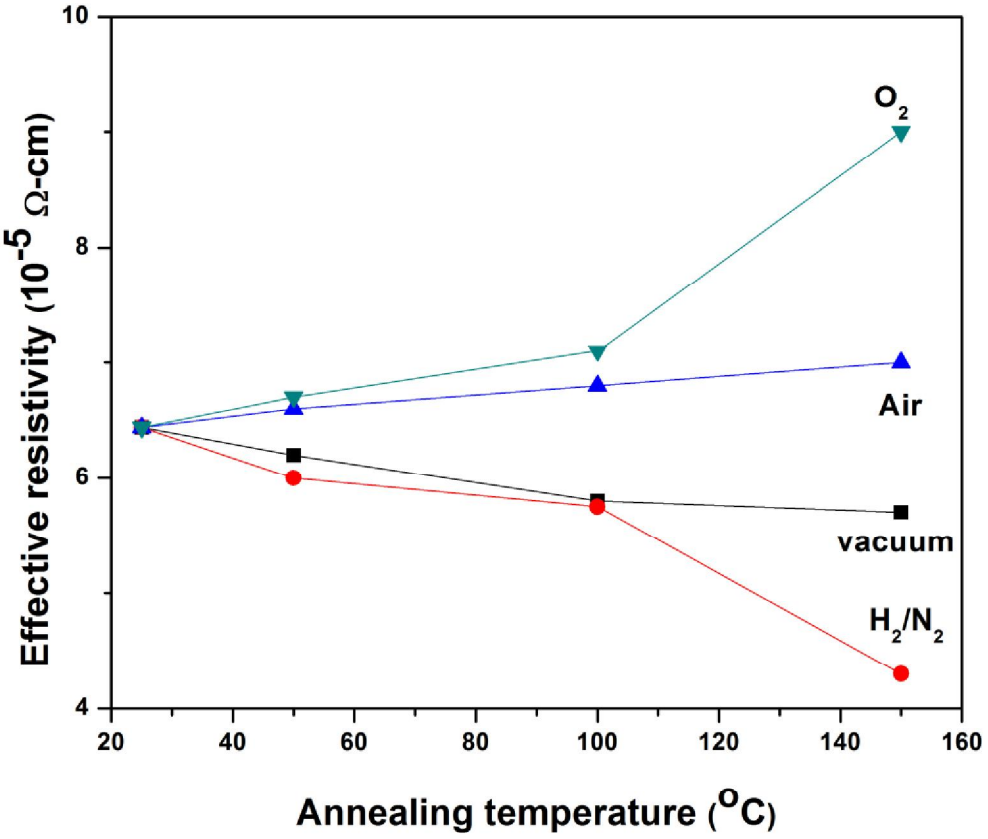

Fig.5.4. Effect of annealing on effective resistivity of NAN multilayers in various environments.

Figure 5.4 and 5.5 shows the effect of annealing of the NAN multilayer thin films in various environments. The thin film with critical Ag thickness were annealed for 3 hours upto 150 ^{o}C. It is seen that the effective resistivity of the thin film improved when annealed in forming gas (H_2/N_2) and vacuum but detoriated in air and O_2. However, the improvement was more significant in case of forming gas. Although the average transmittance slightly improved on O_2 annealing but the electric properties showed a sharp increase in effective resistivity when annealed at 150 ^{o}C.

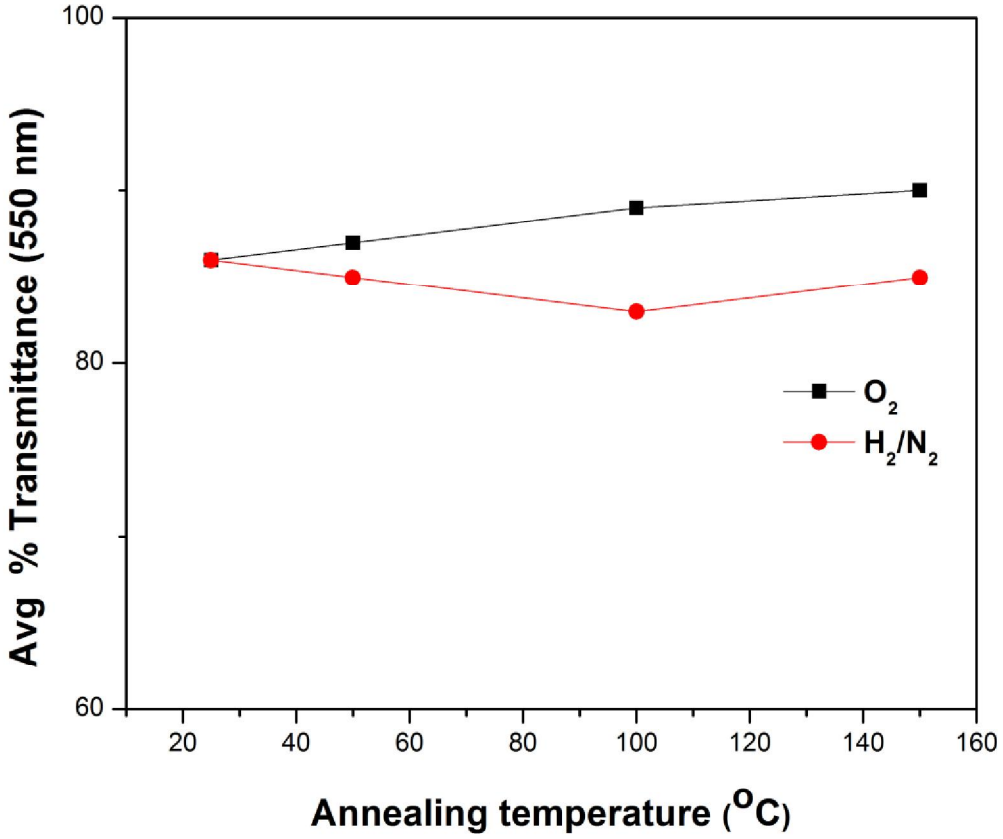

Fig.5.5. Average transmittance spectra (at 550 nm) for $Nb_2O_5/Ag/Nb_2O_5$ multilayers when annealed in O_2 and H_2/N_2 environments

A figure of merit, $\varphi_{TC,}$ (as defined by Haacke) was estimated for each of the NAN multilayers using the following relationship:

$$\varphi_{TC} = \frac{T_{av}^{10}}{R_{sh}} \tag{5.5}$$

where, T_{av} is the average transmittance and R_{sh} is the sheet resistance. The multilayer with mid Ag thickness 9.5 nm has the best figure of merit with 31.5 x 10^{-3} Ω/sq.

5.4. CONCLUSION

Different multilayer structures of Nb_2O_5/Ag/Nb_2O_5 have been deposited on PEN, characterized and developed as transparent conductive film with low resistance. Hall measurements and sheet resistance data show that the conductivity of the NAN multilayer is solely due to the Ag mid-layer.. The multilayer stack has been optimized to have sheet resistance of 7.2 ohm/sq and an average optical transmittance of 86 % at 550 nm. The multilayer with mid Ag thickness 9.5 nm has the best figure of merit with 31.5 x 10^{-3} Ω/sq. This makes it possible to synthesize low resistivity electrode at room temperature without using high substrate temperature or post annealing process. Thus the NAN multilayers on PEN substrates can be used as transparent electrode for solar cell and other display application.

CHAPTER 6

HIGH QUALITY TRANSPARENT TiO_2/Ag/TiO_2 COMPOSITE ELECTRODE FILMS DEPOSITED ON FLEXIBLE SUBSTRATE AT ROOM TEMPERATURE BY SPUTTERING

6.1. INTRODUCTION

The constant increase in limitation of Si technology owing to long and expensive fabrication steps that utilize rigid and fragile substrates has created an inherent need for the development of low cost, large area and highly robust flexible electronics. The introduction of a room-temperature route for deposition of highly conductive and transparent material onto flexible substrates could change the future of several photonic and electronic devices with the potential to influence a wide spectrum of applications [1-3]. Flexible thin films of transparent conducting oxide (TCO) are extensively used for a variety of applications in optoelectronic industry, such as solar cells, electrochromic devices, liquid crystal displays, and organic light emitting diodes [1-4].

Until now, amorphous indium tin oxide (a-ITO) have been commonly used as transparent electrodes for flexible optoelectronic applications due to its low resistivity (~ 10^{-4} Ω-cm) and high transmittance (~ 80 %) in the visible region [5]. However, a-ITO film deposited on flexible substrates have some limitations like fairly lower conductivity owing to low process temperature and reduced dopant activation at lower temperatures. The reduction in thickness of the electrode material to attain better mechanical flexibility

also results in the poor conductivity problem. Indium is also a rare and highly expensive metal and thus makes the resulting fabrication costs excessive for future applications. Thus, these factors have attracted a sufficient amount of attention in search for cheaper materials with good opto-electrical properties. Promising alternative materials includes pure SnO_2, ZnO or ZnO doped with metals (*i.e;* aluminum (Al), gallium (Ga), indium (In) *etc.*), Nb_2O_5, TiO_2, graphene, and carbon nanotube (CNT) sheets have been recently studied as potential alternatives to a-ITO electrodes on flexible substrates [5-9]. Recently, insertion of a very thin metal layer sandwiched between the two TCO layers have been studied to develop a transparent composite electrode (TCE) with the desired electrical conductivity [9-12]. Although metals have high reflectivity, very thin films (< 15 nm) shows moderate transmittance in the visible region and also the top dielectric layer helps to obtain a higher transparent effect by diminishing the reflection from the metal layer. This oxide/metal/oxide (OMO) multilayer framework have lower total thickness and more efficient than a single-layer TCO film [7-12].

Titanium dioxide (TiO_2) is such a potential semiconductor material with wide band gap (~ 3 eV) and good adhesion to the substrates [13-14]. It has many excellent physical properties such as a high dielectric constant and a strong mechanical and chemical stability. Due to its high refractive index of about 2.7 and optical transmittance of above 90 % in the visible range, TiO_2 can be used as optical coatings on large area substrates for architectural, automotive and display applications and protective layers for very large-scale integrated circuits [13-14]. In this work, the high transparency of TiO_2 in visible region and low resistivity of thin Ag layer lead us to the detailed study of optical and electrical properties of TiO_2/Ag/TiO_2 (TAT) multilayers as transparent composite

electrode (TCE). The multilayers transparent conductive electrode have been deposited onto flexible substrates by sputtering at room temperature. The performance of this system based on the optical and electrical properties has been evaluated using a figure of merit (FOM).

6.2. EXPERIMENTAL DETAILS

The TiO_2/Ag/TiO_2 multilayer thin films of different silver thickness were sequentially deposited onto 125 μm thick flexible polyethylene naphthalate (PEN) and Si substrates by RF magnetron sputtering of ceramic TiO_2 target (99.999 % purity) and DC sputtering of pure Ag target (99.99 % purity) at room temperature without any vacuum break. The TiO_2 and Ag were deposited using an rf power and dc power of 150 W and 40 W, respectively. Bare TiO_2 layers were also deposited under identical conditions on PEN to compare the physical properties. The top and bottom TiO_2 layers were approximately 30 nm thick; while, the silver thickness was varied between 5 to 13 nm. The thicknesses of the TAT multilayer films were determined using optical ellipsometry. Scanning electron microscope (XL30 ESEM, Philips) at an operating voltage of 20 kV was used to analyze the surface morphology of different thicknesses of Ag layers grown on the bottom TiO_2 layer. Hall measurements by the van der Pauw technique with a magnetic field of 0.98 T were done using the Ecopia HMS 3000 instrument. Four-point-probe technique was used for sheet resistance measurements. Optical transmittance of the multilayers were measured using an Ocean Optics double channel spectrometer (model DS200) in the wavelength range of 300–800 nm with an air reference for transmittance.

Deuterium and tungsten halogen lamps were used as sources for UV and visible light, respectively.

6.3. RESULTS AND DISCUSSION

A systematic study is done in order to determine the effect of Ag mid-layer on the opto-electrical properties of multilayer thin films. The most vital factor that influences the performance of the composite is the morphology of the middle metal layer. It is known that the Ag film growing on an amorphous TiO_2 surface should follow the islands growth mechanism of Volmer-Weber model [15-16] which is verified from the microstructure in Fig. 6.1. The SEM images correspond to different Ag thickness before and after the critical thickness of 9.5 nm. Fig. 6.1(a) showed the presence of island structures which gradually form contagious as it approaches the critical thickness [Fig.6.1 (b)]. Finally, the Ag islands form a continuous layer [Fig.6.1 (c)] at 13nm. In order to achieve high transmittance in the visible region, the thickness of the Ag layer is limited to an optimum thickness so that the TAT multilayers exhibit high conductivity as well as transparency.

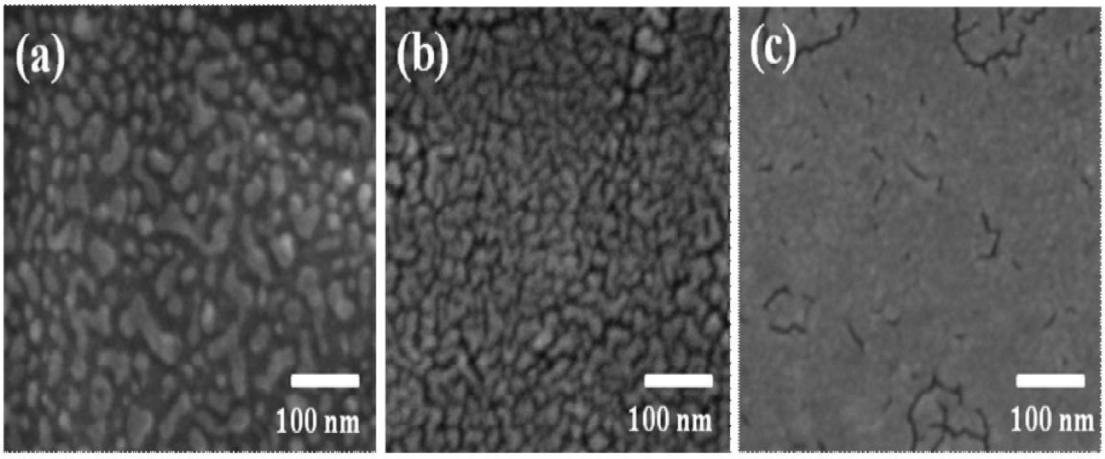

Fig.6.1. SEM images of Ag thin film deposited on bottom TiO_2 surface with different Ag thicknesses: (a) 5 nm, (b) 9.5 nm, (c) 13 nm.

Figure 6.2. shows the change in carrier concentration and Hall mobility as a function of Ag thickness for various TAT multilayers. The plot indicates that carrier concentration depends strongly on the Ag thickness. The carrier concentration of the TAT multilayer has increased from 6.8 x 10^{21} to 1.46 x 10^{22} cm^{-3} upon increase of Ag thickness from 5 to 13 nm. Hence, metallic conduction is dominant in this TAT system. There is a rapid increase in Hall mobility that occurs with increasing Ag layer thickness from 3.7 cm^2/V-s at 5 nm to 13.1 cm^2/V-s at 13 nm, respectively. There are many scattering mechanisms such as phonon scattering, grain-boundary scattering, surface scattering, interface scattering, and ionized-impurity scattering [7-9]. Since TiO_2 is an intrinsic semiconductor and amorphous, one can exclude the possibility of ionized-impurity scattering. In our TCE, interface scattering takes place above the critical thickness of 9.5 nm; whereas, island boundary scattering dominates at the TiO_2/Ag interface below the critical thickness due to the presence of Ag island structures. These

boundaries are expected to have fairly high densities of interface states which scatter free carriers due to the presence of trapped charges and inherent disorders. As a result, a space charge region is created in the island boundaries, which results in potential barriers to charge transport due to band bending. This transport phenomenon in polycrystalline thin films can be expressed by Petritz model [17], where the mobility (μ_i) is written as:

$$\mu_i = \mu_0 \exp(-\frac{\Phi_B}{k_B T}) \tag{6.1}$$

Where $\mu_0 = (\frac{S^2 e^2}{2\pi m^* k_B T})^{\frac{1}{2}}$

S is the island size, e is the elementary charge, Φ_B is the island boundary potential and k_B is the Boltzmann constant.

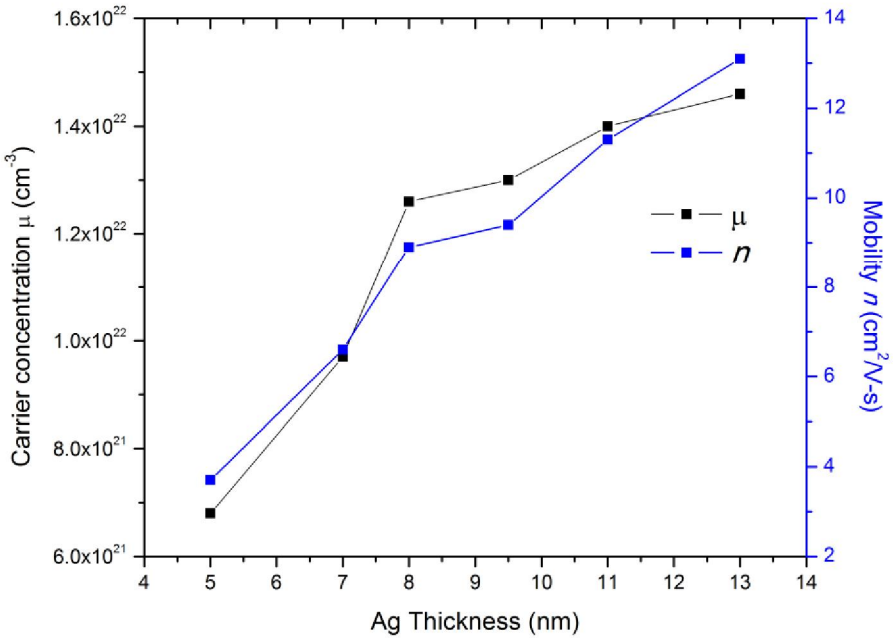

Fig.6.2. Carrier concentration and Hall mobility as a function of Ag thickness for TAT multilayers.

Figure.6.3. shows the effect of Ag mid-layer on the resistivity and sheet resistance of TAT multilayers where both decrease with increasing thickness of the Ag mid-layer in the multilayer. In this case, TiO_2 is an insulator with resistivity of the order 10^7 Ω-cm. On depositing a 5 nm Ag film between the TiO_2 layers, the resistivity decreases to 8.8 $x10^{-4}$ Ω-cm and suggests that there is a 11 fold decrease in resistivity in TAT multilayers when compared to bare TiO_2. As the Ag thickness is increased from 5 nm to 13 nm, the effective resistivity gradually decreases down to 4.45 x 10^{-5} Ω-cm. A more detailed investigation of Fig.6.2 shows that the effective resistivity of the TAT multilayers drops significantly from 5 to 7 nm and indicates the presence of small Ag island structures in case of 5 nm deposition. However, there is a slow decrease in the effective resistivity of the multilayers from 7 to 13 nm with TAT multilayers approaching the resistivity of bulk silver. The change in effective resistivity of the TAT multilayer films with increasing Ag thickness can be explained using the following basic relation:

$$\rho_{eff} = \frac{1}{ne\mu} \tag{6.2}$$

The sheet resistance curve follows similar trend to that of resistivity as a function of Ag thickness achieving data close to bulk Ag on 13 nm thickness. Here also, we see a rapid decrease in sheet resistance from 50.6 Ω/sq to 5.5 Ω/sq as the mid-Ag layer increases from 5 to 9.5 nm. However, the total resistance of the TAT multilayer is a result of parallel combination of the three individual layers of TiO_2/Ag/TiO_2 and can be shown as:

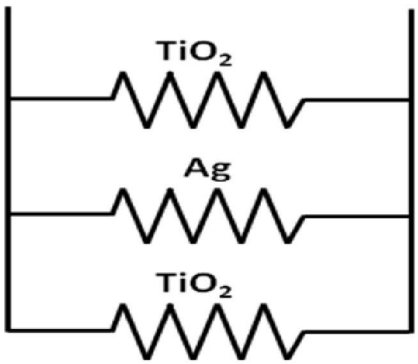

Fig.6.3. Schematic diagram of parallel resistor in TAT multilayer electrode

Figure 6.4. shows the effect of Ag mid-layer on the effective resistivity and sheet resistance of the TAT multilayers where both parameters decrease with increasing thickness of the Ag mid-layer. From the microstructure of the Ag thin film, it is clear that the Ag film deposited was discontinuous below the critical thickness (t_c) and gradually became continuous after t_c. Hence we expect different conduction mechanism before and after critical thickness.

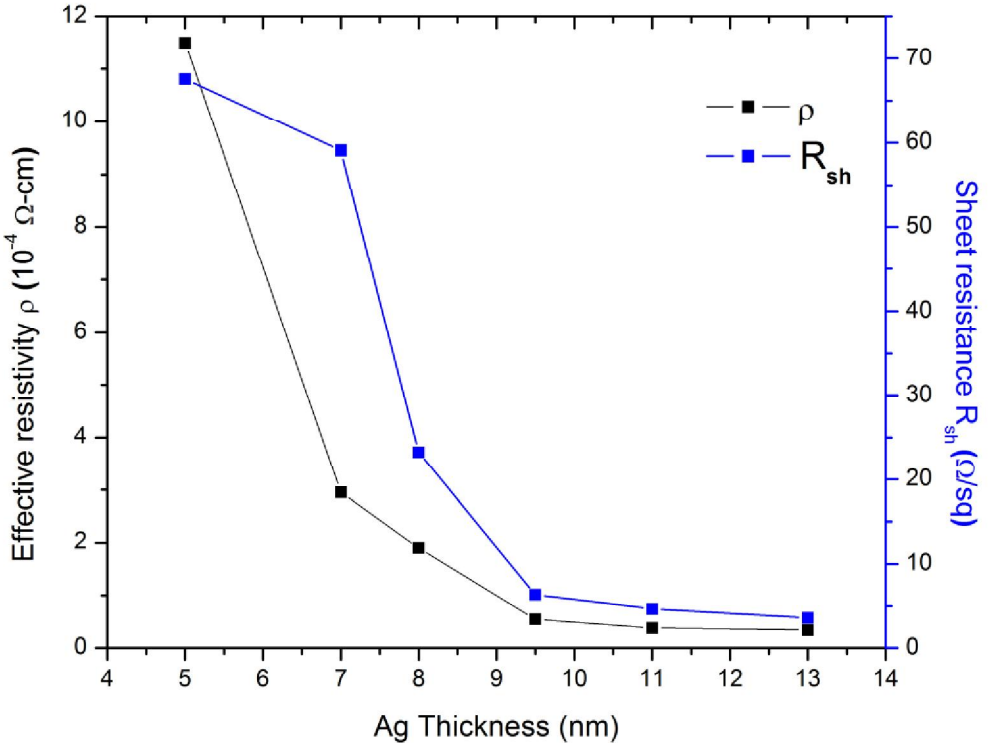

Fig.6.4. Effective resistivity and sheet resistance of TAT multilayer films as a function of Ag thickness.

Conduction through the dielectric dominates when the metal islands are very small and space between islands is large. As the islands grow, the separation between the islands decreases and some of the islands undergo coalesce in large scale. This leads to a radical drop in resistance as observed in lower thickness region of Fig. 6.4. Quantum tunneling occurs between the larger islands with small gaps between them while bulk conduction occurs through the contiguous layer. The effective conductivity (σ) in this region is governed by the following equation [18-19]:

$$\sigma \propto \exp(-2\beta L - \frac{W}{k_B T}) \tag{6.3}$$

where W is the island charging energy, L is the island separation and β is the tunneling exponent of electron wave functions in the insulator, k the Boltzmann constant, and T is the temperature.

A rough surface or interface results in more diffuse scattering and thus increases resistivity of the thin film that can be either surface scattering or grain-boundary scattering. These phenomena are less prominent as the metal thickness approaches the mean free path of the conducting electrons (λ_o). Mayadas and Shatzkes [20] explained that the effect of grain boundary scattering is more predominant in polycrystalline thin films as the grain size are smaller than λ_o. When the Ag islands form a contagious layer, the decrease in resistivity is governed by the combined effect of the increase in carrier concentration of conducting electrons and mobility. At this stage, the dominant factor affecting resistivity was surface boundary scattering. The conductivity (σ) in this region behave according to the following equation [18, 19]

$$\frac{\sigma}{\sigma_0} \propto \frac{3}{4}(1-p)\kappa \log\frac{1}{\kappa} \tag{6.4}$$

Where p is the fraction of the distribution function of the electrons arriving at the surface, σ_o represents the conductivity of the bulk metal, and $\kappa = t/\lambda_o$

Figure 6.5 shows optical transmittance spectra for TiO_2/Ag/TiO_2 (TAT) multilayers on PEN substrate as a function of silver thicknesses. The maximum optical

transmittance of the pure single-layer TiO_2 film is about 95 % in the visible region. TAT multilayers show a maximum transmittance of 90 % for 9.5 nm Ag thickness at ~ 550 nm wavelength.

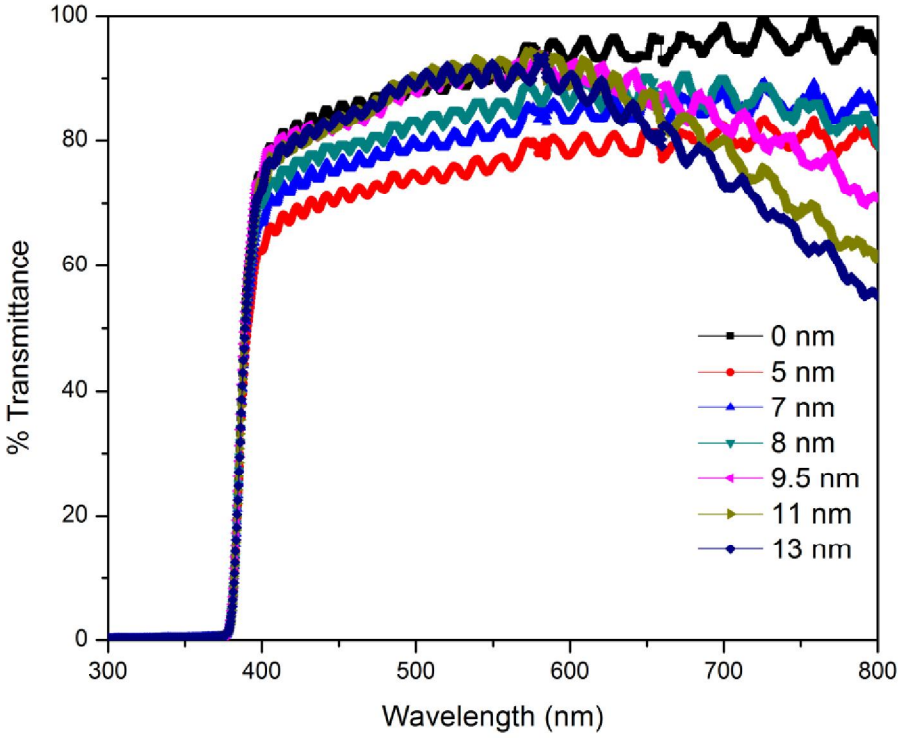

Fig.6.5. Transmittance spectra for TiO_2/Ag/TiO_2 (TAT) multilayers on PEN substrate as a function of silver thickness

It was observed that there is a parabolic increase in average optical transmittance with increasing Ag thickness and also the trend is different for middle (500-600 nm) and longer wavelengths which can be explained based on scattering and absorption by the Ag mid-layer. The difference at 500-600 nm wavelength region is due to light scattering at the TiO_2/Ag interface in Ag isolated islands for Ag thickness below 8 nm and absorption

of light due to interband electronic transitions from the 3*d* to unoccupied levels in the 4*s* band above Fermi level. However, below this thickness, the transmittance decreases because the silver islands are discontinuous. In discontinuous Ag films, a size-dependent variation in the dielectric function was observed due to limitation of the mean free path of the conduction electrons. This leads to a correction to the imaginary part of the overall dielectric function (ε_R) given by [19]:

$$\varepsilon_R = \varepsilon_m + \frac{C}{R} \tag{6.5}$$

Where, ε_m is the dielectric of the bulk metal, c is a constant at a particular wavelength and R is the particle radius. As a result, the transmittance decreases with smaller island size below the critical thickness. As the Ag thickness increases, the Ag becomes a continuous layer from discontinuous islands that causes decrease in light scattering.

In the visible region, higher transmittance was observed which can also be explained on the coupling between the incident light and surface plasmon of the island like structures of Ag thin films [21-23]. However in the longer wavelength (700-800 nm) region the transmittance decreased abruptly for larger Ag thickness (11-13 nm), a trend similar to the optical behavior of bulk metals. In the near IR region, the increase of electron carriers results in low transmission is due to plasmon absorption dependent reflection. From the Drude-Lorentz free electron model, the plasmon frequency (ω_p) can be expressed by the following equation [22-23]:

$$\omega_p = \sqrt{\frac{ne^2}{m\varepsilon_0}} \tag{6.6}$$

Where n is the carrier density of electrons and ε_o is the permittivity of free space.

A figure of merit, $\varphi_{TC,}$ (as defined by Haacke) was estimated for each of the TAT multilayers using the following relationship: [24]

$$\varphi_{TC} = \frac{T_{av}^{10}}{R_{sh}} \tag{6.7}$$

where, T_{av} is the average transmittance and R_{sh} is the sheet resistance. The multilayer with mid Ag thickness 9.5 nm has the best figure of merit with 61.4 x 10^{-3} Ω^{-1} which is the one of the highest FOM reported till date on flexible substrate at room temperature.

6.4. CONCLUSION

In conclusion, different multilayer structures of TiO_2/Ag/TiO_2 have been deposited on PEN, characterized and developed as transparent conductive film with low resistance. Hall measurements and sheet resistance data show that the conductivity of the TAT multilayer is solely due to the Ag mid-layer. The multilayer stack has been optimized to have sheet resistance of 5.7ohm/sq and an average optical transmittance of 90 % at 550 nm. The multilayer with mid Ag thickness 9.5 nm has the best figure of merit with 61.4 x 10^{-3} Ω^{-1}. This makes it possible to synthesize low resistivity electrode at room temperature without using high substrate temperature or post annealing process. Thus the TAT multilayers on PEN substrates can be used as transparent electrode for solar cell and other display application.

CHAPTER 7

OPTIMIZATION OF TiO_2/Cu/TiO_2 MULTILAYER AS TRANSPARENT COMPOSITE ELECTRODE (TCE) DEPOSITED ON FLEXIBLE SUBSTRATE AT ROOM TEMPERATURE

7.1. INTRODUCTION

In recent years, transparent conductive oxides play an integral role in many thin films optoelectronic devices, such as organic light emitting diodes, liquid crystal displays, electro chromic, electroluminescent, flat panel displays and photovoltaic cells [1-5]. TCO thin films are important due to their unique combination of high electrical conductivity and high visible transparency. Recent developments in the area of flexible electronics have generated substantial interest since flexible substrates can overcome the disadvantages (heavy weight and brittleness) of glass substrates. An ideal material for a flexible substrate should be lightweight, tough, dimensionally stable, high thermal stability, moisture and oxygen resistant, resistant towards chemical, and have a low coefficient of thermal expansion. In order to obtain higher speed and superior energy efficiency of optoelectronic devices, transparent electrodes must have high electrical conductivity combined with high transmittance [6-9]. The material most commonly used for transparent electrodes in optoelectronic applications is indium tin oxide (ITO) due to its low resistivity (~ 10^{-4} Ω-cm) and high transmittance (~ 80 %) in the visible region [5-7]. However, the limited supply of indium increases the resulting fabrication costs which

are prohibitive for future industry. Also, a-ITO films deposited on flexible substrates have fairly poor conductivity owing to reduced dopant activation at lower temperatures. These factors have promoted the search for inexpensive materials with good optoelectrical properties. Promising alternative materials includes pure SnO_2, ZnO or ZnO doped with metals (*i.e.,* aluminum (Al), gallium (Ga), indium (In) *etc.*), Nb_2O_5 and TiO_2 have been recently studied as potential alternatives to a-ITO electrodes on flexible substrates [6-15]. Recently, insertion of a very thin metal layer sandwiched between the two TCO layers (TCO/metal/TCO) has been studied to develop a transparent composite electrode (TCE) where various metals like Ag, Cu, Au, Pt, Al *etc.* had been used as the embedded metal layer due to their low resistivities [7-15]. However, to achieve metallic conductivity in TCOs without significant loss in transmittance, the metal layer should be uniform, thin and continuous. Among the metals, although Ag had been widely studied [8-11], but some reports suggests that Cu can have comparable electrical properties and also less expensive [14-16]. In this study, we exploit the conductive properties of thin Cu films and the antireflecting properties of the TiO_2 dielectric by inserting a Cu nanolayer in between two TiO_2 layers on flexible polyethylene naphthalate (PEN) substrates to produce very high transparent and conductive structures. The conduction and transmission mechanisms of the multilayer and the role of copper have been investigated. Titanium dioxide (TiO_2) is a potential semiconductor material with wide band gap (~ 3.2 eV) and a strong mechanical and chemical stability [17-18]. It has many excellent physical properties such as a high dielectric constant and good adhesion to the both polymer and metal substrates. In this work, we report on the optical and electrical

characteristics of thin TiO_2 (30 nm)/Cu (3–9 nm)/ TiO_2 (30 nm) TCEs grown on a PEN substrate by sputtering at room temperature.

7.2. EXPERIMENTAL DETAILS

The TiO_2 / Cu / TiO_2 TCEs were deposited on flexible PEN substrate by rf sputtering of TiO_2 target and dc sputtering of pure Cu target at room temperature. PEN polymer substrates of 125 μm thickness (Dupont Teijin Films, Teonex® Q65) were used. The base pressure of the sputter system prior to each deposition was approximately 1×10^{-7} Torr. The deposition was performed at a pressure of 10 mTorr for both TiO_2 and Cu in pure Ar gas (99.999%) without any vacuum break. The TiO_2 and Cu were deposited using a rf and dc power of 100 W and 40 W, respectively. The target-to-substrate distance was maintained same at 6 cm for all the depositions. The thickness for the top and bottom TiO_2 layers was kept constant at 30 nm while Cu thickness was varied between 3 to 9 nm. Bare TiO_2 was also deposited under identical conditions on PEN to compare the physical properties.

Thickness of the TiO_2 multilayer films were determined using variable angle spectroscopic ellipsometry (VASE) analysis. The optical transmittance of the multilayers was measured using an Ocean Optics double channel spectrometer (model DS200) in the wavelength range of 300–800 nm with air reference for transmittance. Tungsten halogen and deuterium lamps were used as sources for visible and UV light, respectively. Four-point-probe technique equipped with a 100 mA Keithley 2700 digital multimeter was used for sheet resistance measurements. Hall measurements were done using an Ecopia

HMS3000 tool. Electrical resistivity, Hall mobility and carrier concentration of the films were measured by means of the Van der Pauw method. A magnetic field of 0.98 T was applied perpendicular to the sample surface. Surface topography was evaluated using atomic force microscopy (AFM) in acoustic mode (tapping mode), using a Molecular Imaging Pico scanning probe microscope system.

7.3. RESULTS AND DISCUSSION

Figure 7.1 shows the surface topography of the TCE structures as measured by AFM using 1 x 1 μm^2 scans. With the insertion of the Cu layer to the bare TiO_2, the root mean square (rms) roughness changes from 0.8 to 1.7 nm. Henceforth, as the Cu layer thickness increases, the morphology changes from isolated islands to continuous layer and thus the surface roughness gradually decreases. It is expected that the Cu film grown on an amorphous TiO_2 surface should follow the islands growth mechanism of Volmer-Weber model [19-20]. The surface roughness of TCO film plays an important role in determining the optical and electrical properties of the multilayer films; smoother films will have less scattering and hence superior mobility and better transparency.

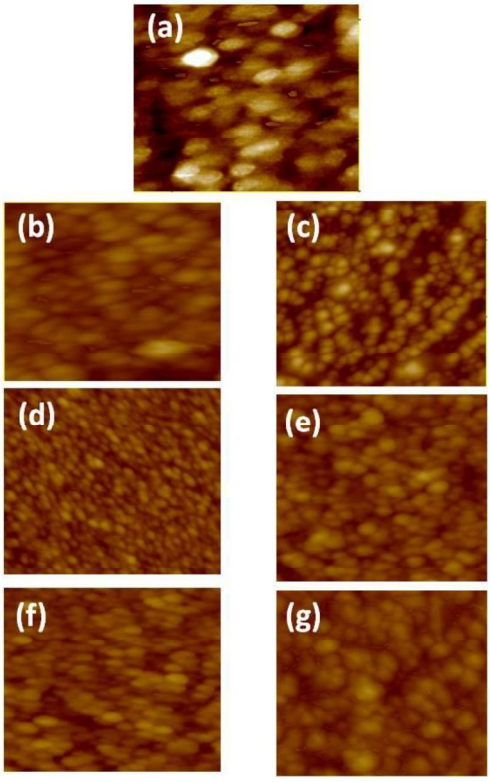

Fig.7.1. AFM images from as-deposited TCEs on PEN for different Cu thicknesses: (a) bare TiO_2, (b) 3 nm Cu, (c) 4.5 nm Cu, (d) 6 nm Cu, (e) 7 nm Cu, (f) 8 nm Cu , and (g) 9 nm Cu.

Figure 7.2. shows the effect of Cu mid-layer thickness on the effective resistivity and sheet resistance of TCE. Inspection of the plots shows that the effective resistivity decreases with increasing thickness of the Cu mid-layer. On addition of a 3 nm Cu thin film between the two TiO_2 layers, the effective resistivity decreases to 9.3 $\times 10^{-4}$ Ω-cm. Now, as the Cu thickness is increased from 3 nm to 9 nm, there is a gradual decrease in resistivity from 9.3 $\times 10^{-4}$ Ω-cm down to 4.9 $\times 10^{-5}$ Ω-cm. A further detailed investigation of the plot showed that the resistivity of the TCE dropped significantly from 3 to 6 nm. This can be attributed due to the presence of small Cu island structures in case of 3 nm

deposition. As the thickness increases, the island size increase and slowly formed a contiguous layer at 6 nm. However, there is a slower drop in the resistivity of the multilayers from 7 to 9 nm of Cu thickness. A detailed investigation depicts the phenomenon of quantum tunneling between the larger islands with small gaps between them while bulk conduction occurs through the contiguous layer.

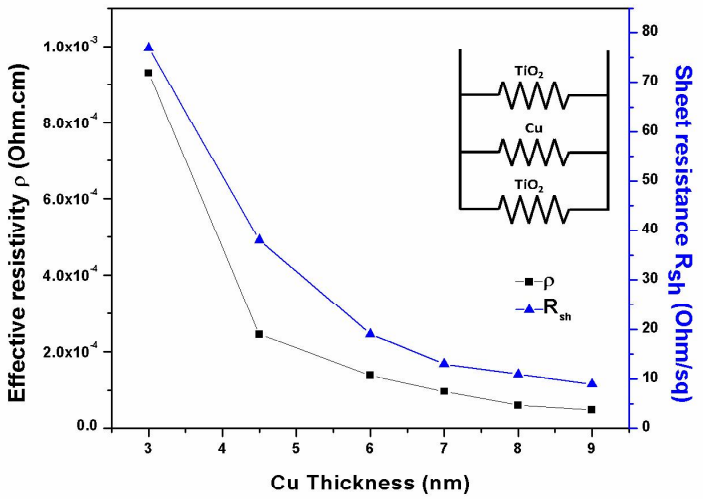

Fig.7.2. Effective resistivity and sheet resistance of TiO_2/Cu/TiO_2 multilayer films as a function of Cu thickness.

Figure 7.2 also shows a similar change in sheet resistance as a function of Cu thickness. Here also, we see a significant decrease in sheet resistance from 10^4 Ω/sq to 77 Ω/sq with the insertion of Cu layer to the bare TiO_2. Further, the sheet resistance drops significantly to 13 Ω/sq at 7 nm Cu thickness. At 9nm thickness, the Cu forms a thin uniform layer and thus behaves similar to the bulk metal.

Figure 7.3 shows the change in carrier concentration as a function of Cu thickness for TCEs. The carrier concentration increased remarkably by 3 folds of magnitude from 10^{19} to 10^{22} cm^{-3} on addition of 3 nm Cu layer to the bare TiO_2. The plot

indicates that carrier concentration depends strongly on the Cu thickness. The carrier concentration of the TCEs has increased from 1.3×10^{22} to 4.4×10^{22} cm^{-3} upon increase of Cu thickness from 3 nm to 9 nm. Hence, metallic conduction is taking place in this TCE system.

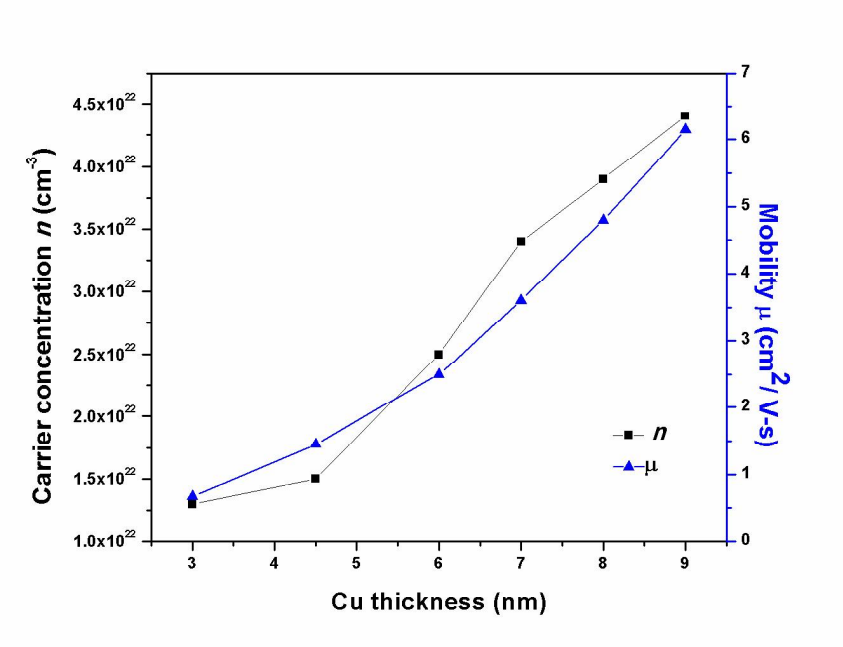

Fig.7.3. Carrier concentrations and mobility of TCE as a function of Cu thickness.

The mobility can be affected by different scattering mechanisms such as phonon scattering, interface scattering, grain-boundary scattering, surface scattering, and ionized-impurity scattering. Due to the amorphous nature of TiO_2, grain boundary scattering can be ruled out. The presence of isolated Cu island structures leads to island boundary scattering at TiO_2/Cu interface while interface scattering is the dominant mechanism at the bulk thickness.

Table7.1. discuss about the impact of interface quality on the optical and electrical properties of the bilayer and multilayer films. The thin film with top TiO_2/Cu is

seen to have moderate drop in the optical transmittance followed with a little detoriation in the electrical properties. The drop in the optical transmittance is due to the absence of the anti-reflecting TiO_2 layer on the bottom. However in case of Cu/bottom TiO_2, a little improvement was observed in the electrical properties due to the top Cu layer. But the optical transmittance dropped significantly in the near IR region due to the typical high reflection property of the metals.

	TiO_2/PEN (60 nm)	**TiO_2/Cu/PEN (30/6 nm)**	**Cu/TiO_2/PEN (6/30 nm)**	**TiO_2/Cu/TiO_2/PEN (30/6/30 nm)**
Resistivity (Ω-cm)	10^{-1}	2.6 x 10^{-4}	1.1 x 10^{-4}	1.4 x 10^{-4}
Mobility(cm^2/V-s)	0.07	2.35	2.9	2.5
Career concentration (cm^{-3})	10^{19}	2.5 x 10^{22}	3.2 x 10^{22}	2.7 x 10^{22}
Sheet resistance (Ω/sq)	10^4	17.6	14.4	16.2
Transmittance (%)	95	57	41	83

Table7.1. Comparison of optical and electrical properties of single layered TiO_2, bilayered TiO_2/Cu and TiO_2/Cu/TiO_2 multilayered thin films

Figure 7.4. shows optical transmittance spectra for TCE on PEN substrate as a function of copper thicknesses. These spectra show a steady decrease of transmittance

with increase of Cu thickness. The maximum optical transmittance of a single-layer TiO_2 film of 60 nm thickness is about 95 % in the visible region.

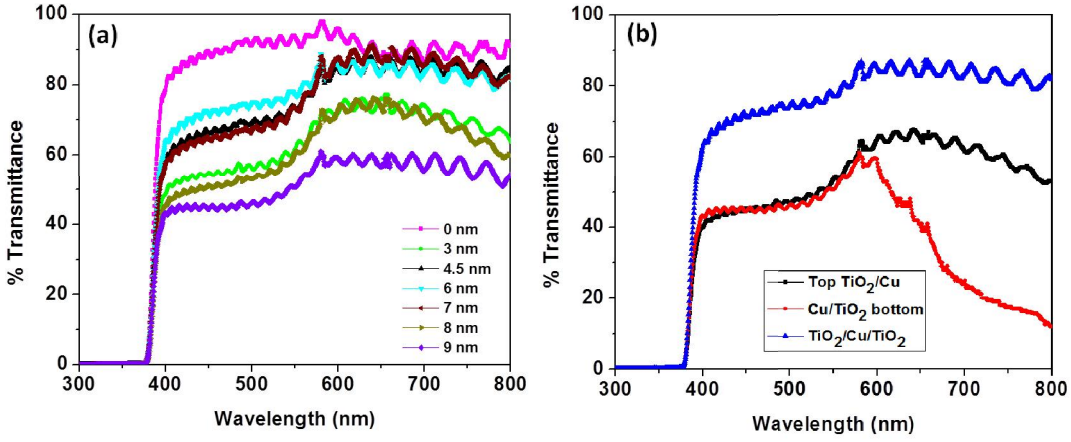

Fig.7.4. (a) Transmittance spectra for TCE multilayers as a function of copper thickness. (b) Comparison of optical transmittance of different bilayered TiO_2/Cu and TiO_2/Cu/TiO_2 multilayered thin films

The decrease in transmittance due to the addition of the Cu middle layer can be attributed to the reflectivity of the free electrons of the metal. However for the TCEs in Fig. 7.4 (a), increasing the Cu thickness from 3 to 6 nm results in little or no decrease in the optical transmittance with average optical transmittance around 80 % at ~ 630 nm wavelength. At lower wavelength region (500-600 nm), the decrease in transmittance is due to absorption of light by interband electronic transitions At a higher Cu thickness of 7-8 nm, a fairly low transmittance of 70 % is observed at a wavelength of 630 nm due to the absorption by the aggregated Cu islands. The transmittance drops sharply from ~ 70 % to 55 % with a further increase in the Cu thickness to 9 nm. This is attributed to the increase in reflectivity of the contiguous islands of Cu layer that has typical electrical conduction characteristic similar to metals. In case of metals, the

increase of electron carriers results in low transmission which is due to plasmon absorption dependent reflection. The plasmon frequency (ω_p) can be expressed from Drude-Lorentz theory by the following equation [24-25]:

$$\omega_p = \sqrt{\frac{ne^2}{m\varepsilon_0}} \tag{7.1}$$

An ongoing research had been done in the Alford Group to fit optical properties of TCE multilayer films with theoretical simulation. A theoretical model is developed and validated using transfer-matrix method [21-23] to efficiently undergo materials selection and design thickness for developing TCEs for future optoelectronics applications. The details of the model and the theoretical validation are beyond the scope of this letter and will be published in the near future.

A figure of merit, $\varphi_{TC,}$ (as defined by Haacke [27]) was estimated for each of the TCEs using the following relationship:

$$\varphi_{TC} = \frac{T_{av}^{10}}{R_{sh}} \tag{7.2}$$

Where, T_{av} is the average transmittance and R_{sh} is the sheet resistance.

The multilayer with mid Cu thickness 6 nm has the best figure of merit 6.4×10^{-3} Ω/sq among the various TCEs. Below 6 nm, the poor FOM value corresponds to low average transmittance and high sheet resistance due to discontinuous Cu island growth as discussed earlier. Table 1 compares the optical and electrical properties of single layered TiO_2 with TiO_2/Cu/TiO_2 multilayered thin films. The TCE multilayer has improved several folds in both electrical and optical properties compared to the bare TiO_2. The

insertion of a thin and uniform 6 nm thick Cu layer had reduced the FOM to 6.4×10^{-3} Ω/sq from 5×10^{-6} Ω/sq in case of a single layered TiO_2 thin film.

7.4. CONCLUSION

Different multilayer structures of $TiO_2/Cu/TiO_2$ had been deposited on PEN, characterized and optimized as TCEs with superior opto-electrical properties. The conductivity mechanism of the TCE multilayer is solely due to the Cu mid-layer. The multilayer stack has been optimized to have sheet resistance of 19 ohm/sq and an average optical transmittance of 81 % at 630 nm at room temperature with no post-deposition anneals. The improved FOM of the optimized TCE is due to the better electrical performance on addition of the middle Cu layer. Thus the $TiO_2/Cu/TiO_2$ multilayers on PEN substrates can be used as cheap transparent conductive electrode (TCE) for flexible optoelectronics applications.

CHAPTER 8

HIGH QUALITY TiO_2/Au/TiO_2 MULTILAYERS AS TRANSPARENT COMPOSITE ELECTRODE ON FLEXIBLE SUBSTRATE

8.1. INTRODUCTION

Transparent conducting oxides (TCOs) are unique class of materials that are essential components for a large variety of optoelectronics applications. TCOs act as a transparent electrodes or electrical contacts in flat-panel displays (*e.g.*, LCDs), solar cells, electromagnetic shielding of CRTs used for video display terminals [1-4], electrochromic windows and low-emissivity windows in buildings. Transparent conducting oxides (TCOs) are wide band gap semiconductors which are optically transparent and show conductivities intermediate to metals and semiconductors. The key requirement for the TCO applications is that optical transmittance (%T) should be greater than 80%, while resistivity (ρ) is less than 10-4 Ω-cm [5,6]. In this regard, a lot of research has been going to find an ideal material with optimum optical and electrical properties. A good understanding of the fundamental materials structure/property relationships is required to elucidate the present challenge for achieving novel materials that retains optical transparency while becoming more electrically conductive.

The material most commonly used for transparent electrodes in optoelectronic applications is indium tin oxide (ITO) due to its low resistivity (~ 10^{-4} Ω-cm) and high transmittance (~ 80 %) in the visible region [5]. However, the limited supply of indium

increases the resulting fabrication costs are prohibitive for future industrial implementation. Also, a-ITO films deposited on flexible substrates have fairly poor conductivity owing to it limited low process temperatures and reduced dopant activation at lower temperatures. These factors have promoted the search for inexpensive materials with good electricoptical properties. Promising alternative materials includes pure SnO_2, ZnO or ZnO doped with metals (*i.e.,* aluminum (Al), gallium (Ga), indium (In)), Nb_2O_5, TiO_2 *etc* have been recently studied as potential alternatives to a-ITO electrodes on flexible substrates [5-10]. Recently, insertion of a very thin metal layer sandwiched between the two TCO layers has been studied to develop a transparent composite electrode (TCE) with the desired electrical conductivity [10-12]. A lot of research had been ongoing with using Ag and Cu as the middle layer [7-12]. However, Au is another potential metal to substitute Ag as the inter metallic layer. Although, it is far costlier than Ag, the chemical inertness and stability of Au is an advantage for device fabrication. It is well known that thin gold films show good transmission properties. In this study, we exploit the transmittive properties of thin gold films and the antireflecting properties of the TiO_2 dielectric by inserting a gold nanolayers in between two TiO_2 layers on flexible polyethylene naphthalate (PEN) substrates to produce very high transmittivity and conductivity structures. The conduction and transmission mechanisms and the role of gold are investigated. Titanium dioxide (TiO_2) is such a potential semiconductor material with wide band gap (~ 3 eV) and good adhesion to the both polymer and metal substrates [13, 14]. In this work, the high transparency of TiO_2 in visible region and low resistivity of thin Au layer lead to the detailed study of optical and electrical properties of TiO_2/Au/TiO_2 (TAuT) multilayers as transparent composite electrode (TCE).

8.2 EXPERIMENTAL DETAILS

Thin film of TiO_2/Au/TiO_2 tri-layered structures were sequentially sputter deposited at room temperature onto flexible polyethylene napthalate (PEN) substrate in a magnetron sputter deposition system equipped with DC and RF power suppliers. Prior to deposition, the chamber was evacuated to a base pressure of approximately 2×10^{-7} Torr. A sputter ceramic target of pure TiO_2 (99.999% purity, 5.08 cm diameter and 0.64 cm thickness) was used for the oxide layer and pure Au foil (99.99% purity, 5.08 cm diameter and 0.01 cm thickness) was used for the metal layer. PEN polymer substrates of 125 μm thickness (Dupont Teijin Films, Teonex® Q65) were used. The substrate was ultrasonically cleaned in isopropanol and acetone and subsequently dried in N_2 before deposition. The sputtering was performed in pure argon atmosphere (99.999%) at a pressure of 10 mTorr for both TiO_2 and Au with a target to substrate distance of 6 cm without any vacuum break. The TiO_2 and Au were deposited using an RF power of 150 W and DC power of 40 W, respectively. The thickness of the top and bottom TiO_2 layers were same at approximately 30 nm and those of Au were varied between 4 and 17 nm. The film thicknesses of the TAuT multilayer were determined using optical ellipsometry. Surface morphology of different Au thicknesses was observed by scanning electron microscope (XL30 ESEM, Philips) at an operating voltage of 20 kV Optical transmittance of the multilayers were measured using an Ocean Optics double channel UV-Vis spectrometer (model DS200) in the wavelength range of 300–800 nm with air reference for transmittance. Hall measurements were done using an Ecopia HMS3000 tool by means of the Van der Pauw method. A magnetic field of 0.98 T was applied

perpendicular to the sample surface. Four-point-probe technique was used for sheet resistance measurements. The TCE thin films were annealed upto 150 ^{o}C in vacuum, forming gas, air and O_2 for 24 hours.

8.3 RESULTS AND DISCUSSION

A systematic study is done in order to determine the effect of Au mid-layer on the opto-electrical properties of multilayer thin films. The most vital factor that influences the performance of the composite is the morphology of the middle metal layer. According to Volmer-Weber model [15, 16], the Au film growing on an amorphous TiO_2 surface should follow the islands growth mechanism of which is verified from the SEM image in Fig. 1. The SEM images correspond to different Au thickness before and after the critical thickness of 10 nm. Figure 8.1(a) shows the presence of island structures at 7 nm which gradually form contagious as it approaches the critical thickness. Finally, the Au islands form a uniform continuous layer [Fig.8.1 (b)] at 14 nm.

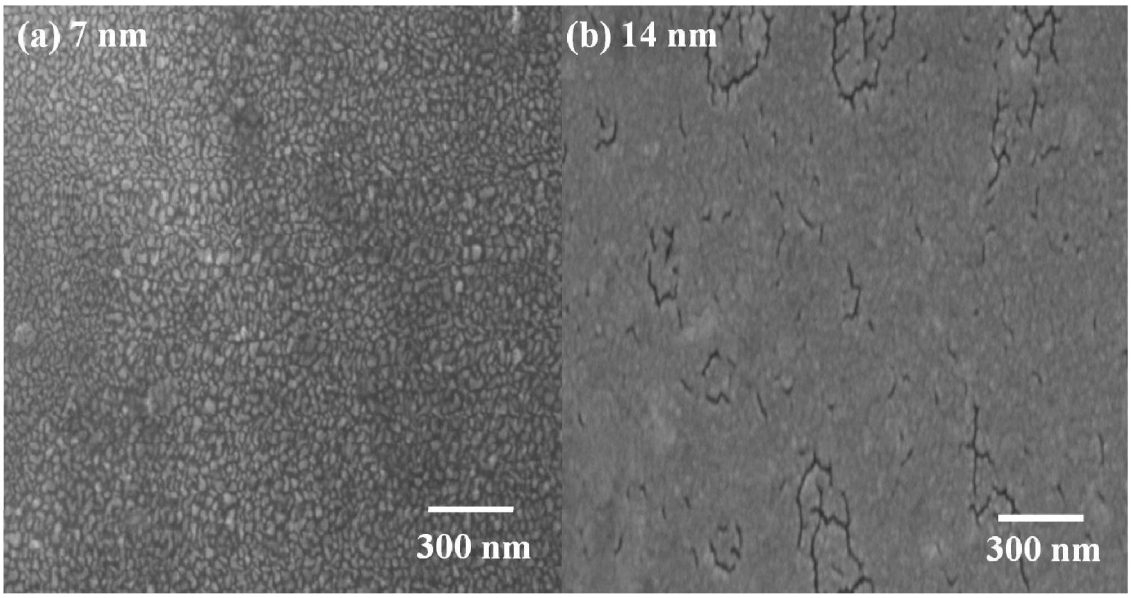

Fig. 8.1 SEM images of Au thin film deposited on bottom TiO_2 surface with different Au thicknesses: (a) 7 nm, (b) 14 nm.

Figure 8.2 shows the change in carrier concentration and Hall mobility as a function of Au thickness for various TAuT multilayers. The plot indicates that carrier concentration depends strongly on the Au thickness. The carrier concentration of the TAuT multilayer has increased from 3.3×10^{21} to 1.4×10^{22} cm^{-3} upon increase of Au thickness from 4 to 17 nm, respectively. Hence, metallic conduction is dominant in this TAuT system. There is a rapid increase in Hall mobility that occurs with increasing Au layer thickness from 5.4 cm^2/V-s (at 4 nm) to 10.3 cm^2/V-s (at 17 nm), respectively. There are many scattering mechanisms such as phonon scattering, grain-boundary scattering, surface scattering, interface scattering, and ionized-impurity scattering [7-9]. In our TCE, interface scattering takes place above the critical thickness of 10 nm; whereas, island boundary scattering dominates at the TiO_2/Au interface below the critical thickness due to the

presence of Au island structures. These boundaries are expected to have fairly high densities of interface states that scatter free carriers due to the presence of trapped charges and inherent disorders. As a result, a space charge region is created in the island boundaries and this produces potential barriers to charge transport due to band bending.

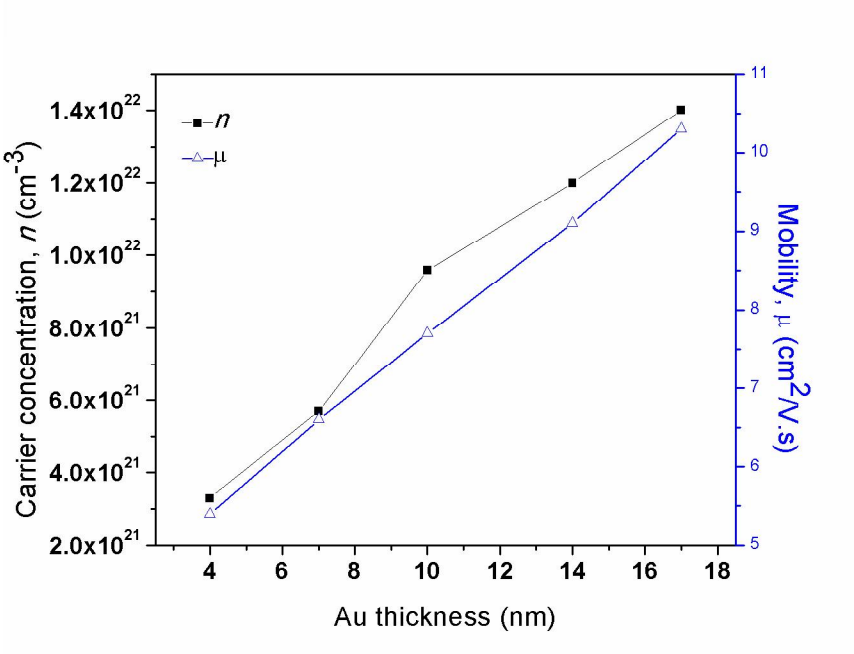

Fig. 8.2 Carrier concentration and Hall mobility as a function of Au thickness for TAuT multilayers.

Figure 8.3 shows the effect of Au mid-layer on the resistivity and sheet resistance of TAuT multilayers, where both decrease with increasing thickness of the Au mid-layer. The TiO_2 used in our study is an insulator with resistivity of the order 10^7 Ω-cm. Upon the deposition of a 4 nm Au film between the TiO_2 layers, the resistivity decreases to 7.4×10^{-4} Ω-cm and suggests that there is a 11 fold decrease in resistivity in TAuT multilayers when compared to bare TiO_2. As the Au thickness is increased from 4 nm to 17 nm, the effective resistivity gradually decreases down to 5.3×10^{-5} Ω-cm. A more

detailed assessement of Fig. 3 shows that the effective resistivity of the TAuT multilayers drops significantly for thicknesses 4 to 10 nm and thus indicates the presence of small Au island structures in case of 4 nm deposition. However, there is a slow decrease in the effective resistivity of the multilayers for thicknesses over the range 10 to 17 nm with TAT multilayers approaching the resistivity of bulk gold (2.4×10^{-6} Ω-cm). The change in effective resistivity of the TAT multilayer films with increasing Au thickness can be explained using the following basic relation:

$$\rho_{eff} = \frac{1}{n\mathrm{e}\mu} \tag{8.1}$$

The sheet resistance curve follows similar trend to that of resistivity as a function of Au thickness achieving values close to that of bulk Au for thicknesses of 14 nm or greater. Here also, we see a rapid decrease in sheet resistance from 34.5 Ω/sq to 12.2 Ω/sq as the mid-Au layer increases from 4 to 10 nm.

Figure 8.3 shows the effect of Au mid-layer on the effective resistivity and sheet resistance of the TAuT multilayers where both parameters decrease with increasing thickness of the Au mid-layer. From the microstructure of the Au thin film, it is clear that the Au film has islands below the critical thickness (t_c) and gradually became uniform after t_c. Thus, a different conduction mechanism is expected before and after critical thickness.

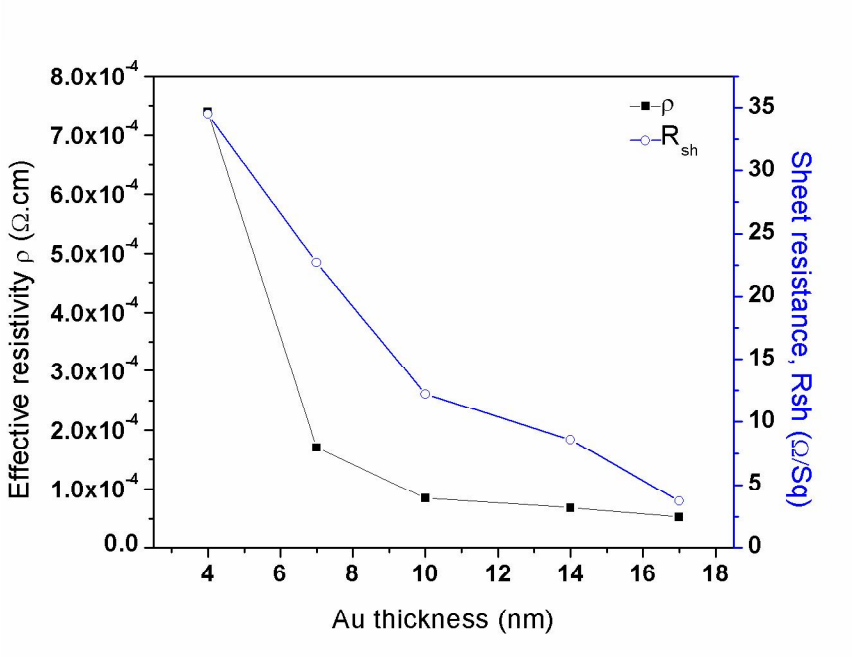

Fig. 8.3 Effective resistivity and sheet resistance of TAuT multilayer films as a function of Au thickness.

As the islands grow, the separation between the islands decreases and some of the islands undergo coalesce in large scale. This leads to a radical drop in resistance as observed in lower thickness region of Fig. 8.4. Quantum tunneling occurs between the larger islands with small gaps between them while bulk conduction occurs through the contiguous layer. A rough surface or interface results in more diffuse scattering and thus increases resistivity of the thin film that can be either surface scattering or grain-boundary scattering. These phenomena are less prominent as the metal thickness approaches the mean free path of the conducting electrons (λ_o). When the Au islands form a contagious layer, the decrease in resistivity is governed by the combined effect of the increase in carrier concentration of conducting electrons and mobility.

Figure 8.4 shows optical transmittance spectra for TiO_2/Au/TiO_2 (TAuT) multilayers on PEN substrate as a function of gold thicknesses. TAuT multilayers show a maximum transmittance of 86 % for 10 nm Au thickness at ~ 550 nm wavelength. In the TAuT multilayered structure, TiO_2 acts as the layers for transmitting light. Typically, the light absorption in this type of layer is so small that it can be neglected. Most of the light transmits through this transparent oxide layer. Although there is a large degree of reflection at the metal and oxide interface, the light reflected from the back surface will again be bounced back from the air/TiO_2 interface and then some portion of the light will penetrate through the air/oxide interface, and the rest of the light will experience the similar multiply reflections process in the oxide layer [11]. The sum of all the transmission is the light transmitted through the oxide layer [11]. The advantage of the multiply reflections happened in oxide layer is it successfully constrains the light reflected from the oxide/metal interface in oxide layer and force those reflected light enter into the metal layer by the reflection at the air/oxide interface. Hence, it allows more light enter into metal layer, compared to the structure where has no transparent oxide layer on top of the thin metal layer.

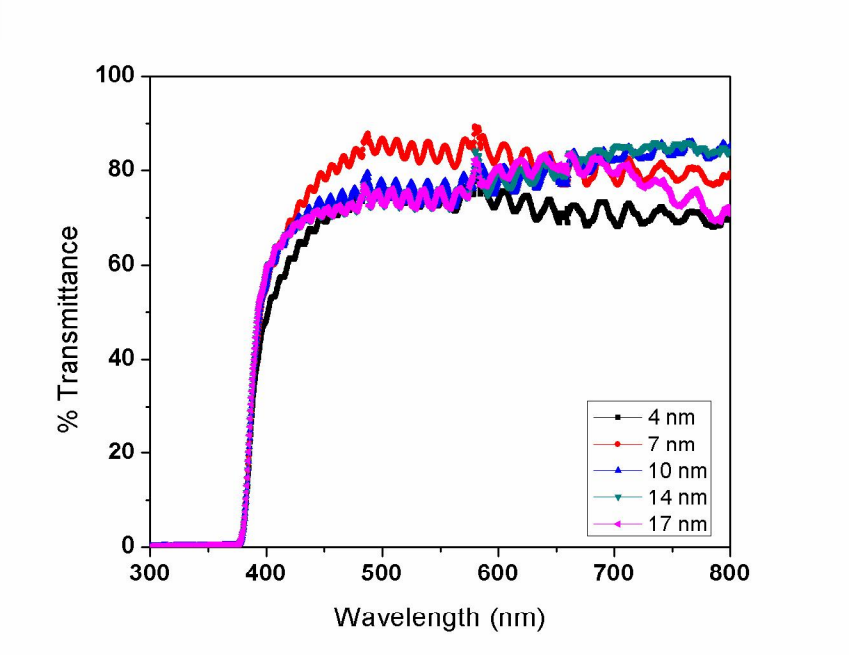

Fig 8.4. Transmittance spectra for $TiO_2/Au/TiO_2$ (TAuT) multilayers on PEN substrate as a function of gold thickness

Metals show different optical properties from dielectric oxides materials. Bulk metals are a good reflector and hardly transmits light in visible light region. The free carriers in metal interact with light (magnetic field), and experience interband and intraband transition of electrons, leading to the light absorption and low transmittance in visible and near ultra-violet region [22, 23]. That explains why the copper and gold look reddish and yellowish under the sunlight. However when the thickness of metal goes down below a certain point, the metal thin film can transmit light over the whole visible light spectrum. Depending on the deposition times and conditions, the formation of thin film experiences isolated islands, continuous islands and complete thin film. The topography of the thin film strongly affects its optical properties. In case of metal thin films with islands, the absorption band of films depends on the islands' (particles') size

[22, 23]. Small islands (particles) results in wide absorption bands since its conductivity σ is low when the particle size is less than the mean free path of electrons in the particle [22, 23]. However, when the film becomes thicker and the islands become continuous, the theory for islands film is invalid, therefore, the maximum absorption band cannot be predicted by above equations [22, 23]. I n the visible region, higher transmittance is observed and can also be explained by the coupling between the incident light and surface plasmon of the island like structures of Au thin films [21-23]. However in the longer wavelength (700-800 nm) region the transmittance decreased abruptly for larger Au thickness (14-17 nm). This trend is similar to the optical behavior of bulk metals. In the near IR region, the increase of electron carriers results in low transmission is due to plasmon absorption dependent reflection. From the Drude-Lorentz free electron model, the plasmon frequency (ω_p) can be expressed by the following equation [22,23]:

$$\omega_p = \sqrt{\frac{ne^2}{m\varepsilon_0}} \tag{8.2}$$

where n is the carrier density of electrons and ε_o is the permittivity of free space.

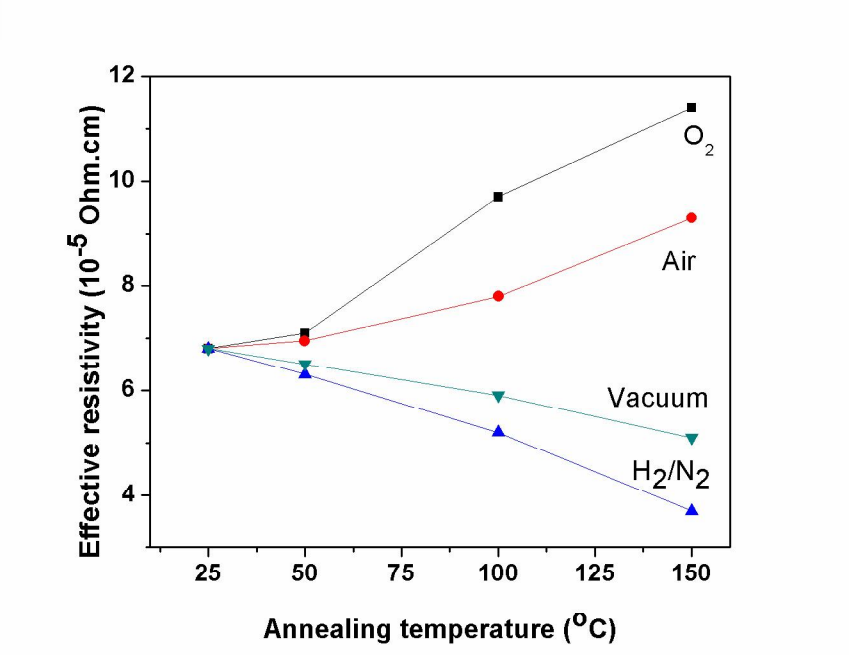

Figure 8.5 Effect of annealing on the effective resistivity of the TCE in different ambients

Post-deposition, the TAuT multilayer (30/10/30) was annealed in different ambients. Figure 8.5 shows the effect of annealing on the effective resistivity of the TCE. It was seen that the resistivity decreased in case of vacuum and forming gas but went higher for air and O_2. A possible explanation can be absorption of the O_2 adsorbed on the TCE surface. Also, forming gas and vacuum can create more vacancy in the metal oxides and thus improve the conductivity.

A figure of merit, $\varphi_{TC,}$ (as defined by Haacke [24]) was estimated for each of the TAuT multilayers using the following relationship:

$$\varphi_{TC} = \frac{T_{av}^{10}}{R_{sh}} \tag{8.3}$$

where, T_{av} is the average transmittance and R_{sh} is the sheet resistance. The multilayer with mid Au thickness 10 nm has the best figure of merit with 18 $\times 10^{-3}$ Ω^{-1}

8.4 CONCLUSION

In conclusion, different multilayer structures of TiO_2/Au/TiO_2 have been deposited on PEN, characterized and developed as transparent conductive film with low resistance. Hall measurements and sheet resistance data show that the conductivity of the TAuT multilayer is solely due to the Au mid-layer. The multilayer stack has been optimized to have sheet resistance of 12.2 Ohm/sq and an average optical transmittance of 86 % at 550 nm. The multilayer with mid Au thickness 10 nm has the best figure of merit with 18×10^{-3} Ω^{-1}. This makes it possible to synthesize low resistivity electrode at room temperature without using high substrate temperature or post annealing process. Thus the TAuT multilayers on PEN substrates can be used as transparent electrode for solar cell and other display application.

CHAPTER 9

CONCLUSION

9.1 SUMMARY OF RESEARCH

In conclusion, the research done in this dissertation has enabled a detailed study of the structure-property relationship and optimization of two types of transparent electrode on flexible substrate with a view to engineer them for improved optoelectronics applications. The work focused on optimizing Indium gallium zinc oxide thin films with low indium content and a new indium free multilayered transparent composite electrode, making them an effective low cost alternative to indium tin oxide, the most used transparent conducting oxides in the industry.

The first study was on the optimization of a mixed oxide – Indium gallium zinc oxide (IGZO) on both glass and flexible PEN substrates. Highly transparent and conductive thin films of indium gallium zinc ozide (IGZO) of varying thicknesses (25-150 nm) were deposited onto glass and PEN substrates by RF sputtering at room temperature. A systematic investigation of film thickness dependence on the structural, optical and electrical properties was done. The Haacke figure of merit (FOM) had been calculated to evaluate the performance of the different thin films and the 100 nm thick film had the best FOM value of $20.3 \times 10^{-4}\ \Omega^{-1}$. The annealed films showed superior opto-electrical properties in vacuum and forming gas. The wettability of both as-deposited and annealed thin films had been studied and efficiently controlled by engineering surface topography. The as-deposited IGZO film showed hydrophobic behavior while the annealed films were distinctly hydrophilic with contact angle of around 63.5° against water.

The second study was on the improved processing of the above mixed oxide IGZO thin films for superior optical and electrical properties. Amorphous Indium Gallium zinc oxides (IGZO) of 100 nm thickness were deposited onto glass substrates by sputtering at room temperature. The films were subsequently annealed in air, vacuum, forming gas and O_2 environments by both conventional and microwave methods. The optical and electrical properties of the as-deposited and annealed samples were measured and compared. It was seen that microwave annealing had a dual advantage of reduced time and lower temperature compared to conventional annealing. The optical and electrical properties of the IGZO thin films were measured UV–Visible spectrophotometry, Hall measurement and four point probe analyses. On microwave anneals of 4 minutes at 200 ^{o} C, the resistivity of IGZO thin films was lowered to 4.45 and 4.24 x 10^{-3} ohm-cm in vacuum and forming gas, respectively. However in conventional annealing at 400 ^{o} C, it took 24 hours to reach 4.5 and 4.2 x 10^{-3} ohm-cm in vacuum and forming gas, respectively. The average transmittance of IGZO improved from 80% to almost 86% for microwave annealing.

In the next chapter, a new multilayered indium free transparent composite electrode was developed. This dielectric/metal/dielectric multilayered structure can exhibit better electrical and optical properties than a single layered TCO thin film. Different multilayer structures of Nb_2O_5/Ag/Nb_2O_5 have been deposited onto flexible substrates by sputtering at room temperature to develop an indium free transparent composite electrode. The effect of Ag thickness on the electrical and optical properties of the multilayer stack has been studied in accordance with the Ag morphology. The critical thickness of Ag to form a continuous conducting layer is found to be 9.5 nm. A new

conduction mechanism has been proposed to describe the conduction before and after the critical thickness. The effective Hall resistivity of the optimized films is as low as 6.44 x 10^{-5} Ω-cm with a carrier concentration and mobility of 7.4 x 10^{21} cm^{-3} and 13.1 cm^2/V-s, respectively at the critical Ag layer thickness. The multilayer stack has been optimized to obtain a sheet resistance of 7.2 Ω/sq and an average optical transmittance of 86 % at 550 nm without any substrate heating or post-annealing process. The Haacke figure of merit (FOM) has been calculated for the films, and the multilayer with a 9.5 nm thick Ag layer has the highest FOM at 31.5 x 10-3 Ω/sq. A detailed study was done on the post-deposition annealing of the above mentioned Nb_2O_5/Ag/Nb_2O_5 TCE for improved opto-electrical properties. The samples were annealed upto 150 ^oC in various environments like air, O_2, vacuum and forming gas.

The next work was on the same TCE structure with a very cheap material like TiO_2 as a low cost alternative to ITO. Multilayer structures of TiO_2/Ag/TiO_2 have been deposited onto flexible substrates by room temperature sputtering to develop indium-free transparent composite electrodes. The effect of Ag thicknesses on optical, electrical properties and the mechanism of conduction have been discussed. The study revealed that the inner meatl layer is the sole contributor for the electrical properties of the entire stack. The critical thickness (t_c) of Ag mid-layer to form a continuous conducting layer is 9.5 nm and the multilayer has been optimized to obtain a sheet resistance of 5.7 ohm/sq and an average optical transmittance of 90 % at 590 nm. The Haacke figure of merit (FOM) for t_c has FOM with 61.4 x 10^{-3} Ω/sq, which is one of the highest FOM values reported for TCE deposited at room temperature on a flexible substrate.

Finally, a similar follow up study was done on the same TiO_2/metal/TiO_2 TCE with different metals like Cu and Au. The motivation for selecting Cu was that it was cheap and widely used in semiconductor industry. Although the resistivity of bulk Cu is lower than Au, the optical transmittance of the Cu-based TCEs is lower compared to Au. As a result, The FOM of Au based TCE was higher than that of Cu. The advantage with gold is its chemical inertness and lower diffusion problems. Thus, the TiO_2/metal/TiO_2 multilayers on PEN substrates can be used as cheap transparent conductive electrode (TCE) for flexible optoelectronics applications.

9.2. FUTURE WORK

It would be very interesting to fabricate the different dielectric/metal/dielectric multilayer TCEs in some optoelectronic devices, such as organic photovoltaics, organic light emitting diodes, flat-panel displays and analyze the device performance. A lot of study can be done on the impact of long anneals and different ambients on the device performance and stability owing to improvement in the interface quality. The other important study on the device performance includes detailed understanding of the different layer thicknesses and surface morphology.

Another important aspect is to understand the mechanical properties of the IGZO and TCE thin films on flexible polymer substrates. Also, the thin films deposited on plastic substrates may be exposed to humidity at different temperatures for moisture uptake. It would be interesting to investigate the effects of mechanical stress and electrical stress on the electrical and optical properties of the thin films.

REFERENCES

CHAPTER 1

[1] D.S. Ginley and C. Bright., MRS Bulletin, 2000. **25**.

[2] J.C.C. Fan and J.B. Goodenough., Journal of Applied Physics, 1977. **48**.

[3] 3. R.G. Gordon, MRS Bulletin, 2000. **25**.

[4] 4. H. Kawazoe, M. Yasukawa, and M. Hyodou., Nature, 1997. **389**.

[5] H. Hosono, Thin Solid Films, 2007. **515**.

[6] T. Dutta , N. C. State University, **2011**

[7] K.Badeker, *Annals of Physics* **1907,** (22), 749.

[8] G. Haacke, *J. Appl. Phys*. **47**, 4086 (1976).

[9] G.J. Exarhos and X.D. Zhou, Thin Solid Films, 2007. **515**: p. 7025.

[10] J.R. Bellingham, W.A. Phillips, and C.J. Adkins., J.Mater.Sci.Lett., 1992. **11**.

[11] H. Brooks., *Advances in Electronics and Electron Physics*, L. Martin., Editor. 1955, New York: Accademic: New York.

[12] R.L. Petriz., Physical Review 1956. **104**.

[13] M. Chen, Z.L. Pei, X. Wang, Y.H. Yu, X.H. Liu, C. Sun, and L.S. Wen, Journal of Physics D: Applied Physics., 2000. **33**.

[14] K.Ellmer., Journa of Physics D, 2001. **34**.

[15] F. Simonis, M.V. Leij, and C.J. Hoogendoorn, solar energy materials, 1979. **1**.

[16] J.C.C Fan and J.B. Goodenough., Journal of applied physics, 1977. **48**.

[17] O.N. Mryasov and A.J. Freeman., physical Review B, 2001. **64**.

[18] E. Burnstein., Physical Review, 1954. **93**.

[19] I. Hamberg and C.J. Granqvist, Journal of Applied Physics, 1986. **60**. 90

[20] A.P. Roth, J.B. Webb, and D.F. Williams., physical Review B, 1982. **25**.

[21] T. Minami., Semicond. Sci. Techno., 2005. **20**.

[22] T. Minami, MRS Bulletin, 2000. **25**.91

[23] M. Hiramatsu, K. Imaeda, N. Horio, and M. Nawata, Journal of Vacuum Science and Technology A, 1998. **16**.

[24] P.K. Song, M. Watanabe, M. Kon, A. Mitsui, and Y. Shigesato., Thin Solid Films, 2002. **82**.

[25] T. Minami., Journal of Vacuum Science and Technology A, 1999. **17**.

[26] T. Minami., Thin Solid Films, 2008. **516**.

[27] K.L. Chopra, S. Major, and a.D.K. Pandya., Thin Solid Films, 1983. **102**.

[28] C. Guillén, J. Herrero , Thin Solid Films **520** (2011) 1

[29] C. Guillén, J. Herrero, Opt. Commun. 282 (2009) 574.

[30] Y.S. Park, K.H. Choi, H.K. Kim, J. Phys. D: Appl. Phys. 42 (2009) 235109, 7

[31] J.A. Jeong, H.K. Kim, Sol. Energy Mater. Sol. Cells 93 (2009) 1801.

[32] D.R. Sahu, S.Y. Lin, J.L. Huang, Appl. Surf. Sci. 252 (2006) 7509.

[33] C. Guillén, J. Herrero, Phys. Status Solidi A 207 (2010) 1563.

CHAPTER 2

[1] G. Gustafsson, Y. Cao, G.M. Treacy, F. Klavetter, N. Colaneri, and A. J. Heeger, *Nature* **357**, 477 (1992).

[2] D. C. Look, K. D. Leedy, D. H. Tomich, and B. Bayraktaroglu, *Appl. Phys. Lett.* **96**, 062102 (2010).

[3] A. Dhar and T. L. Alford, *APL MATERIALS* **1**, 012102 (2013)

[4] C. Guillén, J. Herrero , *Thin Solid Films* **520,** 1, (2011)

[5] Eun Mi Kim, In-Seok Choi, Jeong-Pyo Oh, Young-Baek Kim, Jong-Ho Lee, Yong-Sung Choi, Jung-Dae Cho, Yang-Bae Kim and Gi-Seok Heo, *Jpn. J. Appl. Phys.* **53** 095505, (2014)

[6] Zhong Zhi You, Gu Jin Hua, *Materials Letters* **65**, 3234 (2011)

[7] Hung-Wei Wu, Chien-Hsun Chu, *Materials Letters* **105**, 65 (2013)

[8] Chu-Chi Ting, Shiep-Ping Chang, Wei-Yang Li, Ching-Hua Wang, *Applied Surface Science* **284** (2013) 397

[9] P.K. Ooi, S.S. Ng, M.J. Abdullah and Z. Hassan, *Materials Letters* **116**, 396 (2014)

[10] *V. Craciun, C. Martin, G. Socol, D. Tanner, H.C. Swart, N. Becherescu, D. Craciun, Applied Surface Science* **306** (2014) 52

[11] C.H. Jung, D.J. Kim, Y.K. Kang, D.H. Yoon, *Thin Solid Films* **517**, 4078 (2009).

[12] A. Dhar and T. L. Alford, *ECS Solid State Letters*, **3** (11) N1 (2014)

[13] S.H. Yu, C.H. Jia, H.W. Zheng, L.H. Ding, W.F. Zhang, *Materials Letters* 85, 68 (2012)

[14] A. Dhar and T. L. Alford, *J. Appl. Phys.* **112**, 103113 (2012).

[15] Haitian Chen, Yu Cao, Jialu Zhang and Chongwu Zhou, *Nature Communications,* (2014), DOI: 10.1038/ncomms5097

[16] Shang-Chao Hung,1 Kin-Tak Lam,2 Cheng-Fu Yang,3 and Yu-Jhen Liou, *International Journal of Photoenergy,* (2014), DOI: 10.1155/2014/739096

[17] Gwang Jun Lee, Joonwoo Kim, Jung-Hye Kim, Soon Moon Jeong, Jae Eun Jang and Jaewook Jeong, *Semicond. Sci. Technol.* **29** 035003, (2014)

[18] J Niu, R Ma, Y Wang, S Li, S Cheng, *Z Liu*, Optoelectronics Letters, **10**, 347, (2014)

[19] M. Gadre and T. L. Alford, *Applied Physics Lett.* **99**, 051901 (2011)

[20] Shiu-Jen Liu, Shih-Hao Su, Hau-Wei Fang, Jang-Hsing Hsieh, Jenh-Yih Juang, *Applied Surface Science* **257** (2011) 10018

[21] Keisuke Ide, Yutomo Kikuchi, Kenji Nomura, Toshio Kamiya, Hideo Hosono, *Thin Solid Films* **520,** 3787 (2012).

[22] Haifeng Pu, Qianfei Zhou, Lan Yue, Qun Zhang, *Applied Surface Science* **283** (2013) 722

[23] Ijaz Ahmad Bhatti, T.A. Nirmal Peiris, Thomas D. Smith, K.G. Upul Wijayantha, *Materials Letters* **93**, 333 (2013)

[24] B Jung, K Kim, W Kim, *J. Mater. Chem. A*, (2014), **2**, 15175

[25] Kim, Jong-Woong; Choi, Jang-Woo; Hong, Sung-Jei; Kwak, Min-Gi, *Journal of Nanoscience and Nanotechnology,* Volume 13, (2013), 6005

[26] Ping Wei, Dongmei Zhu, Shanshan Huang, Wancheng Zhou, Fa Luo, *Applied Surface Science* **285** (2013) 577

[27] Byung Du Ahn, Sang Hoon Oh, Choong Hee Lee, Gun Hee Kim, Hyun Jae Kim, Sang Yeol Lee, *Journal of Crystal Growth*, **309**, (2007), 128

[28] M Gulen, G Yildirim, S Bal, A Varilci, I Belenli and M. Oz, *J Mater Sci: Mater Electron,* **24**, (2013), 467

[29] G. Haacke, *J. Appl. Phys*. **47**, 4086 (1976).

CHAPTER 3

[1] G. Gustafsson, Y. Cao, G.M. Treacy, F. Klavetter, N. Colaneri, and A. J. Heeger, *Nature* **357**, 477 (1992).

[2] D. C. Look, K. D. Leedy, D. H. Tomich, and B. Bayraktaroglu, *Appl. Phys. Lett.* **96**, 062102 (2010).

[3] A. Dhar and T. L. Alford, *APL MATERIALS* **1**, 012102 (2013)

[4] C. Guillén, J. Herrero , *Thin Solid Films* **520,** 1, (2011)

[5] Eun Mi Kim, In-Seok Choi, Jeong-Pyo Oh, Young-Baek Kim, Jong-Ho Lee, Yong-Sung Choi, Jung-Dae Cho, Yang-Bae Kim and Gi-Seok Heo, *Jpn. J. Appl. Phys.* **53** 095505, (2014)

[6] Zhong Zhi You, Gu Jin Hua, *Materials Letters* **65**, 3234 (2011)

[7] Hung-Wei Wu, Chien-Hsun Chu, *Materials Letters* **105**, 65 (2013)

[8] Chu-Chi Ting, Shiep-Ping Chang, Wei-Yang Li, Ching-Hua Wang, *Applied Surface Science* **284** (2013) 397

[9] P.K. Ooi, S.S. Ng, M.J. Abdullah and Z. Hassan, *Materials Letters* **116**, 396 (2014)

[10] *V. Craciun, C. Martin, G. Socol, D. Tanner, H.C. Swart, N. Becherescu, D. Craciun, Applied Surface Science* **306** (2014) 52

[11] C.H. Jung, D.J. Kim, Y.K. Kang, D.H. Yoon, *Thin Solid Films* **517**, 4078 (2009).

[12] A. Dhar and T. L. Alford, *ECS Solid State Letters*, **3** (11) N1 (2014)

[13] S.H. Yu, C.H. Jia, H.W. Zheng, L.H. Ding, W.F. Zhang, *Materials Letters* 85, 68 (2012)

[14] A. Dhar and T. L. Alford, *J. Appl. Phys.* **112**, 103113 (2012).

[15] Haitian Chen, Yu Cao, Jialu Zhang and Chongwu Zhou, *Nature Communications,* (2014), DOI: 10.1038/ncomms5097

[16] Shang-Chao Hung,1 Kin-Tak Lam,2 Cheng-Fu Yang,3 and Yu-Jhen Liou, *International Journal of Photoenergy,* (2014), DOI: 10.1155/2014/739096

[17] Gwang Jun Lee, Joonwoo Kim, Jung-Hye Kim, Soon Moon Jeong, Jae Eun Jang and Jaewook Jeong, *Semicond. Sci. Technol.* **29** 035003, (2014)

[18] J Niu, R Ma, Y Wang, S Li, S Cheng, *Z Liu*, Optoelectronics Letters, **10**, 347, (2014)

[19] M. Gadre and T. L. Alford, *Applied Physics Lett.* **99**, 051901 (2011)

[20] Shiu-Jen Liu, Shih-Hao Su, Hau-Wei Fang, Jang-Hsing Hsieh, Jenh-Yih Juang, *Applied Surface Science* **257** (2011) 10018

[21] Keisuke Ide, Yutomo Kikuchi, Kenji Nomura, Toshio Kamiya, Hideo Hosono, *Thin Solid Films* **520,** 3787 (2012).

[22] Haifeng Pu, Qianfei Zhou, Lan Yue, Qun Zhang, *Applied Surface Science* **283** (2013) 722

[23] Ijaz Ahmad Bhatti, T.A. Nirmal Peiris, Thomas D. Smith, K.G. Upul Wijayantha, *Materials Letters* **93**, 333 (2013)

[24] B Jung, K Kim, W Kim, *J. Mater. Chem. A*, (2014), **2**, 15175

[25] Kim, Jong-Woong; Choi, Jang-Woo; Hong, Sung-Jei; Kwak, Min-Gi, *Journal of Nanoscience and Nanotechnology,* Volume 13, (2013), 6005

[26] Ping Wei, Dongmei Zhu, Shanshan Huang, Wancheng Zhou, Fa Luo, *Applied Surface Science* **285** (2013) 577

[27] Byung Du Ahn, Sang Hoon Oh, Choong Hee Lee, Gun Hee Kim, Hyun Jae Kim, Sang Yeol Lee, *Journal of Crystal Growth*, **309**, (2007), 128

[28] M Gulen, G Yildirim, S Bal, A Varilci, I Belenli and M. Oz, *J Mater Sci: Mater Electron,* **24**, (2013), 467

[29] G. Haacke, *J. Appl. Phys*. **47**, 4086 (1976).

CHAPTER 4

[1] E. Harlev, T. Gulakhmedova, I. Rubinovich, and G. Aizenshtein, *Adv. Mater*. **8**, 994, (1996).

[2] U. Bach, D. Lupo, P. Comte, J.E. Moser, F. Weissörtel, J. Salbeck, H. Spreitzer, and M. Grätzel, *Nature* **395**, 477, (1998).

[3] G. Gustafsson, Y. Cao, G.M. Treacy, F. Klavetter, N. Colaneri, and A. J. Heeger, *Nature* **357**, 477, (1992).

[4] H. Sato, T. Minami, S. Takata, T. Miyata, and M. Ishii, *Thin Solid Films* **102**, 1,(1983).

[5] C. G. Granqvist, *Appl. Phys. A* **52**, 83, (1991).

[6] H. C. Lee, and O. O. Park, *Vacuum* **75**, 275, (2004).

[7] A. E. Hichou, A. Kachouane, J. L. Bubendorff, M. Addou, J. Ebothe, M. Troyon, and A. Bougrine, *Thin Solid Films* **458**, 263, (2004).

[8] S. Kim, Y. Moon, D. Moon, M. Hong, Y. Jeon, and J. Park, *J. Korean Phys.Soc*. **49**, 1256, (2006).

[9] D. C. Look, *Semicond. Sci. Technol.* **20**, S55, (2005).

[10] H. Han, N. D. Theodore, and T. L. Alford, *J. Appl. Phys.* **105,** 123528 (2009).

[11] A. Indluru and T. L. Alford, *J. Appl. Phys.* **103,** 013708, (2008).

[12] S. W. Chen, and C. H. Koo, *Mater. Lett*. **61,** 4097, (2007).

[13] K. H. Choi, J. Y. Kim, Y. S. Lee, and H. J. Kim, *Thin Solid Films* **341**, 152, (1999).

[14] M. K. Sinha, S. K. Mukherjee, B. Pathak, R. K. Paul, P. K. Barhai, *Thin Solid Films* **515**, 1753, (2006).

[15] F. Laia, M. Lia, H. Wanga, H. Hua, Y. Songc, Y. Jiang *Thin Solid Films* **488,** 314, (2005).

[16] R. Romero, J. R. Ramos-Barrado, F. Martin and D. Leinen *Surf. Interface Anal*. , **36**, 888, (2004).

[17] C. C. Lee, C. L. Tien, and J. C. Hsu *Applied Optics* **41**, 10 (2002)

[18] L. R. Doolittle, *Nucl. Instrum. Methods Phys. Res. B* **9**, 344 (1985).

[19] H. Han, J. W. Mayer, and T. L. Alford, *J. Appl. Phys*. **100**, 083715 (2006).

[20] H. Han, J. W. Mayer, and T. L. Alford, *J. Appl. Phys*. **99**, 123711 (2006).

[21] G. Haacke, *J. Appl. Phys*. **47**, 4086 (1976).

[22] T. Muller and H. Nienhaus, *J. Appl. Phys.* **93**, 924 (2003).

[23] R. Koch *J. Phys.: Condens. Matter* **6,** 9519, (1994)

[24] P. Bieganski, *Vacuum* **74**, 211, (2004)

[25] R. Doremus, *Thin Solid Films* **326,** 205, (1998).

CHAPTER 5

[1] Q. Wan, E. N. Dattoli, and W. Lu, *Appl. Phys. Lett.* **90**, 222107 (2007).

[2] G. Gustafsson, Y. Cao, G.M. Treacy, F. Klavetter, N. Colaneri, and A. J. Heeger, *Nature* **357**, 477 (1992).

[3] D. C. Look, K. D. Leedy, D. H. Tomich, and B. Bayraktaroglu, *Appl. Phys. Lett.* **96**, 062102 (2010).

[4] H. C. Lee, and O. O. Park, *Vacuum* **75**, 275 (2004).

[5] A. El Hichou, A. Kachouane, J. L. Bubendorff, M. Addou, J. Ebothe, M. Troyon, and A. Bougrine, *Thin Solid Films* **458**, 263 (2004).

[6] S. Kim, Y. Moon, D. Moon, M. Hong, Y. Jeon, and J. Park, *J. Korean Phys. Soc*. **49**, 1256 (2006).

[7] D. C. Look, *Semicond. Sci. Technol.* **20**, S55 (2005).

[8] H. Han, N. D. Theodore, and T. L. Alford, *J. Appl. Phys.* **105,** 123528 (2009).

[9] A.Indluru and T. L. Alford, *J. Appl. Phys.* **103,** 013708 (2008).

[10] S. W. Chen, and C. H. Koo, *Mater. Lett*. **61,** 4097 (2007).

[11] K. H. Choi, J. Y. Kim, Y. S. Lee, and H. J. Kim, *Thin Solid Films* **341**, 152 (1999).

[12] M. K. Sinha, S. K. Mukherjee, B. Pathak, R. K. Paul, P. K. Barhai, *Thin Solid Films* **515** 1753 (2006).

[13] F. Laia, M. Lia, H. Wanga, H. Hua, Y. Songc, Y. Jiang *Thin Solid Films* **488** (2005) 314

[14] T. Muller and H. Nienhaus, *J. Appl. Phys.* **93**, 924 (2003).

[15] D. Zhang, H. Yabe, E. Akita, P. Wang, R. Murakami and X. Song *J. Appl. Phys.* **109**, 104318 (2011)

[16] Yeongseok Zoo and T. L. Alford *J. Appl. Phys.* **101**, 033505 (2007)

[17] G. Haacke, *J. Appl. Phys*. **47**, 4086 (1976).

CHAPTER 6

[1] Q. Wan, E. N. Dattoli, and W. Lu, *Appl. Phys. Lett.* **90**, 222107 (2007).

[2] G. Gustafsson, Y. Cao, G.M. Treacy, F. Klavetter, N. Colaneri, and A. J. Heeger, *Nature* **357**, 477 (1992).

[3] D. C. Look, K. D. Leedy, D. H. Tomich, and B. Bayraktaroglu, *Appl. Phys. Lett.* **96**, 062102 (2010).

[4] S. X. Zhang, S. Dhar, W. Yu, H. Xu, S. B. Ogale, and T. Venkatesan, *Appl.Phys. Lett.* **91**, 112113 (2007).

[5] V. Bhosle, A. Tiwari, and J. Narayan, *Appl. Phys. Lett.* **88**, 032106 (2006).

[6] K. L. Chopra, S.K. Major, and D. K. Pandya, *Thin Solid Films* **102**, 1 (1983)
.

[7] H. Han, N. D. Theodore, and T. L. Alford, *J. Appl. Phys.* **103**, 013708 (2008).

[8] A. Dhar and T. L. Alford, *J. Appl. Phys.* **112**, 103113 (2012).

[9] A. Indluru and T. L. Alford, *J. Appl. Phys.* **105**, 123528 (2009).

[10] T. Y. Park, Y. S. Choi, J. W. Kang, J. H. Jeong, S. J. Park, D. M. Jeon, J. W. Kim, and Y. C. Kim, *Appl. Phys. Lett.* **96**, 051124 (2010).

[11] C. Guillén, J. Herrero , *Thin Solid Films* **520** (2011) 1

[12] D. S. Ghosh, T. L. Chen, and V. Pruneri, *Appl. Phys. Lett.* **96**, 041109 (2010).

[13] I. Dima, B. Popescu, F. Iova and G. Popescu, *Thin Solid Films* **200**, 11 (1991).

[14] C. H. Heo, S-Bo. Lee, J-Hyo. Boo Jiang *Thin Solid Films* **475** (2005) 183

[15] T. Muller and H. Nienhaus, *J. Appl. Phys.* **93**, 924 (2003).

[16] R. Koch, *J. Phys.: Condens. Matter* **6**, 9519 (1994)

[17] R. L. Petritz *Phys. Rev.* **104** 1508 (1956)

[18] D. Zhang, H. Yabe, E. Akita, P. Wang, R. Murakami and X. Song *J. Appl. Phys.* **109**, 104318 (2011)

[19] K. Sivaramakrishnan and T. L. Alford, *Appl. Phys. Lett.* **96**, 201109 (2010)

[20] F. Mayadas and M. Shatzkes, *Phys. Rev. B* **1**, 1382 (1970)

[21] D. Zhang, P. Wang, R. Murakami and X. Song, *Appl. Phys. Lett.* **96**, 233114 (2010)

[22] P. Wang, D. Zhang, D. H. Kim, Z. Qiu, L. Gao, R. Murakami and X. Song *J. Appl. Phys.* **106**, 103104 (2009)

[23] R. Doremus, Thin Solid Films **326**, 205 (1998).

[24] G. Haacke, *J. Appl. Phys*. **47**, 4086 (1976).

CHAPTER 7

[1] G. Gustafsson, Y. Cao, G.M. Treacy, F. Klavetter, N. Colaneri, and A. J. Heeger, *Nature* **357**, 477 (1992).

[2] D. C. Look, K. D. Leedy, D. H. Tomich, and B. Bayraktaroglu, *Appl. Phys. Lett.* **96**, 062102 (2010).

[3] G. Exarhos *; ECS Trans*. **19**, 29, (2009)

[4] H-K Kim *et.al* , *Journal of The Electrochemical Society*, **155,** 1, J1, (2008)

[5] K. L. Chopra, S.K. Major, and D. K. Pandya, *Thin Solid Films* **102**, 1 (1983).

[6] T. Minami, *Semicond. Sci. Technol*. **20,** S35, (2005)

[7] H Xu, L Lan, M Xu, M Li, D Luo, P Xiao and J Peng, *ECS J. Solid State Sci. Technol.* **2,** 11, R245 (2013)

[8] A. Dhar and T. L. Alford, *APL MATERIALS* **1**, 012102 (2013)

[9] A. Dhar and T. L. Alford, *J. Appl. Phys.* **112**, 103113 (2012).

[10] Y-S Park *et.al*, *Journal of The Electrochemical Society*, **156**, 7, H588, (2009)

[11] Y-S Park, H-K Kim, and S-W Kim, *Journal of The Electrochemical Society,* **157**, 8, J301, (2010)

[12] K-H Choi, Y-Y Choi, J-A Jeong, H-K Kim, S Jeon, *Electrochem. Solid-State Lett.* **14**, 4, H152, (2011)

[13] H-K Park, J-A Jeong, Y-S Park, S-Y Na, D-Y Kim and H-K Kim, *Electrochem. Solid-State Lett.* **12**, 8, H309, (2009)

[14] C. Guillén, J. Herrero , *Thin Solid Films* **520,** 1, (2011)

[15] K. Sivaramakrishnan, N. D. Theodore, J. F. Moulder, and T. L. Alford; *J. Appl. Phys.* **106**, 063510 (2009).

[16] T. Ghosh, M. Dutta, S. Mridha and D. Basak, *Journal of The Electrochemical Society,* **156**, 4, H285, (2009)

[17] I. Dima, B. Popescu, F. Iova and G. Popescu, *Thin Solid Films* **200**, 11 (1991).

[18] C. H. Heo, S-Bo. Lee, J-Hyo. Boo Jiang *Thin Solid Films* **475** (2005) 183

[19] T. Muller and H. Nienhaus, *J. Appl. Phys.* **93**, 924 (2003).

[20] R. Koch, *J. Phys.: Condens. Matter* **6**, 9519 (1994)

[21] Z. B. Wang, M. G Helander,X. F. Xu, D. P. Puzzo, J. Qiu, M. T. Greiner and Z. H. Lu, Journal of Applied Physics, **109**, 053107 (2011).

[22] C. C. Katsidis, Dimitrios I. Siapkas, Applied optics **41**, 3978 (2002).

[23] E. Centurioni, Applied Optics **44**, 7532 (2005).

[24] D. Zhang, P. Wang, R. Murakami and X. Song, *Appl. Phys. Lett.* **96**, 233114 (2010)

[25] P. Wang, D. Zhang, D. H. Kim, Z. Qiu, L. Gao, R. Murakami and X. Song *J. Appl. Phys.* **106**, 103104 (2009)

[26] R. Doremus, Thin Solid Films **326**, 205 (1998).

[27] G. Haacke, *J. Appl. Phys*. **47**, 4086 (1976).

CHAPTER 8

[1] Q. Wan, E. N. Dattoli, and W. Lu, *Appl. Phys. Lett.* **90**, 222107 (2007).

[2] G. Gustafsson, Y. Cao, G.M. Treacy, F. Klavetter, N. Colaneri, and A. J. Heeger, *Nature* **357**, 477 (1992).

[3] A. Dhar, Z. Zhao and T. L. Alford, *JOM* **67**,4, 840 (2015).

[4] S. X. Zhang, S. Dhar, W. Yu, H. Xu, S. B. Ogale, and T. Venkatesan, *Appl.Phys. Lett.* **91**, 112113 (2007).

[5] V. Bhosle, A. Tiwari, and J. Narayan, *Appl. Phys. Lett.* **88**, 032106 (2006).

[6] K. L. Chopra, S.K. Major, and D. K. Pandya, *Thin Solid Films* **102**, 1 (1983).

[7] H. Han, N. D. Theodore, and T. L. Alford, *J. Appl. Phys.* **103**, 013708 (2008).

[8] A. Dhar and T. L. Alford, *J. Appl. Phys.* **112**, 103113 (2012).

[9] A. Dhar, Z. Zhao and T. L. Alford, *JOM* **67**,4, 845 (2015).

[10] T. Y. Park, Y. S. Choi, J. W. Kang, J. H. Jeong, S. J. Park, D. M. Jeon, J. W. Kim, and Y. C. Kim, *Appl. Phys. Lett.* **96**, 051124 (2010).

[11] C. Guillén, J. Herrero , *Thin Solid Films* **520** (2011) 1

[12] D. S. Ghosh, T. L. Chen, and V. Pruneri, *Appl. Phys. Lett.* **96**, 041109 (2010).

[13] I. Dima, B. Popescu, F. Iova and G. Popescu, *Thin Solid Films* **200**, 11 (1991).

[14] C. H. Heo, S-Bo. Lee, J-Hyo. Boo Jiang *Thin Solid Films* **475** (2005) 183

[15] T. Muller and H. Nienhaus, *J. Appl. Phys.* **93**, 924 (2003).

[16] R. Koch, *J. Phys.: Condens. Matter* **6**, 9519 (1994)

[17] R. L. Petritz *Phys. Rev.* **104** 1508 (1956)

[18] D. Zhang, H. Yabe, E. Akita, P. Wang, R. Murakami and X. Song *J. Appl. Phys.* **109**, 104318 (2011)

[19] K. Sivaramakrishnan and T. L. Alford, *Appl. Phys. Lett.* **96**, 201109 (2010)

[20] F. Mayadas and M. Shatzkes, *Phys. Rev. B* **1**, 1382 (1970)

[21] D. Zhang, P. Wang, R. Murakami and X. Song, *Appl. Phys. Lett.* **96**, 233114 (2010)

[22] P. Wang, D. Zhang, D. H. Kim, Z. Qiu, L. Gao, R. Murakami and X. Song *J. Appl. Phys.* **106**, 103104 (2009)

[23] R. Doremus, Thin Solid Films **326**, 205 (1998).

[24] G. Haacke, *J. Appl. Phys*. **47**, 4086 (1976).

APPENDIX A

COPYRIGHT PERMISSIONS

ELSEVIER LICENSE
TERMS AND CONDITIONS

Dec 05, 2014

This is a License Agreement between Aritra Dhar ("You") and Elsevier ("Elsevier") provided by Copyright Clearance Center ("CCC"). The license consists of your order details, the terms and conditions provided by Elsevier, and the payment terms and conditions.

All payments must be made in full to CCC. For payment instructions, please see information listed at the bottom of this form.

Supplier	Elsevier Limited The Boulevard,Langford Lane Kidlington,Oxford,OX5 1GB,UK
Registered Company Number	1982084
Customer name	Aritra Dhar
Customer address	1265 E UNIVERSITY DR APT 3060 TEMPE, AZ 85281
License number	3522790936703
License date	Dec 05, 2014
Licensed content publisher	Elsevier
Licensed content publication	Solar Energy Materials
Licensed content title	Physics of doped tin dioxide films for spectral-selective surfaces
Licensed content author	F. Simonis, M. van der Leij, C.J. Hoogendoorn
Licensed content date	March–May 1979
Licensed content volume number	1
Licensed content issue number	3-4
Number of pages	11
Start Page	221
End Page	231
Type of Use	reuse in a thesis/dissertation
Intended publisher of new work	other
Portion	figures/tables/illustrations
Number of figures/tables/illustrations	1
Format	both print and electronic
Are you the author of this Elsevier article?	No

ELSEVIER LICENSE
TERMS AND CONDITIONS

Dec 05, 2014

This is a License Agreement between Aritra Dhar ("You") and Elsevier ("Elsevier") provided by Copyright Clearance Center ("CCC"). The license consists of your order details, the terms and conditions provided by Elsevier, and the payment terms and conditions.

All payments must be made in full to CCC. For payment instructions, please see information listed at the bottom of this form.

Supplier	Elsevier Limited The Boulevard,Langford Lane Kidlington,Oxford,OX5 1GB,UK
Registered Company Number	1982084
Customer name	Aritra Dhar
Customer address	1265 E UNIVERSITY DR APT 3060 TEMPE, AZ 85281
License number	3522780776630
License date	Dec 05, 2014
Licensed content publisher	Elsevier
Licensed content publication	Thin Solid Films
Licensed content title	TCO/metal/TCO structures for energy and flexible electronics
Licensed content author	C. Guillén,J. Herrero
Licensed content date	31 October 2011
Licensed content volume number	520
Licensed content issue number	1
Number of pages	17
Start Page	1
End Page	17
Type of Use	reuse in a thesis/dissertation
Portion	figures/tables/illustrations
Number of figures/tables/illustrations	2
Format	both print and electronic
Are you the author of this Elsevier article?	No
Will you be translating?	No
Title of your	Novel Transparent Composite Electrodes and Mixed Oxide Layers for

CAMBRIDGE UNIVERSITY PRESS LICENSE TERMS AND CONDITIONS

Dec 05, 2014

This is a License Agreement between Aritra Dhar ("You") and Cambridge University Press ("Cambridge University Press") provided by Copyright Clearance Center ("CCC"). The license consists of your order details, the terms and conditions provided by Cambridge University Press, and the payment terms and conditions.

All payments must be made in full to CCC. For payment instructions, please see information listed at the bottom of this form.

License Number	3522781335617
License date	Dec 05, 2014
Licensed content publisher	Cambridge University Press
Licensed content publication	MRS Bulletin
Licensed content title	New *n*-Type Transparent Conducting Oxides
Licensed content author	Tadatsugu Minami
Licensed content date	Jan 31, 2011
Volume number	25
Issue number	08
Start page	38
End page	44
Type of Use	Dissertation/Thesis
Requestor type	Not-for-profit
Portion	Text extract
Number of pages requested	5
Order reference number	None
Territory for reuse	World
Title of your thesis / dissertation	Novel Transparent Composite Electrodes and Mixed Oxide Layers for Improved Flexible Electronics
Expected completion date	Dec 2014
Estimated size(pages)	120
Billing Type	Invoice
Billing address	1265 E UNIVERSITY DR APT 3060 TEMPE, AZ 85281 United States
TAX (0.00%)	0.00 USD
Total	0.00 USD

ELSEVIER LICENSE
TERMS AND CONDITIONS

Dec 05, 2014

This is a License Agreement between Aritra Dhar ("You") and Elsevier ("Elsevier") provided by Copyright Clearance Center ("CCC"). The license consists of your order details, the terms and conditions provided by Elsevier, and the payment terms and conditions.

All payments must be made in full to CCC. For payment instructions, please see information listed at the bottom of this form.

Supplier	Elsevier Limited The Boulevard,Langford Lane Kidlington,Oxford,OX5 1GB,UK
Registered Company Number	1982084
Customer name	Aritra Dhar
Customer address	1265 E UNIVERSITY DR APT 3060 TEMPE, AZ 85281
License number	3522790040948
License date	Dec 05, 2014
Licensed content publisher	Elsevier
Licensed content publication	Thin Solid Films
Licensed content title	Present status of transparent conducting oxide thin-film development for Indium-Tin-Oxide (ITO) substitutes
Licensed content author	Tadatsugu Minami
Licensed content date	1 July 2008
Licensed content volume number	516
Licensed content issue number	17
Number of pages	7
Start Page	5822
End Page	5828
Type of Use	reuse in a thesis/dissertation
Intended publisher of new work	other
Portion	figures/tables/illustrations
Number of figures/tables/illustrations	1
Format	both print and electronic
Are you the author of this Elsevier article?	No